Thermal Aspects of Using Alternative Nuclear Fuels in Supercritical Water-Cooled Reactors

by

Lisa Christine Grande

A Thesis Submitted in Partial Fulfillment

of the Requirements for the Degree of

Master of Applied Science

Nuclear Engineering

The Faculty of Energy Systems and Nuclear Science

University of Ontario Institute of Technology

November, 2010

ABSTRACT

A SuperCritical Water-cooled Nuclear Reactor (SCWR) is a Generation IV concept currently being developed worldwide. Unique to this reactor type is the use of light-water coolant above its critical point. The current research presents a thermal-hydraulic analysis of a single fuel channel within a Pressure Tube (PT) - type SCWR with a single-reheat cycle. Since this reactor is in its early design phase many fuel-channel components are being investigated in various combinations. Analysis inputs are: steam cycle, Axial Heat Flux Profile (AHFP), fuel-bundle geometry, and thermophysical properties of reactor coolant, fuel sheath and fuel.

Uniform and non-uniform AHFPs for average channel power were applied to a variety of alternative fuels (mixed oxide, thorium dioxide, uranium dicarbide, uranium nitride and uranium carbide) enclosed in an Inconel-600 43-element bundle. The results depict bulk-fluid, outer-sheath and fuel-centreline temperature profiles together with the Heat Transfer Coefficient (HTC) profiles along the heated length of fuel channel. The objective is to identify the best options in terms of fuel, sheath material and AHFPS in which the outer-sheath and fuel-centreline temperatures will be below the accepted temperature limits of 850°C and 1850°C respectively.

The 43-element Inconel-600 fuel bundle is suitable for SCWR use as the sheath-temperature design limit of 850°C was maintained for all analyzed cases at average channel power. Thoria, UC_2, UN and UC fuels for all AHFPs are acceptable since the maximum fuel-centreline temperature does not exceed the industry accepted limit of 1850°C. Conversely, the fuel-centreline temperature limit was exceeded for MOX at all AHFPs, and UO_2 for both cosine and downstream-skewed cosine AHFPs. Therefore, fuel-bundle modifications are required for UO_2 and MOX to be feasible nuclear fuels for SCWRs.

ACKNOWLEDGMENTS

My research could not have been possible without the ongoing patience and encouragement from my family and friends. Many thanks for the inspiration and collaboration from my undergraduate thesis team: Bryan Villamere, Adrianexy Rodriguez-Prado, Sally Mikhael, and Leyland Allison. The guidance and mentorship from Dr. I. Pioro are fundamental to my success. Assistance from my fellow graduate students has been crucial to my academic performance. Thank you: Sarah Mokry, Andrew Lukomski, Wargha Peiman, Eugene Saltanov and Jeffery Samuel for all of your help. I am truly appreciative for all the continuous support from my UOIT's FESNS "family".

Financial supports from the NSERC Discovery Grant and NSERC/NRCan/AECL Generation IV Energy Technologies Program (NNAPJ) are also gratefully acknowledged.

SUMMARY

SuperCritical Water-cooled nuclear Reactors (SCWRs) are a renewed technology being pursued as one of the six Generation IV International Forum (GIF) reactor concepts. The reactor coolant is light water at pressures and temperatures above its critical point. Some fossil generating power plants use SuperCritical Water (SCW) as the working fluid. However, SCWRs are the only Generation IV reactor concept to be cooled with SCW. These elevated operating conditions will improve SCW Nuclear Power Plant (NPP) thermal efficiencies by 10 – 15% compared to those of current NPPs. Also, SCWRs will have the ability to employ a direct cycle, thus decreasing NPP capital and maintenance costs.

The SCWR core has 2 configurations: 1) Pressure Vessel (PV) -type enclosing a fuel assembly and 2) Pressure Tube (PT) -type consisting of individual pressure channels containing fuel bundles. Canada and Russia are developing PT-type SCWRs. In particular, the Canadian SCWR reactor has an output of 1200 MW_{el} and will operate at a pressure of 25 MPa with inlet and outlet fuel-channel temperatures of 350°C and 625°C, respectively.

The challenge is defining fuel-channel-material combinations that are able to withstand SCW conditions. This research places emphasis on thermal aspects of the core design. Reactor-physics calculations were not conducted; however neutronic characteristics of the fuel are discussed. Operational behaviors and issues of the alternative fuels are presented. The current PT-type nuclear-reactor fuel-channel design is based on the use of zirconium alloy pressure tube, Inconel-sheath bundle and uranium dioxide (UO_2) fuel. Previous studies have indicated that UO_2 fuel may not be acceptable within the SCWR operating conditions. Alternative fuels with increased thermal conductivity should be considered for application in SCWRs due to lower the fuel centerline temperatures.

Previous studies have shown that the maximum fuel centreline temperature of a UO_2 pellet might exceed the industry accepted temperature limit of 1850°C at SCWR conditions. Therefore, alternative fuels such as Mixed OXides (MOX) and Thoria (ThO_2) are analyzed, because of resource availability and can supplement depleting uranium reserves. Uranium dicarbide (UC_2), uranium carbide (UC) and uranium nitride (UN) are also potential fuel

options as they all have higher thermal conductivities compared to conventional nuclear fuels such as UO_2.

The SCWR sheath temperature is restricted with the design limit of 850°C. Inconel-600 has been selected as the sheath material due its high corrosion resistance and high yield strength in aggressive SCW at high temperatures.

The thermal-hydraulic analysis presented in this thesis is versatile since all fuel-design inputs are interchangeable. The developed computer code may be adapted to model the globally popular PV-type reactor core. This is possible since the design parameters are based on coolant mass flux and hydraulic-equivalent diameter of the fuel bundle. The PT-type was selected due to the availability of detailed core specifications.

The 43-element Inconel-600 fuel bundle is suitable for SCWR use as the sheath-temperature design limit of 850°C was maintained for all analyzed cases at average channel power. Thoria, UC_2, UN and UC fuels for all AHFPs are acceptable since the maximum fuel-centreline temperature does not exceed the industry accepted limit of 1850°C. Conversely, the fuel centreline-temperature limit was exceeded with MOX at all AHFPs, and UO_2 for both cosine and downstream-skewed cosine AHFPs. Therefore, fuel bundle-modifications are required for UO_2 and MOX and to be feasible fuels for SCWRs.

TABLE OF CONTENTS

LIST OF FIGURES

LIST OF TABLES

NOMENCLATURE

A	area, m^2
A_{flow}	flow area, m^2
a_i	polynomial coefficient
c_p	specific heat, J/kg K
$\overline{c_p}$	average specific heat, J/kg K; $\left(\frac{h_{o,sh}-h_b}{T_{o,sh}-T_b}\right)$
D	diameter, m
E	modulus of elasticity, Pa
$\dot{E}_{gen}$	heat generation rate, W,
$\dot{e}_{gen}$	volumetric heat flux, W/m^3
G	mass flux, kg/m^2s; $\left(\frac{\dot{m}}{A_{flow}}\right)$
h	enthalpy, J/kg
HTC	Heat Transfer Coefficient, W/m^2 K
k	thermal conductivity, W/m K
l	length, m
$\dot{m}$	mass-flow rate, kg/s
N	number of fuel rods
Nu	Nusselt number; $\left(\frac{HTC\ D_{hy}}{k}\right)$
P	pressure, Pa
p	perimeter, m

Pr	Prandtl number, $\left(\frac{c_p\,\mu}{k}\right)$
$\overline{\mathbf{Pr}}$	average Prandtl number, $\left(\frac{\overline{c_p}\,\mu}{k}\right)$
Q	heat transfer, J
$\dot{Q}$	heat transfer rate, W
$\dot{q}$	heat flux, W/m^2, $\left(\frac{\dot{Q}}{A_h}\right)$
$\dot{q}'$	power ratio, $\left(\frac{\dot{q}_{loc}}{\dot{q}_{ave}}\right)$
r	radius, m
Re	Reynolds number, $\left(\frac{GD_{hy}}{\mu}\right)$
T	temperature, ℃
x	axial location, m

Greek Symbols

Δ	difference
δ	minimum wall thickness (sheath), m
ε	porosity, volume fractions
μ	dynamic viscosity, Pa•s
ν	kinematic viscosity, m^2/s
ν	Poisson's ratio
ρ	density, kg/m^3

Subscripts

ave	average
b	bulk
c	centre
cr	crush (pressure)
cond, cyl	conduction through a cylinder
Ch	channel
el	electrical
fc	fuel centreline
flow	cross sectional flow area
fuel	fuel
fuel bundle	cross sectional area of fuel bundle blocking fluid flow
h	heated
hy	hydraulic equivalent
i	inner
ir	inner ring
in	inlet
loc	local
max	maximum
mm	per millimetre increment
mr	middle ring

n	radial location within fuel pellet
o	outer
or	outer ring
out	outlet
pc	pseudocritical point
pt	pressure tube
sh	sheath
th	thermal
w	wall
wetted	wetted
x	axial location along heated length

Acronyms

ABWR	Advanced Boiling light-Water Reactor
AGR	Advanced Gas-cooled Reactor
AHFP	Axial Heat Flux Profile
AECL	Atomic Energy of Canada Limited
BWR	Boiling light-Water Reactor
CANDU	CANada Deuterium Uranium (reactor)
ChUWR	Channel-type Uranium-graphite Water Reactor with annular-type elements cooled from inside
CL	centreline (related to fuel pellet)

CRL	Chalk River Laboratory
DUPIC	Direct Use of spent PWR fuel In CANDU
GCR	Gas Cooled Reactor
GIF	Generation IV International Forum
GFR	Gas-cooled Fast Reactor
HF	Heat Flux
HTC	Heat Transfer Coefficient
HP	High Pressure (turbine)
HT	Heat Transfer
IAEA	International Atomic Energy Agency
IHT	Improved Heat Transfer
IP	Intermediate Pressure (turbine)
LOCA	Loss Of Coolant Accident
LFR	Lead-cooled Fast Reactor
LGR	Light-water Graphite moderated Reactor
LMFBR	Liquid Metal Fast-Breeder Reactor
LOCA	Loss Of Coolant Accident
LP	Low Pressure (turbine)
LWR	Light Water Reactor
MATLAB	MATrix LABoratory (software)
MOX	Mixed OXide

MSaR	Molten Salt-cooled Reactor
MSR	Moister-Separator-Reheater
NHT	Normal Heat Transfer
NIST	National Institute of Standards and Technology (USA)
NPP	Nuclear Power Plant
OD	Outer Diameter
PC	PseudoCritical
PCh	Pressure Channel (reactor)
PT	Pressure Tube (reactor)
PV	Pressure Vessel (reactor)
PHWR	Pressurized Heavy Water Reactor
PWR	Pressurized light-Water Reactor
RDIPE	Research and Development Institute of Power Engineering
REFPROP	REference Fluid thermodynamic and transport PROPerties
SC	SuperCritical
SCW	SuperCritical Water
SCWR	SuperCritical Water-cooled Reactor
SFR	Sodium-cooled Fast Reactor
SH	sheath (fuel)
SRH	Steam-ReHeat (channel)
VHTR	Very High-Temperature gas-cooled Reactor
UCG	Uranium Carbide Grit

GLOSSARY

Prior to a general discussion on Supercritical Water-cooled nuclear Reactor (SCWR) concepts it is important to define special terms and expressions used at these conditions.

Definitions of Selected Terms and Expressions Related to Critical and Supercritical Regions[1]

Compressed fluid is a fluid at a pressure above the critical pressure, but at a temperature below the critical temperature.

Critical point (also called a *critical state*) is a point in which the distinction between the liquid and gas (or vapour) phases disappears, i.e., both phases have the same temperature, pressure and volume or density. The *critical point* is characterized by the phase-state parameters T_{cr}, P_{cr} and V_{cr} (or ρ_{cr}), which have unique values for each pure substance.

Deteriorated Heat Transfer (DHT) is characterized with lower values of the wall heat transfer coefficient compared to those at the normal heat transfer; and hence has higher values of wall temperature within some part of a test section or within the entire test section.

Improved Heat Transfer (IHT) is characterized with higher values of the wall heat transfer coefficient compared to those at the normal heat transfer; and hence lower values of wall temperature within some part of a test section or within the entire test section. In our opinion, the improved heat-transfer regime or mode includes peaks or "humps" in the heat transfer coefficient near the critical or pseudocritical points.

Near-critical point is actually a narrow region around the critical point, where all thermophysical properties of a pure fluid exhibit rapid variations.

[1] Based on the book by Pioro & Duffey (2007).

Normal Heat Transfer (NHT) can be characterized in general with wall heat transfer coefficients similar to those of subcritical convective heat transfer far from the critical or pseudocritical regions, when are calculated according to the conventional single-phase Dittus-Boelter-type correlations: $\mathbf{Nu} = 0.0023\ \mathbf{Re}^{0.8}\ \mathbf{Pr}^{0.4}$.

Pseudocritical line is a line, which consists of pseudocritical points.

Pseudocritical point (characterized with P_{pc} and T_{pc}) is a point at a pressure above the critical pressure and at a temperature ($T_{pc} > T_{cr}$) corresponding to the maximum value of the specific heat at this particular pressure.

Supercritical fluid is a fluid at pressures and temperatures that are higher than the critical pressure and critical temperature. However, in the present chapter, a term *supercritical fluid* includes both terms – a *supercritical fluid* and *compressed fluid*.

Supercritical "steam" is actually supercritical water, because at supercritical pressures fluid is considered as a single-phase substance. However, this term is widely (and incorrectly) used in the literature in relation to supercritical "steam" generators and turbines.

Superheated steam is a steam at pressures below the critical pressure, but at temperatures above the critical temperature.

1 INTRODUCTION

1.1 Generation IV Nuclear Reactors.

SuperCritical Water-cooled Reactors (SCWRs) are one of six next-generation nuclear-reactor design options under consideration worldwide. These nuclear-reactor design options are included in the major international treaties such as: Generation IV International Forum (GIF). The premise of GIF is to support the evolution of Nuclear Power Plant (NPP) technology that enhances safety, sustainability, economics, and operational performance.

The other five GIF reactor types with coolant operating parameters are: 1) Gas-cooled Fast Reactors (GFRs) (helium, 7 MPa, 485 – 850°C) (Figure 1.1), 2) Very High-Temperature gas-cooled Reactors (VHTRs) (helium, 9 MPa, 500 – 1000°C) (Figure 1.2), 3) Sodium-cooled Fast Reactors (SFRs) (520 – 550°C) (Figure 1.3), 4) Lead-cooled Fast Reactors (LFRs) (up to 550 – 800°C) (Figure 1.4) and 5) Molten Salt-cooled Reactors (MSaRs) (sodium fluoride salt with dissolved uranium fuel, up to 700 – 800°C) (Figure 1.5).

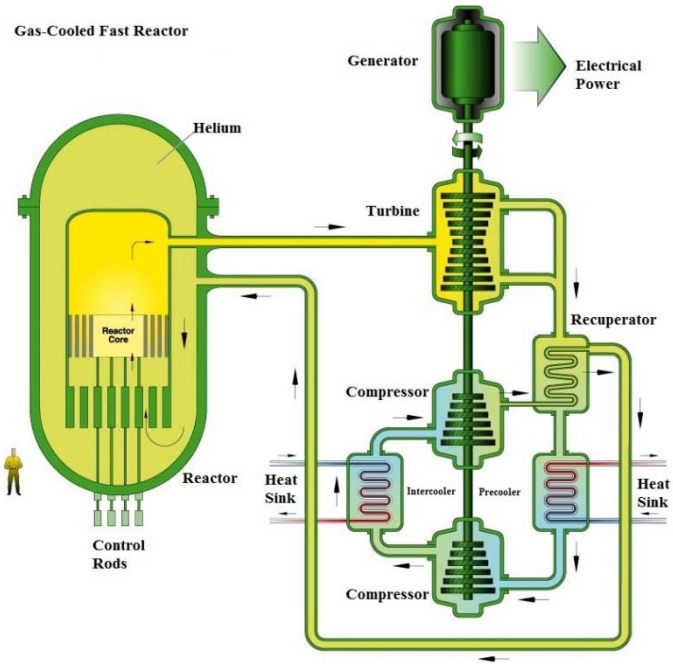

Figure 1.1. GFR GIF concept (DOE & GIF, 2002).

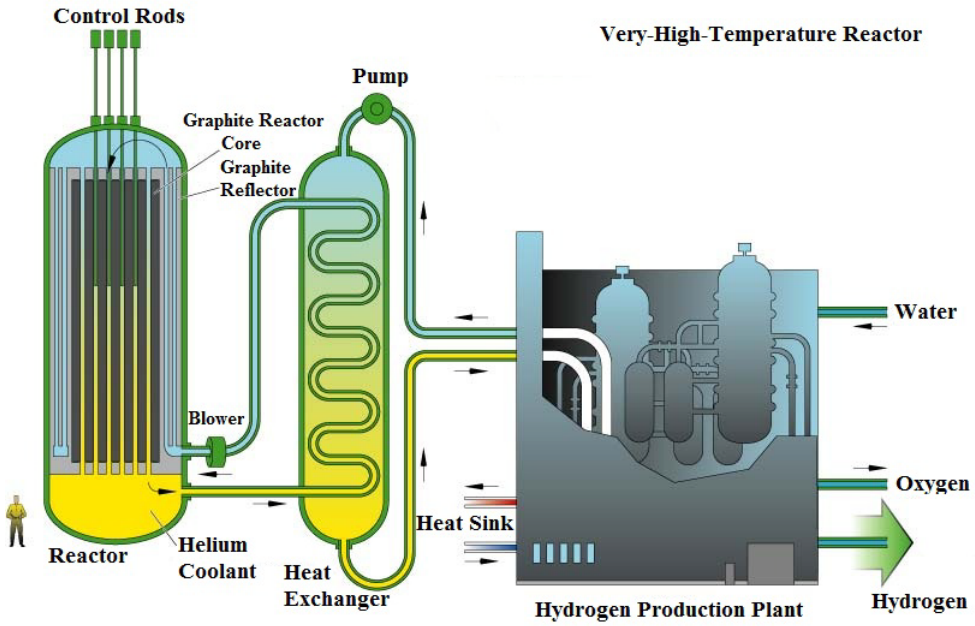

Figure 1.2. VHTR GIF concept (DOE & GIF, 2002).

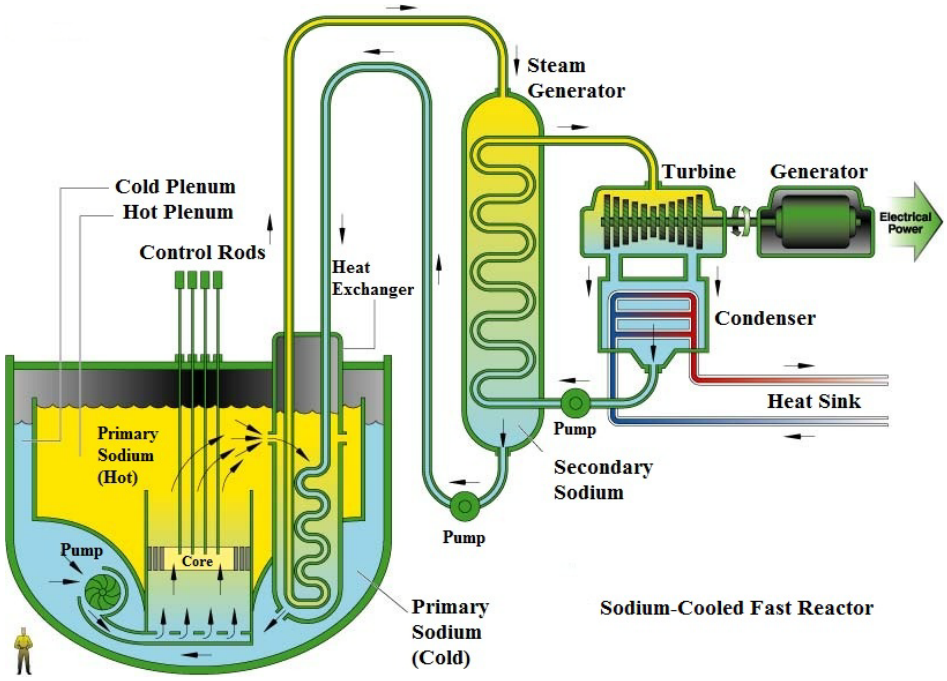

Figure 1.3. SFR GIF concept (DOE & GIF, 2002).

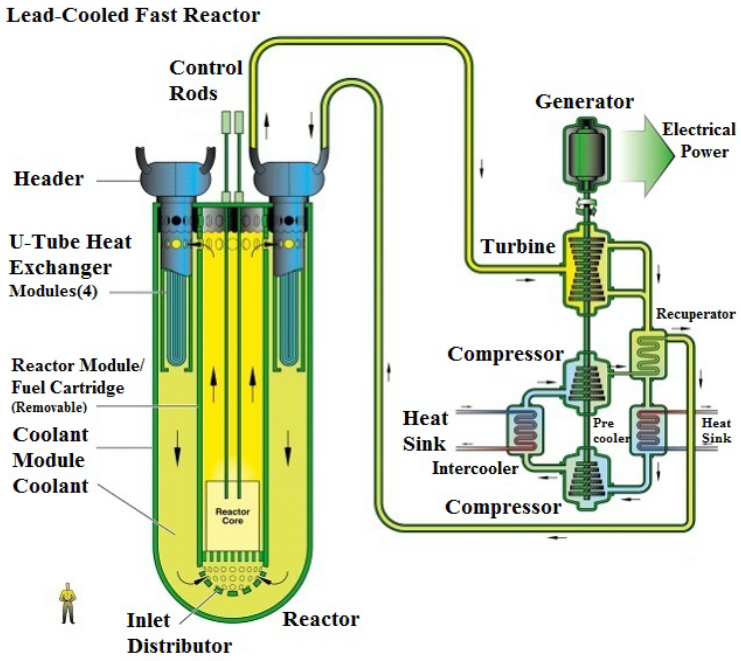

Figure 1.4. LFR GIF concept (DOE & GIF, 2002).

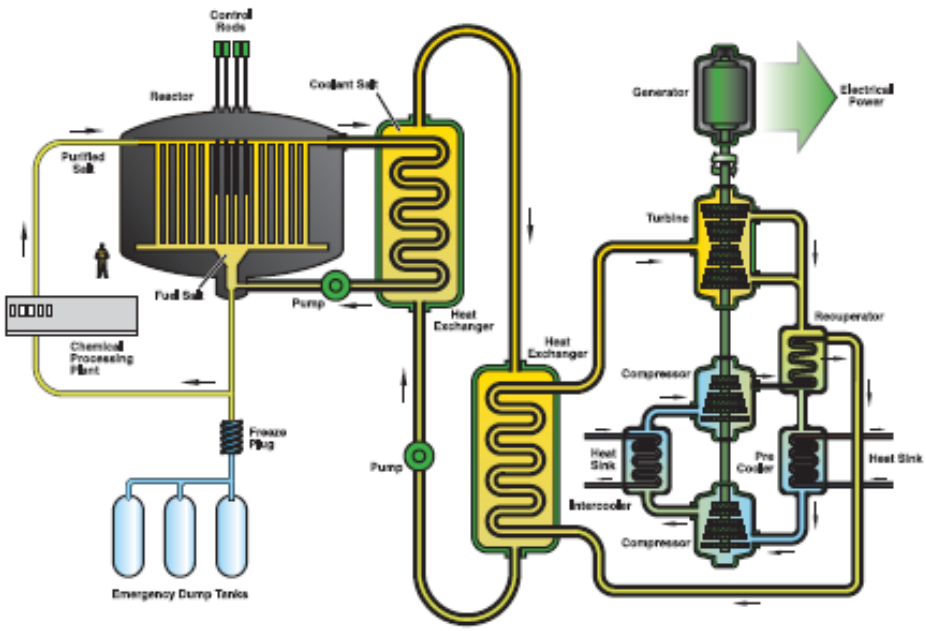

Figure 1.5. MSaR GIF concept (DOE & GIF, 2002).

The SCWR was selected prime GIF concept, because the vast majority of nuclear reactors around the world are water-cooled reactors (see Table 1.1). Therefore, further development of water-cooled reactors in terms of higher thermal efficiencies is a logical way forward. Moving to supercritical pressures is considered as an enhancement for water-cooled reactors. However, it is a conventional way to increase thermal efficiency, which was iniated 50 years ago in the thermal power industry.

Table 1.1. Operating-nuclear power reactors.

Reactor Type	Electrical Output, GW_{el}	Quantity
Pressurized light-Water Reactors (PWRs)	237	262
Boiling light-Water Reactors (BWRs) or Advanced Boiling light-Water Reactors (ABWRs)	83	94
Gas-Cooled Reactors (GCRs) or Advanced Gas-Cooled Reactors (AGRs)	11	22
Pressurized Heavy-Water Reactors (PHWRs)	23	44
Light-water Graphite-moderated Reactors (LGRs)	11	15
Liquid-Metal Fast-Breeder Reactors (LMFBRs)	0.8	2
Total		**439**

Dating back to the end of 1950s and 1960s, SuperCritical Water (SCW) was proposed as a coolant for coal-fired thermal power plants and later on, in nuclear reactors. The United States and Russia led this research. However, this interesting and promising development, i.e., SCWRs, was abandoned at the end of the 1960s – early 1970s. After a

30-year break, the idea of developing nuclear reactors cooled with SCW became attractive once again.

A reason why SCWRs have regained popularity is because they can be operated with a simplified reactor circuit (direct cycle) while increasing the efficiency of an NPP. The number of SCWR components is reduced since steam separators and dryers are not required. This advantage drives down capital and maintenance costs. Safety is also increased, because a dryout phenomenon does not occur at SCW conditions; SCW remains in a single phase.

SCWR technology is currently in its early design phase. A demonstration unit has yet to be designed and constructed. Fuel materials and configurations suited to supercritical conditions are currently being studied. Typical SCWR coolant operating parameters are 25 MPa and 350 – 625°C. These SCWR operating conditions significantly increase the thermal efficiency of current NPPs from 33 – 35% to approximately 45 – 50%. Additionally, use of SCW as a reactor coolant supports hydrogen co-generation through thermal-chemical cycles due to relatively high outlet temperatures of the reactor coolant (Naterer et al., 2010, 2009).

The benefits of SCWRs are: 1) improved thermal efficiency; 2) decreased operational and capital costs, thus reduced overall electrical energy cost; and 3) co-generation of hydrogen. A drawback is determining, which fuel channel-materials are suited for these elevated reactor-coolant operationing parameters. This research describes mainly a preliminary material (nuclear fuel) study focusing on the thermal aspects of SCWR fuel-channel design.

1.2 SuperCritical Water-cooled nuclear Reactors

This fuel-channel analysis provides a potential configuration of an SCWR. This particular Generation IV reactor is in its conceptual design phase. It is currently undergoing research and development activities; a prototype has yet to be built. The benefit of conceptual plant design is the ability to interchange and conduct analysis of

various equipment combinations. This paper discusses a selection of nuclear fuels, sheath materials, sheath geometries, and steam cycles suitable for SCWRs.

1.3 Reactor Core Configurations

There are two basic SCW reactors' design options: 1) Pressure-Vessel (PV) type and 2) Pressure-Channel (PCh) or Pressure-Tube (PT) type. The PV-type SCWR uses a large pressure vessel to contain the fuelling assembly analogous to conventional Pressurized light-Water Reactors (PWRs) and Boiling light-Water Reactors (BWRs). This SCWR core concept is developed to a large extent in USA, EU, Japan, Korea and China (Pioro & Duffey, 2007). A PV-type SCWR is depicted in Figure 1.6.

The PT-type SCWR core configuration is similar to general Pressurized Heavy Water Reactors (PHWRs). The PT-type SCWR concepts are currently being develop by Atomic Energy of Canada Limited (AECL, Canada) and Research and Development Institute of Power Engineering (RDIPE, Russia) (Duffey et al., 2008a).

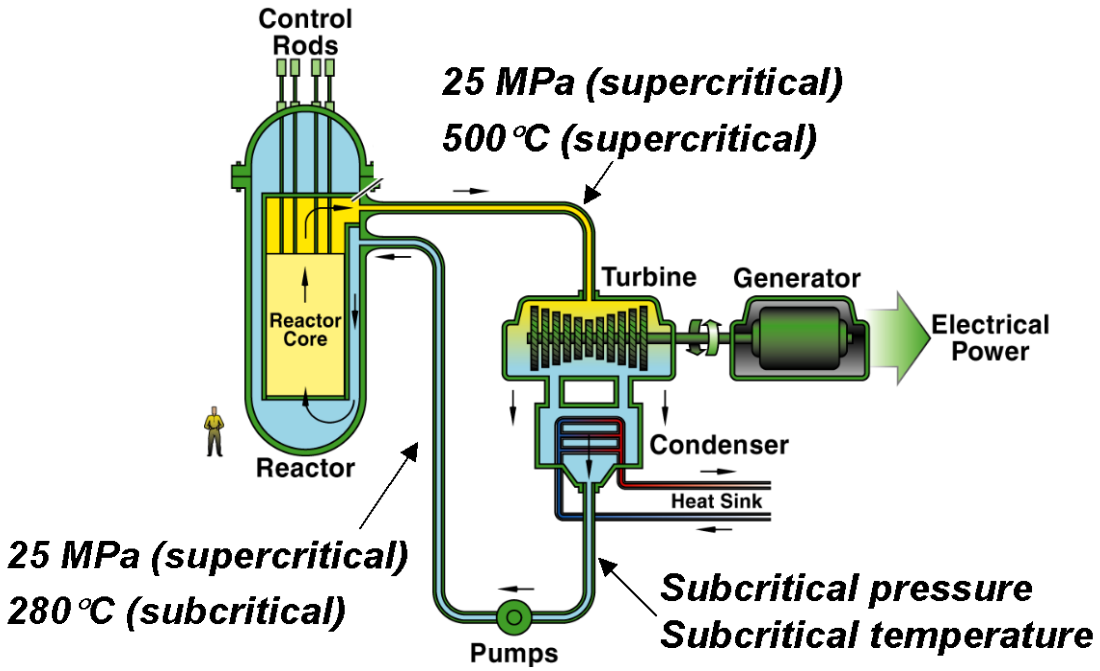

Figure 1.6. PV-type SCWR (DOE & GIF, 2002).

A potential SCWR plant layout is shown in Figure 1.7. This unit has several output features that compliment electrical generation. SCWRs may also produce industrial isotopes, process heat to support hydrogen cogeneration and the desalination of potable water. PT-type SCWR specifications from Russia and Canada are listed in Table 1.2.

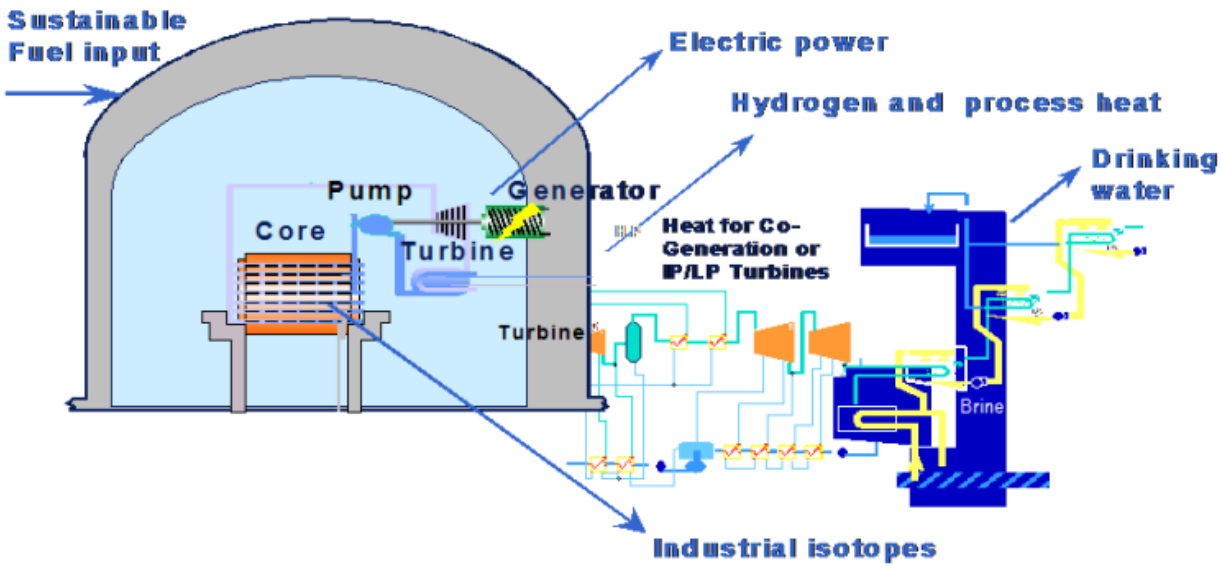

Figure 1.7. General concept of pressure-tube SCW CANDU Reactor (Intermediate-Pressure (IP) turbine, and Low-Pressure (LP) turbine) (Pioro & Duffey, 2007).

Parameters of an SCW CANadian Deuterium Uranium nuclear reactor (CANDU®) were used in the present heat -transfer calculations to determine suitable fuel-channel designs. The PT-type reactor was selected as a basic unit due to its higher flexibility to flow, flux and density changes, as opposed to the PV-type SCWR.

Table 1.2. Modern concepts of PT-type nuclear reactors cooled with SCW.

Parameters	Unit	SCW CANDU®	ChUWR
Reference	–	(Khartabil et al., 2005)	(Pioro et al., 2007)
Country	–	Canada	Russia
Organization	–	AECL	Kurchatov Institute
Reactor spectrum	–	Thermal	Thermal
Power - thermal	MW	2540	2730
Power - electrical	MW	1220	1200
Thermal efficiency	%	48	44
Pressure	MPa	25	24.5
T_{in} coolant	ºC	350	270
T_{out} coolant	ºC	625	545
Flow rate	kg/s	1300	1020
Core height	m	–	6
Core diameter	m	~4	11.8
Fuel	–	UO_2/Th	UCG
Enrichment	% wt.	4	4.4
Cladding material	–	Ni alloy	SS
# of fuel bundles	–	300	1693
# of fuel rods in bundle	–	43	10
D_{rod}/δ_w	mm/mm	11.5 and 13.5*	10/1
T_{max} cladding	ºC	<850	700
Moderator	–	D_2O	D_2O

* For a 43-element bundle.

A current PT-type fuel channel, for example, a CANDU nuclear-reactor fuel channel; the fuel sheath, pressure tube and calandria tube are composed of zirconium based alloys (for details, see Figure 1.8). Zirconium cannot be used at SCWR conditions since between 350 – 450°C the corrosion rates increase drastically (Duffey & Hedges, 1999).

Sheath (clad) materials being examined for these harsh SCW conditions include Inconel-600, Inconel-718 and Stainless Steel (SS-304). The basis for this thermal-hydraulic study of fuel-channel design options is to ensure the fuel centreline temperature does not exceed the industry accepted limit of 1850°C, and the sheath temperature does not exceed the design limit of 850°C.

SCW NPPs will have much higher coolant operating parameters in comparison to those of current NPPs. These operating parameters require research of alternative sheath material and fuel configurations to ensure safe and reliable operation of SCWRs. Therefore, further research is needed before an SCWR fuel-channel design can be finalized and implemented. A proposed SCWR fuel channel is shown in Figure 1.9. The function of the ceramic insulator is to decrease heat losses from SCW to the moderator. The liner or flow tube was added to protect the ceramic insulator from mechanical impact from the bundles. However, for the presented calculations only the fuel, sheath and pressure tube are incorporated into the model.

1.4 Research Scope

The previous study (Pioro et al., 2008) was performed to assess the feasibility of uranium dioxide (UO_2) at SCWR conditions. A generic 43-element fuel bundle with UO_2 fuel was analyzed. However, this study considered only preliminary steady-state heat-transfer calculations with a uniform Axial Heat Flux Profile (AHFP) and an average fuel thermal conductivity. This study has shown that the UO_2 fuel centreline temperature might exceed the industry accepted limit.

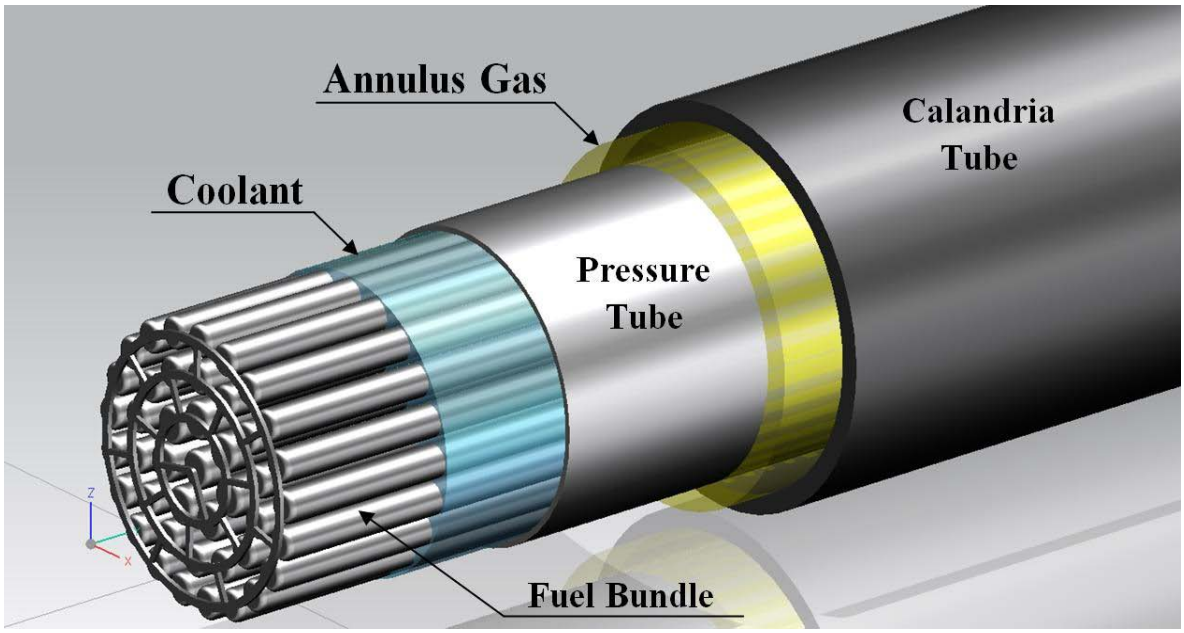

Figure 1.8. Current CANDU-reactor fuel channel design (figure is courtesy of W. Peiman, UOIT).

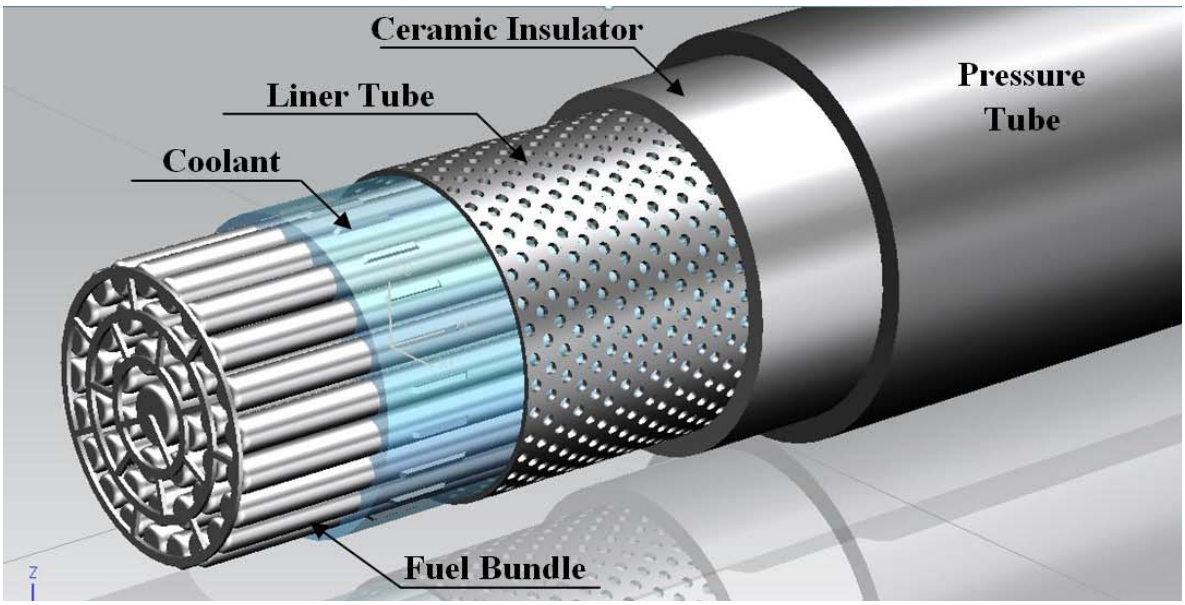

Figure 1.9. SCWR CANDU-reactor fuel channel design (figure is courtesy of W. Peiman, UOIT).

Therefore, the present work is dedicated to more representative PT-type nuclear-reactor AHFPs, such as cosine, upstream-skewed and downstream-skewed cosine profiles. These non-uniform AHFPs are representative of various online fuelling activities and actually, envelop the extreme cases. Additionally, the effect of the temperature on thermal conductivities of sheath materials and nuclear fuels were accounted for in calculations.

This research provides a thermal-hydraulic analysis of a single PT-type fuel channel cooled with light SCW with an inlet temperature of 350°C, an outlet temperature of 625°C, at a constant pressure of 25 MPa, a mass flow rate of 4.4 kg/s and an average channel-power output of 8.5 MW_{th}.

This revised bundle design has been updated to include a large central unheated element with an Outer Diameter (OD) of 20 mm. This central rod is anticipated to be filled with a neutron poison. This revised design will increase safety by suppressing the positive reactivity swing in the event of a Loss Of Coolant Accident (LOCA). The sheath material options are all non-zirconium based alloys to avoid undesired high corrosion rates at the SCW conditions. A sheath material will be deemed acceptable if the maximum temperature remains below the design limit of 850°C.

Several nuclear fuels were analyzed to determine all the potential heat sources for this futuristic reactor cooled with SCW. A fuel is deemed acceptable if the fuel centreline temperature remains below the industry accepted limit of 1850°C. The bulk-fluid, outer-sheath and fuel centreline temperature profiles together with the Heat Transfer Coefficient (HTC) profile were plotted for each nuclear fuel at all AHFPS along the heated length of the fuel channel.

2 SUPERCRITICAL WATER

2.1 Thermophysical-Properties Profiles

One of the distinctive design features of a SCWR is the thermophysical properties of the coolant. The light water reaches supercritical conditions, which means the presence of a single-phase flow only. Therefore, the dryout will not occurs, because this phenomena is related only to two-phase flow.

The pseudocritical point, which is characterized with T_{pc}, is a point at a pressure above the critical pressure and at a temperature corresponding to the maximum value of specific heat at this particular pressure (Figure 2.1) (Pioro & Duffey, 2007). For water at 25 MPa the pseudocritical temperature is 384.9°C (Table 2.1).

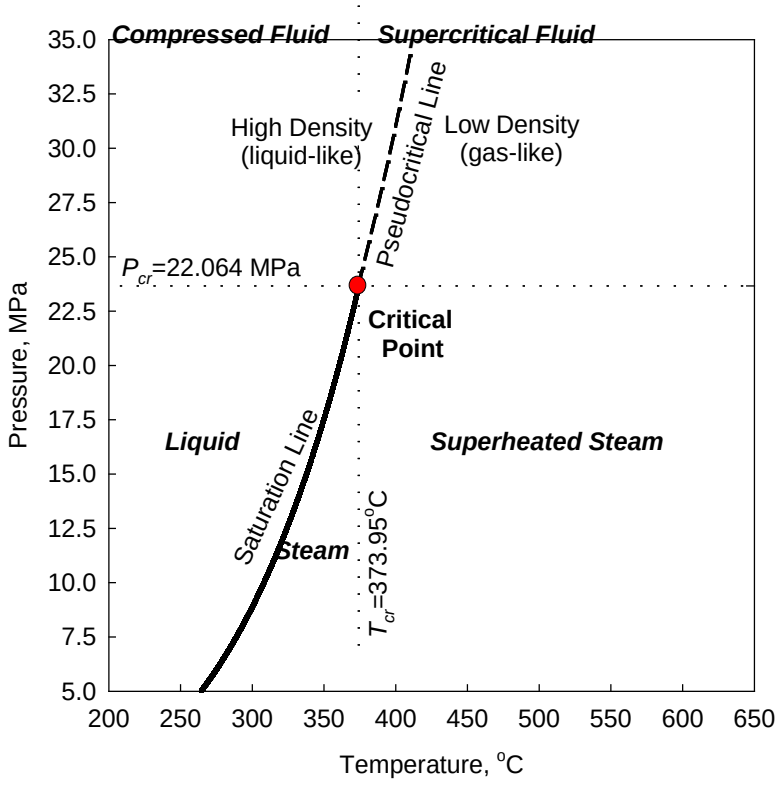

Figure 2.1. Pressure-temperature diagram for water.

Table 2.1. Values of pseudocritical temperature and corresponding peak values of specific heat.

Pressure, MPa	Pseudocritical temperature, °C	Peak value of specific heat, kJ/kg·K
23	377.5	284.3
24	381.2	121.9
25	384.9	76.4
26	388.5	55.7
27	392.0	43.9
28	395.4	36.3
29	398.7	30.9
30	401.9	27.0
31	405.0	24.1
32	408.1	21.7
33	411.0	19.9
34	413.9	18.4
35	416.7	17.2

Figure 2.2 shows thermophysical-property profiles (calculations were performed based on National Institute of Standards and Technology (NIST) software (Lemmon et al., 2007) of the light-water coolant along the heated-channel length for cosine AHFP. All thermophysical properties undergo significant changes within the PseudoCritical (PC) region (±25°C). This statement applies also to all presented AHFPs. The only difference is that the PC-point location along the bundle-string heated length will depend on the particular AHFP.

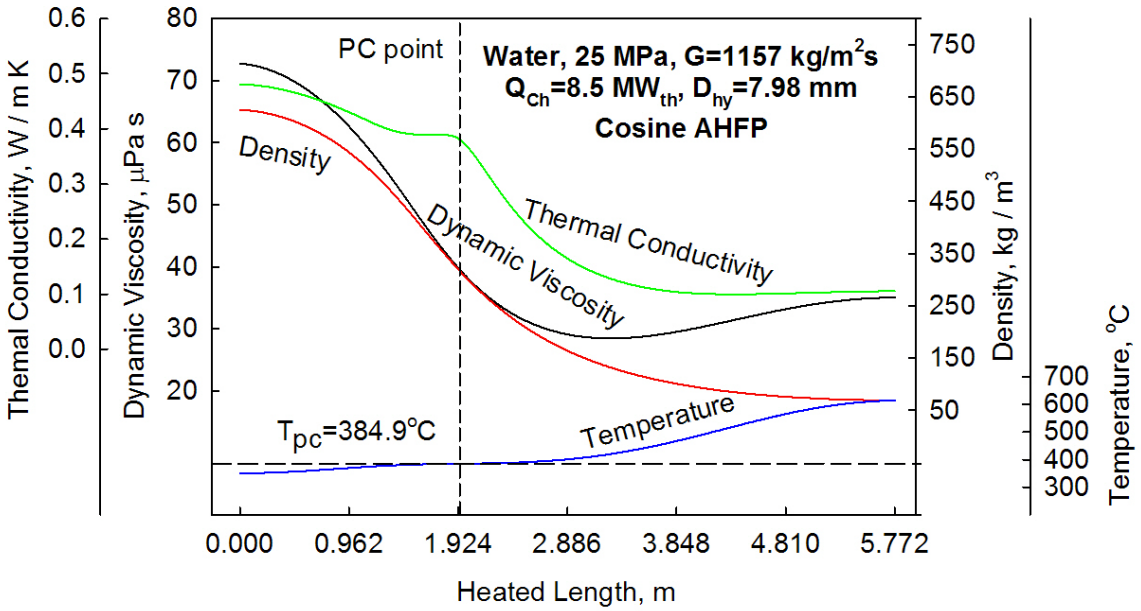

Figure 2.2. Profiles of thermal conductivity, density, dynamic viscosity and bulk-fluid temperature along heated length of fuel channel for cosine AHFP.

The average specific heat, average Prandtl number and density ratio (see Figure 2.3 and Figure 2.4) were used in the Bishop et al. (1964) correlation. These values represent are cross-section averaged of the bulk fluid. The average Prandtl number ($\overline{\mathbf{Pr}}$) and the corresponding average-specific-heat capacity ($\overline{c_p}$) are used in HTC calculations to compute the realistic HTC profile considering both properties at the bulk-fluid temperature and the wall. The Prandtl number ($\mathbf{Pr}$) and specific-heat capacity (c_p) provide an overestimation of HTC within the PC region and does not correspond by magnitude to that of $\overline{\mathbf{Pr}}$ and $\overline{c_p}$.

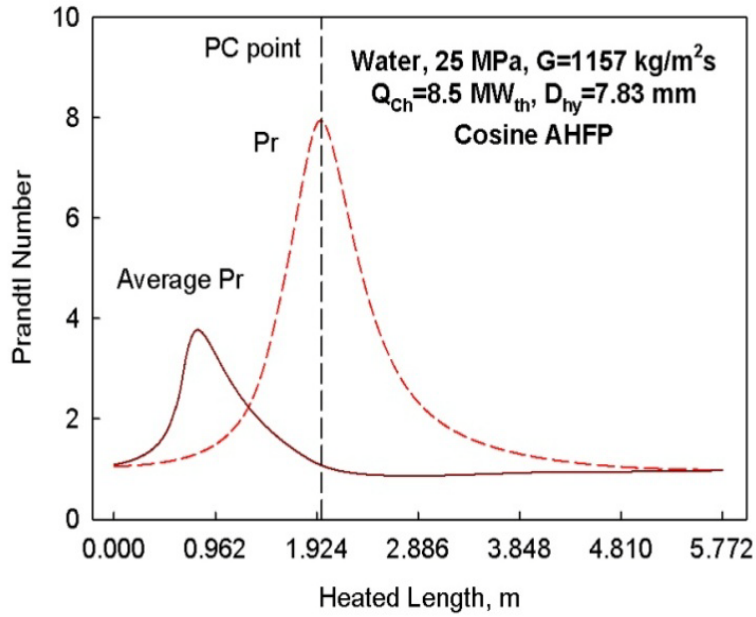

Figure 2.3. Bulk-fluid specific-heat capacity and average specific-heat capacity along heated length with cosine AHFP.

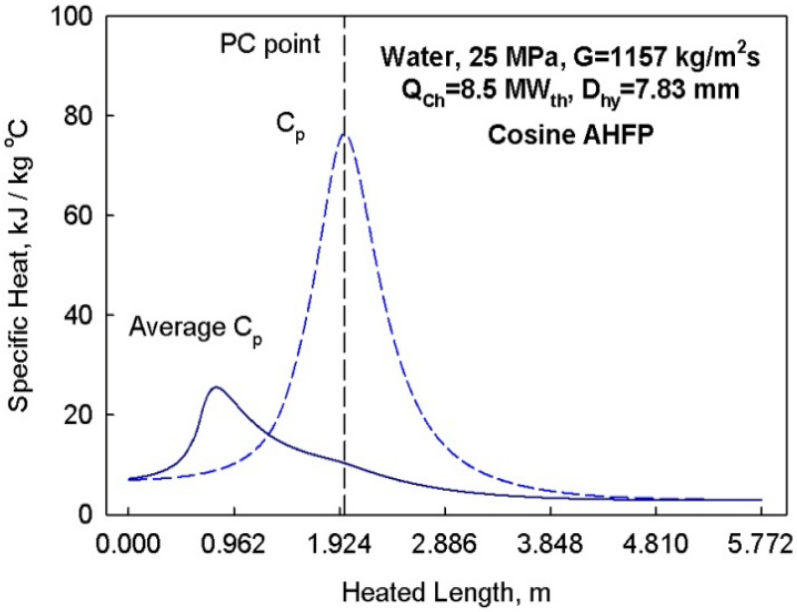

Figure 2.4. Bulk-fluid Prandtl number and average Prandtl number along heated length with cosine AHFP.

2.2 Steam Cycles

Possible steam cycles are discussed in this section for completeness of an SCWR plant layout. A study has been performed by Pioro et al. (2010) to determine if an SCWR can be designed with steam-cycle arrangements similar to those of modern SuperCritical (SC) fossil-fired plants including their SC-turbine technology. All of the steam-cycles arrangements considered were based on the Rankine cycle. From the study performed on the thermodynamic-cycle options, it was determined that the majority of the modern SC turbines are of a single-reheat type. Only a few double-reheat-cycle SC turbines have been manufactured and put into operation.

The reactor coolant is light SCW and is able to operate with a direct steam cycle to maximize thermal efficiency (Pioro et al., 2010). As a result, indirect and dual cycles are not considered in this thesis. The direct steam cycle has the option of steam no-reheat, single-reheat or double-reheat as the SCW cascades through the turbine series. It is assumed that a regenerative cycle is utilized regardless of the reheat arrangement. A regenerative cycle implies the feedwater temperature is increased by the use of steam extracted from various turbines exhausts. Furthermore, heat regeneration improves cycle efficiently and feedwater quality by removal of entrapped air and non-condensable gases.

The potential thermodynamic-cycle options for direct cycle SCWRs are with no-reheat, single-reheat and double-reheat (Pioro et al., 2010). Direct cycles are permitted due to the increased coolant parameters (elevated temperatures and pressures). Supercritical water does not require the use of steam generators and steam dryers, etc. In the no-reheat cycle SCW exits fuel channels and flows directly into the turbine. The single-reheat cycle is achieved by using Steam-ReHeat (SRH) channels or using a Moisture-Separator-Reheater (MSR).

Advantages of the single-reheat cycle include: higher thermal efficiency (45 – 50%), higher reliability through proven state-of-the-art SC-turbine technology, and reduced development cost due to the simplified design (Pioro et al., 2010). The largest disadvantage in implementing the single-reheat cycle via SRH channels in SCW NPPs

would be that significant changes in a reactor-core design because of the addition of the nuclear steam reheat at a lower pressure.

The flow path the no-reheat direct steam cycle is: once the SCW exits the fuel channels it enters and flows directly through the turbine cylinders (high-pressure cylinder, intermediate cylinder and low pressure cylinder(s)) (Pioro et al., 2010). The disadvantages of the no-reheat cycle is slightly decreased thermal efficiency compared to that of single-reheat cycle (by approximately 1 – 2%) and high moisture content in the low-pressure turbine exhaust.

The single-reheat steam scheme is suitable for use with SRH channels or with a MSR (Pioro et al., 2010). For the SRH-channel option, the high-pressure turbine exhaust steam re-enters the reactor within specialized channels devoted to reheating the steam. Re-entrance channels can be used as SRH channels. Currently, this channel design is in the conceptual design stage (for details see (Samuel et al., 2010)). Alternatively, the steam reheat can be accomplished outside the reactor with an MSR as shown in Figure 2.5. The MSR is located between the intermediate and low-pressure turbines and is heated via intermediate-turbine exhaust.

The double-reheat cycle offers the highest thermal efficiency, but the design and capital costs increase substantially (Pioro et al., 2010). Its main benefits compared to that of the single-reheat steam cycle are an increased thermal efficiency. In the current analysis, the direct single-reheat steam cycle with MSR applied is used.

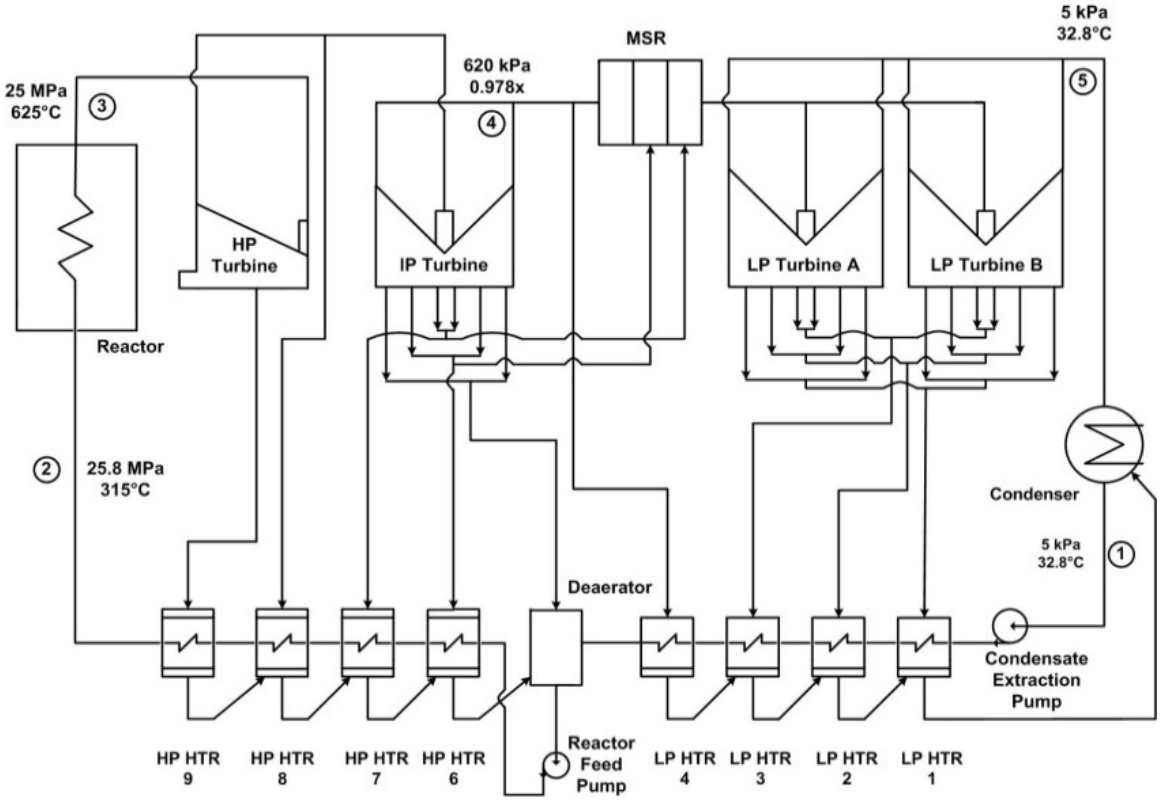

Figure 2.5. SCW NPP single-reheat cycle with MSR (Pioro et al., 2010).

2.3 Heat Transfer Coefficient

A generic SCWR fuel channel analyzed in the presented work is cooled with light water at supercritical pressures and temperatures. HTC correlations for SCW flowing through fuel bundles of power reactors have not been developed yet. Therefore, a renowned HTC correlation Bishop et al. (1964) for flow in bare vertical tubes was modified to suit flow through horizontal channels.

The Bishop et al. correlation (Equation (2.1)) is suitable for pressures from 22.8 to 27.6 MPa, bulk-fluid temperatures between 282 and 527°C, and heat fluxes between 0.31and 3.46 MW/m² (Bishop et al., 1964):

$$\mathbf{Nu}_x = 0.0069\mathbf{Re}_x^{0.9}\overline{\mathbf{Pr}_x}^{0.66}\left(\frac{\rho_w}{\rho_b}\right)_x^{0.43}\left(1 + 2.4\frac{D}{x}\right) \quad (2.1)$$

Although the coolant temperature at the channel exit is anticipated to be 625°C, which is above the upper temperature limit of 527°C for the Bishop et al. correlation; it was deemed the most appropriate empirical correlation based on the present literature survey. The remaining parameters correspond to the generic SCWR operating conditions.

The use of the Bishop et al. correlation is a conservative approach, because this correlation was obtained in bare tubes, but the HTC in bundles will be enhanced with flow turbulization from various appendages (endplates, bearing pads, spacers, etc.). Also, the original Bishop et al. correlation was modified to suit better bundle-flow conditions. Actually, the last term in Equation (2.1), which is responsible for the inlet effect in bare tubes, was eliminated in Equation (2.2) because of significant flow turbulization with endplates.

$$\mathbf{Nu}_x = 0.0069\mathbf{Re}_x^{0.9}\overline{\mathbf{Pr}_x}^{0.66}\left(\frac{\rho_w}{\rho_b}\right)_x^{0.43} \quad (2.2)$$

The most recent SCW HTC correlation for vertical bare tubes was developed by Mokry et al. (2009):

$$\mathbf{Nu}_x = 0.0061\mathbf{Re}_x^{0.904}\overline{\mathbf{Pr}_x}^{0.684}\left(\frac{\rho_w}{\rho_b}\right)_x^{0.564} \quad (2.3)$$

The experimental dataset used for the developing the Mokry et al. correlation was obtained in SCW flowing upward in a vertical bare tube. The applicable operating range of Equation (2.3) is: pressures of about 24 MPa, inlet temperatures from 320 – 350°C,

values of mass flux from 200 – 1500 kg/m^{2}s and heat fluxes up to 1250 kW/m^2. This operational range is also applicable to the proposed generic PT-type SCWR operating conditions, because this correlation was not fully verified within other data sets, it was decided to use well-known in the current calculations.

In general, three heat-transfer regimes exist supercritical pressure (for details see Glossary and Figure 2.6. However, only Normal Heat Transfer (NHT) and Improved Heat Transfer (NHT) regimes will be considered in the current thesis.

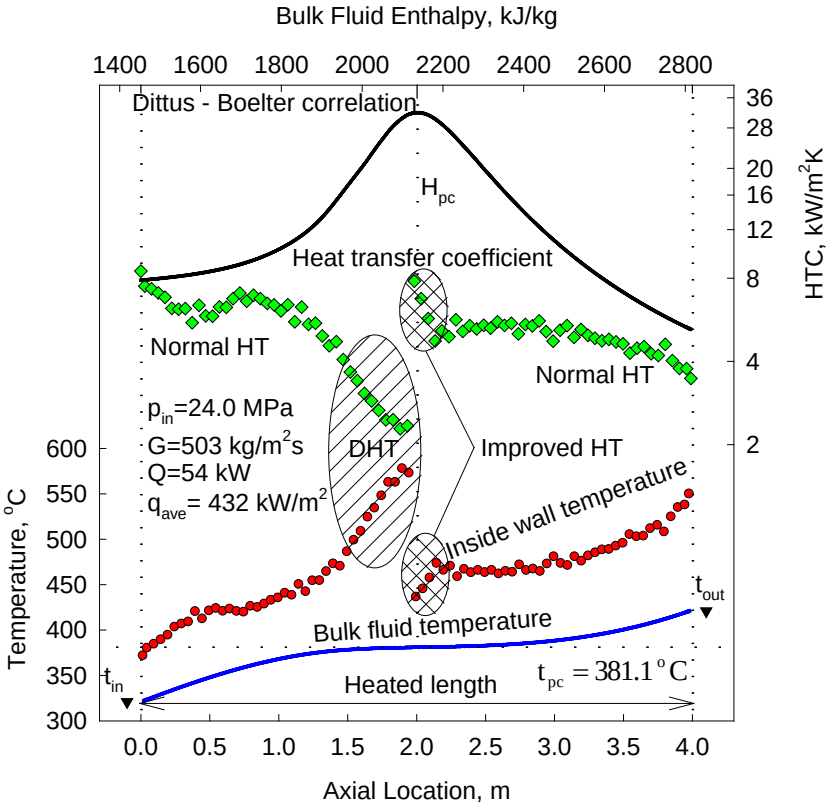

Figure 2.6. Temperature and heat transfer coefficient profiles along heated length of vertical circular tube (data by Kirillov et al., 2007): Water, inside diameter 10 mm and heated length 4 m.

3 FUEL-BUNDLE DESIGN ELEMENTS

3.1 Fuel-Bundle Geometry

Initially, four existing bundle geometries were chosen (one 37-element design and three 43-element designs) as shown in Figure 3.1. The newest AECL bundle design with the large diameter centre rod, so-called Variant-20 bundle described in Leung, (2008) was used in current analysis (Figure 3.1d). The fuel-bundle string consists of 12 Variant 20 bundles with a heated length of 5.772 m. The central rod has an Outer Diameter (OD) of 20 mm and is assumed to be unheated. The remaining 42 elements have the OD of 11.5 mm (Figure 3.1d). The hydraulic-equivalent diameter of the bundle is 7.83 mm. In general, Variant-20 and Variant-28 bundles have approximately the same hydraulic-equivalent diameter. Therefore, the current will be applicable to both of these bundles.

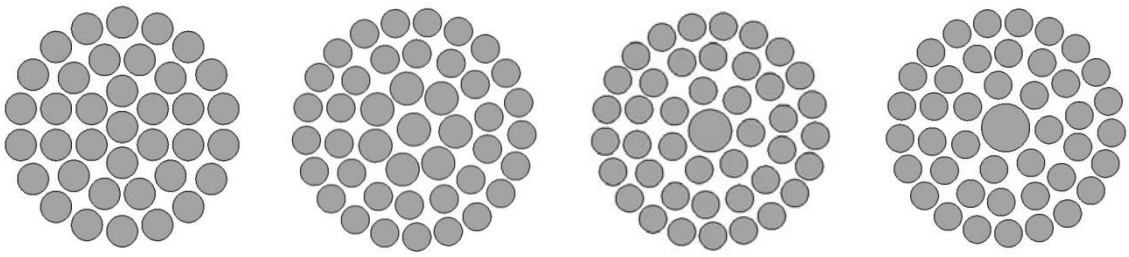

(a) **(b)** **(c)** **(d)**

Figure 3.1. Comparison of fuel-bundle geometries: (a) 37 elements (OD 13.5 mm), (b) 43 elements, centre & inner ring elements with OD 13.5 mm and intermediate OD elements with OD 11.5 mm, (c) 43 elements, Variant-18, centre element OD 18 mm and the rest – 11.5 mm (d) 43 elements, Variant-20, centre element OD 20 mm and the rest – 11.5 mm (based on paper by Leung (2008) (Grande et al., 2010a).

3.2 Sheath Material

An SCWR sheath material should withstand temperatures up to the design limit, defined as 850°C (Chow & Khartabil, 2007). Ideal sheath materials should have high corrosion resistance, neutron economy, mechanical strength, and thermal conductivity. In the current nuclear-power reactors the primary choice for sheath material is zirconium alloy due to its high mechanical strength, excellent neutron transparency and proven performance within a reactor core.

However, when zirconium alloys reach 500°C, the corrosion rate increases significantly (Duffey & Hedges, 1999). For this reason, zirconium alloys are unacceptable as the sheath material in SCWRs, because the channel outlet temperature can reach 625°C

Alternative-sheath material options can be: Inconel-600, Inconel-718 and stainless steel (SS-304). The Inconels are non-magnetic nickel-based high-temperature alloys with high mechanical strength, hot and cold workability, and good corrosion resistance (Blumm et al., 2005). SS-304 also has high corrosion resistance, however its mechanical strength is significantly lower than that of Inconels. Table 3.1 lists the content of the selected Inconel's and SS-304.

Figure 3.2 shows changes in thermal conductivity of Zircaloy-2, SS-304, Inconel-600 and Inconel-718. The figure shows within the expected temperature conditions (600°C – 800°C) SS-304 and Zircaloy-2 have non-linear thermal conductivities. However, the Inconels have nearly linear thermal-conductivity profiles. Inconel-600 has the highest thermal conductivity compared to other alloys within the anticipated SCWR operating range.

Despite the benefits of Inconel alloys, some of them might not be suitable for the SCWR conditions. Young's Modulus of Elasticity is a measure of the stiffness of material that is used to determine the minimum sheath thickness (described in details in the next section). This property is proportional to the mechanical strength. Young's Modulus of Elasticity for the candidate sheath materials are shown in Figure 3.3. At temperatures above 750°C, Inconel-718 exhibits a significant decrease in its yield stress and tensile strength

(Leshock et al., 2001). Inconel-600 has the largest Modulus of Elasticity values compared to those of other sheath material options.

In terms of neutron economy, Inconels have quite high content of nickel, which requires higher fuel enrichment due to significant absorption of thermal neutrons by nickel (Table 3.2).

Table 3.1. Inconel-600, Inconel-718 and SS-304 Content (Matweb).

Material	Inconel 600 % (wt)	Inconel 718 % (wt)	SS-304 % (wt)
Al	0.0	0.5	0
C	0.10	0.02	0.08
Cr	14.0 – 17.0	19	18.0 – 20.0
Cu	0.50	0.0	0
Fe	6.0 – 10.0	17	66.4 – 74.0
Mn	1.0	0.0	2.0
Mo	0.0	3.1	0
Nb	0.0	5.2	0
Ni	72.0 (min)	54	8.0 – 10.5
S	0.015	0.0	0.03
Si	0.50	0.0	1.0
Ti	0.0	0.9	0

*Note: some zero values vary up to 0.9% to balance the alloys.

Table 3.2. Absorptions and scattering cross sections for thermal neutrons (Lamarsh & Baratta, 2001).

Material	Absorption Cross Section, barns	Scattering Cross Section, barns
Chromium	3.10	3.80
Iron	2.55	10.9
Nickel	**4.43**	**17.3**
Zirconium	**0.185**	6.40

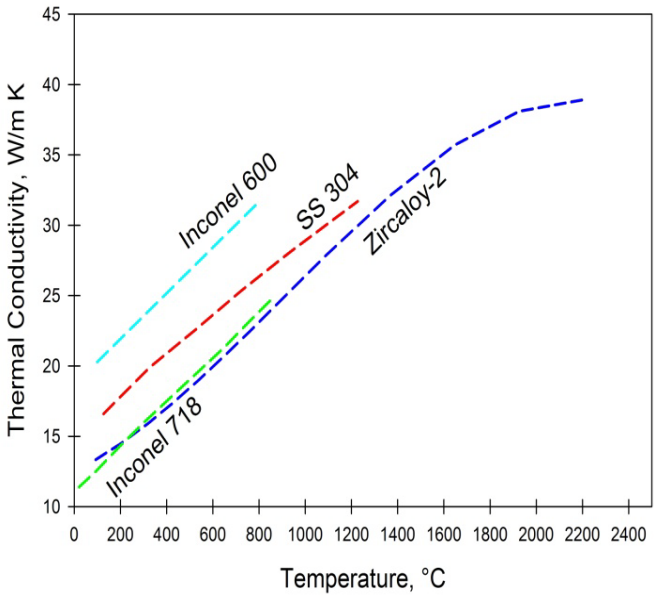

Figure 3.2. Thermal conductivity vs. temperature for Inconel-600 (Matweb), SS-304 (Incorpera et al., 2007), and Inconel-718 (Matweb) and Zircaloy-2 (Lamarsh & Baratta, 2001).

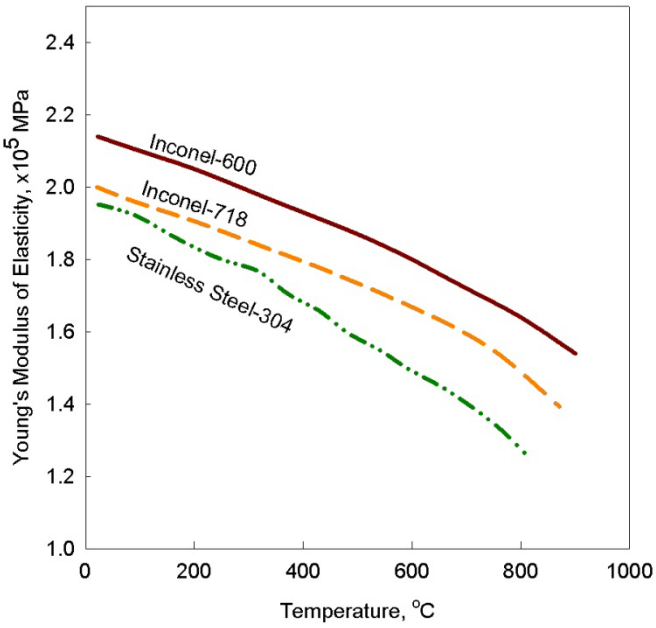

Figure 3.3. Young's Modulus of Elasticity for Inconel-600 (Matweb), Inconel-718 (Matweb) and SS-304 (British Stainless Steel Association).

Based on the abovementioned Inconel-600 was chosen as the best sheath material for SCWR applications. Its thermal conductivity can be calculated through Equation (3.1) (Special Metals, n.d.):

$$k = 14.2214 + 0.01625\,T \tag{3.1}$$

where T is the temperature in Kelvin.

3.3 Sheath Thickness Determination

The required sheath thickness was unknown for all sheath-material options, thus pertinent calculations were performed. The objective is to determine the minimum sheath thickness capable to withstand the SCW coolant pressure of 25 MPa to prevent collapsing. The crush- or collapse-pressure formula (Equation 3.2) was used in order to

calculate the minimum wall thickness capable to withstand the known maximum external pressure:

$$P_{cr} = \frac{2E}{(1-\nu^2)}\left(\frac{\delta}{D_o}\right)^3 \tag{3.2}$$

where P_{cr} is the crush pressure in MPa, E is the modulus of elasticity in MPa, ν is the Poisson's ratio, D_o is the sheath OD in mm, and δ is the minimum wall thickness of the sheath material in mm. For the chosen Variant-20 bundle the central element OD is 20 mm and the OD of the rest of the elements is 11.5 mm. Equation (3.2) is dependent on temperature since the Modulus of Elasticity and Poisson's ratio varies with temperature (Figure 3.3 and Table 3.3). The Equation (3.2) is applicable when Equation (3.3) holds:

$$l > 1.7324 D_o \sqrt{\frac{D_o}{\delta}} \tag{3.3}$$

where l is the heated length per bundle (481 mm).

Equation (3.2) is rearranged to solve for the minimum wall thickness of the sheath material as shown in Equation (3.4). The data used for the sheath-thickness determination data are shown in Table (3.3).

$$\delta = D_o \sqrt[3]{P_{cr}\frac{(1-\nu^2)}{2E}} \tag{3.4}$$

Table 3.3. Sheath thickness calculation data (Inconels (Matweb) and SS-304 (British Stainless Steel Association)).

Material	Temperature, °C	Young's Modulus, MPa	Poisson's Ratio
Inconel-600	22	214000	0.324
	100	210000	0.319
	200	205000	0.314
	300	199000	0.306
	400	193000	0.301
	500	187000	0.300
	600	180000	0.301
	700	172000	0.305
	800	164000	0.320
Inconel-718	21	199948	0.293
	93	195811	0.288
	204	190295	0.280
	316	184090	0.272
	427	177885	0.271
	538	170990	0.271
	649	163406	0.283
	760	153753	0.306
	871	139274	0.331
SS-304	25	19900	0.300
	90	19600	0.300
	150	19100	0.280
	260	18300	0.300
	370	17400	0.320
	480	16300	0.280
	590	15300	0.290
	700	14300	0.280
	820	12700	0.250

The sheath-thickness calculation at 22°C for Inconel-600 fuel bundle for inner, middle and outer ring elements with the OD of 11.5 mm are shown below.

$$\delta = 11.5\ mm \sqrt[3]{25\ MPa \frac{(1-0.324^2)}{2(214000\ MPa)}} \tag{3.4}$$

$\delta = 0.430\ mm$ (Table 3.4)

$$481\ mm > 1.7324(11.5\ mm)\sqrt{\frac{11.5\ mm}{0.430\ mm}} \tag{3.3}$$

$481\ mm > 103\ mm$ holds true

The collapse-pressure calculations were performed at a pressure of 25 MPa and various temperatures for Inconel-600, Inconel-718 and SS-304 (Table 3.4). Variations of minimum sheath thickness for Inconels are shown in Figure 3.4. In the current preliminary calculations the minimum sheath thickness of Inconel-600 at the room temperature was used. In general, increasing the minimum-thichness value from 0.430 mm to 0.470 mm will not affect significantly the temperature difference through the sheath.

Table 3.4. The minimum sheath thickness for Inconel-600, Inconel-718 and SS-304 at room temperature at 25 MPa.

Sheath Material	Centre Element Minimum Sheath Thickness, mm	Inner, Middle, Outer Element Minimum Sheath Thickness, mm
Inconel-600	0.748	0.430
Inconel-718	0.770	0.443
Stainless Steel-304	0.777	0.447

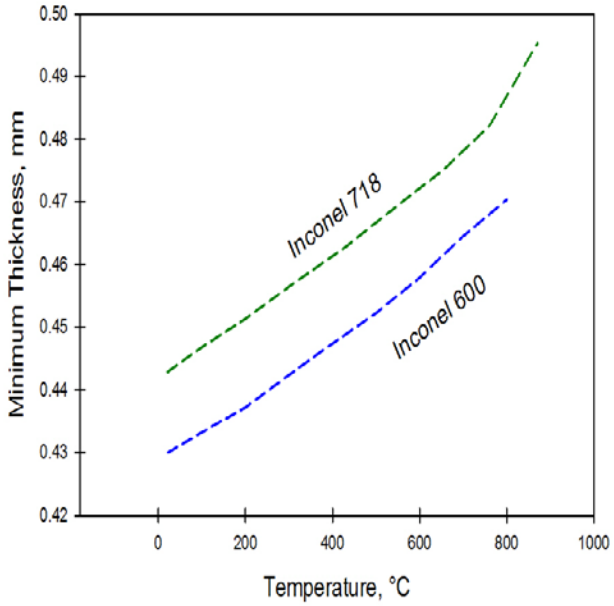

Figure 3.4. The minimum sheath thickness of sheath at different temperatures for Inconel's at 25 MPa.

The design limit of 850°C as the maximum sheath temperature was proposed by Chow and Khartabil (2007). This limit was developed as one of the preliminary specifications for the SCW CANDU nuclear reactor.

3.4 Contact Resistance

The contact resistance between a fuel pellet and sheath has minimal effect on the sheath temperature and therefore, was not considered in the analysis. It is known that the contact thermal resistance between a pellet and inner sheath in a 37 element bundle is about 65.0 kW/m K (Chan et al., 1999). Chan et al., corresponds to a temperature difference of about 15°C.

4 NUCLEAR FUEL OPTIONS

4.1 Uranium dioxide

The conventional nuclear fuel is UO_2, because it has a wealth of operational data and well defined thermalphysical properties. Previously, the UO_2 fuel centreline temperature was analyzed by Pioro et al. (2008) at the SCWR normal operating conditions (Figure 4.1). They have found at the channel outlet, the fuel centreline temperature may exceed the industry accepted limit of 1850°C. Therefore, this result promoted the current investigation in which alternative fuels have been studied.

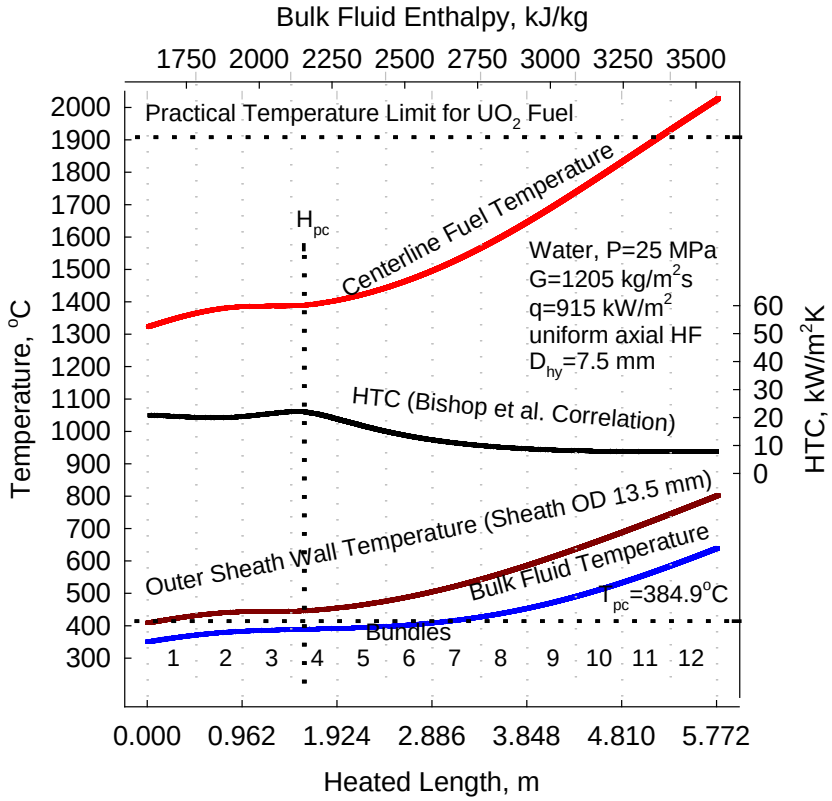

Figure 4.1. Temperature and HTC profiles for UO_2 fuel with constant thermal conductivity along the heated length with uniform AHFP (Pioro et al., 2008).

In general, thermal conductivity of the UO_2 fuel is affected by density changes, methods of manufacturing, neutron fluxes etc. as shown in Figure 4.2. Also, various literature sources might provide quite different thermal-conductivity values and trends. However, all sources showed that the UO_2 thermal conductivity is quite low, and it decreases with temperature increase. Around 1750ºC the UO_2 thermal conductivity has a minimum value close to 2 W/m K.

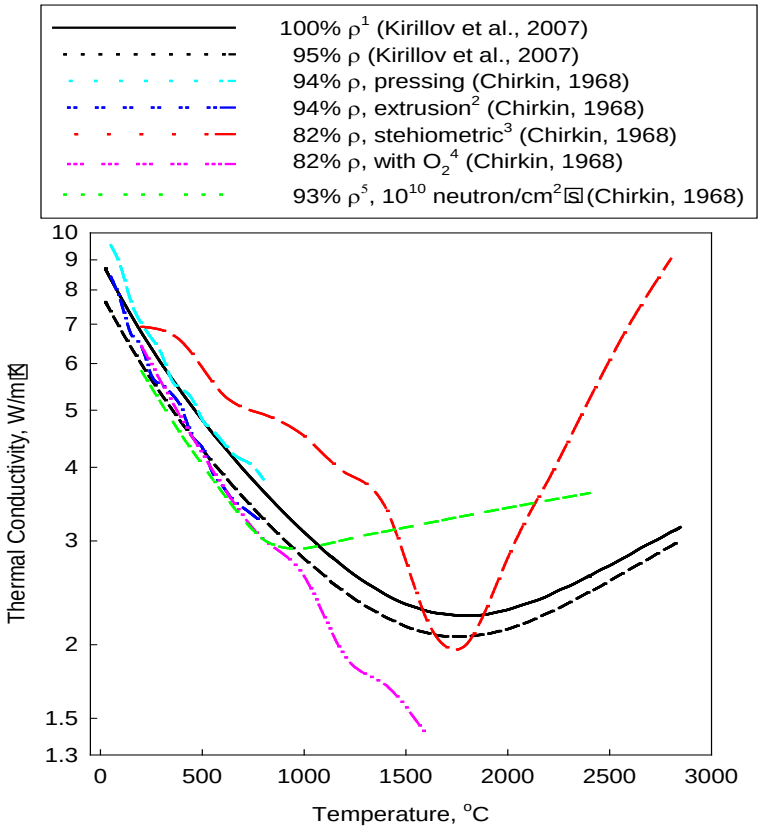

Figure 4.2. Comparison of thermal conductivities of uranium dioxide for various densities, methods of manufacturing fuel and influence of neutron flux: 1 – ρ=10,960 kg/m^3; 2 – extrusion of a rod and sintering; 3 – stehiometric composition; 4 – fine grained with excess of oxygen; 5 – under the influence of neutron flux, samples in the form of cylinder (OD 14 mm) (measurements performed inside a reactor).

Because of the high fuel centreline temperature of UO_2 fuel at the channel outlet in the previous study (Pioro et al, 2008). Alternate nuclear fuels with higher thermal conductivities (Figure 4.3) have to be considered for SCWR applications.

4.2 Alternative Fuels

A variety of nuclear fuels were analysed at the SCWR normal operating conditions. A fuel was deemed to be suitable if the fuel centreline temperature remained below the industry accepted limit of 1850°C. The following non-conventional/alternative fuels have been considered: Mixed OXide (MOX), Thoria (ThO_2), uranium dicarbide (UC_2), uranium nitride (UN), and uranium carbide (UC).

The most important thermophysical parameter in terms of affecting the fuel centreline temperature is the fuel thermal conductivity. The thermal-conductivity profiles of the various are fuels shown in Figure 4.3. In general, estimation of thermal conductivities of nuclear fuels is a complex task, where high uncertainty is expected (as shown in Figure 4.2 and Figure 4.5). Average thermalphysical properties of the alternative fuels are listed in Table 4.1. There are many parameters such as temperature, density, porosity, stoichiometric composition, method of manufacturing as well as burn-up rates that can affect the thermal conductivity of any potential fuel (Kirillov et al., 2007).

Thermal conductivities that increase with the temperature increase are more preferable then the opposite trend because they are responsible for better heat conduction through the fuel pellet. to dissipate the heat faster to decrease fuel-centreline temperature. However, the fuels with these desired trends such as, UC, UN and UC_2 (for details, see Figure 4.3), require extensive testing in terms of their compatibility with SCW. Also such properties as gas release, cracking, swelling, etc. are not well known these alternative fuels within a wide range of temperatures and other conditions (neutron flux, fuel aging and etc.). However, for conventional fuels such as UO2, MOX and ThO_2, such properties are more or less known (IAEA, 2000) and (IAEA, 2003).

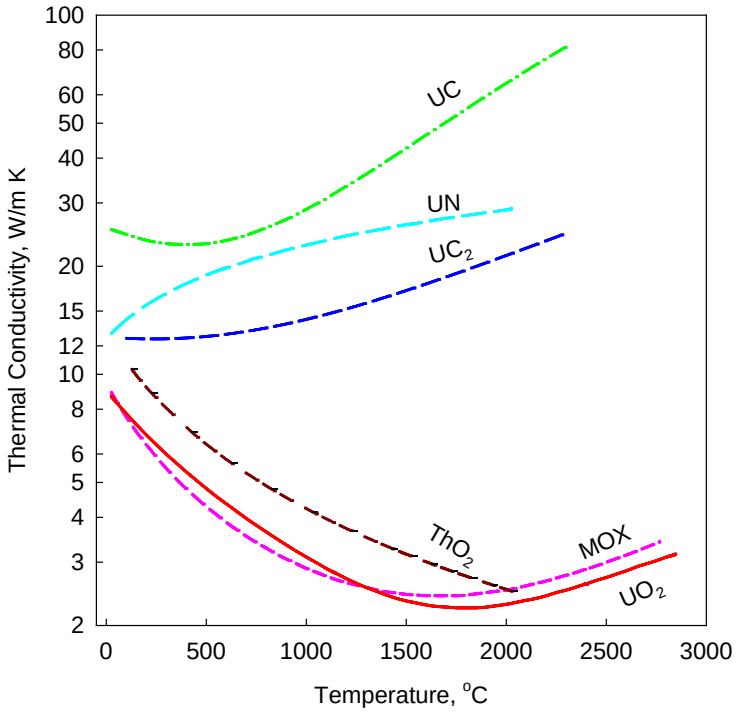

Figure 4.3. Thermal conductivities of selected nuclear fuels (Kirillov et al., 2007) (UC_2 (Chirkin, 1968) and ThO_2 (Jain et al., 2006)).

4.3 Mixed oxide

MOX is a heterogeneous fuel consisting of a mixture of uranium-plutonium oxides. The standard MOX stoichiometric composition is a molar fraction ratio of 0.8 uranium dioxide (UO_2) and 0.2 plutonium dioxide (PuO_2). This composition is described in the form of $(U_{0.8}\,Pu_{0.2})O_2$ (Kirillov et al., 2007).

Table 4.1. Average thermophysical properties of selected ceramic nuclear fuels at 0.1 MPa and 25°C ((Kirillov et al., 2007); ThO_2 (Jain et al., 2006) and UC_2 (Chirkin, 1968)).

Property	Units	Fuel					
		UO_2	MOX*	ThO_2	UC_2	UN	UC
Molar mass	kg /kmol	270.3	271.2	264	262	252	250
Theoretical density	kg/m^3	10,960	11,074	10,000	11,700	14,300	13,630
Melting temperature	°C	2850 ±30	2750 ±30	3227 ±150	2800 ±30	2850 ±30	2365 ±165
Boiling temperature	°C	3542	3538	4227	4370[1]	–	4418
Heat of fusion	kJ/kg	259±15	285.3	69.4[2]	–	–	195.6
Specific heat	kJ/kg·K	0.235	0.240	0.235	0.162	0.190	0.200
Thermal conductivity	W/m·K	8.68	7.82**	9.7	11.57	13.0	25.3
Coefficient of linear expansion, $\times 10^{-6}$	1/K	9.75	9.43[3]	8.9	18.1[4]	7.52	10.1

* Mixed Oxides $(U_{0.8}Pu_{0.2})O_2$, where 0.8 and 0.2 are the molar parts of UO_2 and PuO_2.

** at 95% density.

[1] (International Bio-Analytical Industries, Inc.).

[2] (Fact-index).

[3] at 100°C.

[4] at 1000°C (Bowman, Arnold, Witteman, & Wallace, 1966).

Above 1500°C, the thermal conductivity of MOX is only slightly improved compared to that of UO_2. However, the MOX is beneficial because it is a sustainable resource. MOX reduces the amount of fuel wastes to be disposed of, since it is formed from reprocessing of irradiated fuel. The disadvantages of MOX include: a shorter neutron life, lower

delayed neutron fraction and higher irradiated fuel temperature compared to that of UO_2 (Trellue, 2006).

A MOX-fuelled reactor is able to "burn" plutonium produced from weapons programs. Additionally, MOX fuel enables recycling of plutonium from Light Water Reactor (LWR) fuel. This reprocessing reduces the stockpiling of plutonium in high-level waste facilities and ensures proliferation compliance.

The PT-type core design supports MOX fuel usages. Studies by Boczar et al. (2002) consider the use of MOX fuel, provided by the recycling of LWR fuel in a CANDU reactor. This research considered MOX as an advanced fuel cycle for a CANDU reactor. It was concluded that: fabrication and irradiation tests conducted at Chalk River Laboratories (CRL) were satisfactory, and the core can remain critical by use of MOX fuel only. These studies demonstrated the practical use of irradiated LWR fuel as a MOX supply for PT-type SCWRs.

The interest of MOX as a nuclear fuel was initiated as early as the 1950s. MOX-fuel fabrication activities have been conducted in Belgium and in USA (IAEA, 2003). A decade later, France, Germany, Japan, Russia, and UK became interested; India also supported research into various MOX developments. The initial testing of MOX was in the 1960s (World Nuclear Association, 2009). In the 1980s, MOX became used commercially.

Currently MOX is still a popular fuel choice. MOX is being used extensively in Europe and is intended to be used in Japan (IAEA, 2003). In Belgium, Switzerland, Germany and France, 40 reactors are licensed to use the MOX fuel. Over 30 other countries are in the process of becoming licensed to operate with the MOX fuel. Today, France intends to have all of its 900-MW_{el} series reactors operating with at least one third full of the MOX fuel. Japan has prospects to use MOX in one third of its reactors in the near future and is going to start-up a 1383-MW_{el} reactor at the Ohma plant and start loading MOX by late 2014.

The MOX fuel fabrication operates at a commercial scale around the world. The MOX-fuel fabrication capacities are listed in Table 4.2. There are four plants producing

commercial quantities of MOX fuel (World Nuclear Association, 2009). Two facilities are located in France, one in Belgium, and one was commissioned in the UK in 2001. Presently, the output from MOX reprocessing plants is greater than the amount of plutonium required. This creates a reserve of plutonium. This inventory is expected to exceed 250 tonnes until MOX usage increases.

Currently Canada does not have MOX fabrication facilities. However, it may happen in the future due to utilization of the Direct Use of spent PWR fuel In CANDU (DUPIC) fuel cycle. The DUPIC fuel cycle incorporates irradiated PWR fuel. It is possible the MOX fuel with the low fissile content because of the high neutron economy with the PT-type reactor core. The used PWR fuel would not require manipulation of constituents and would be able to be used as-is (Zhonsheng & Boczar, 1999).

Table 4.2. World known MOX fuel fabrication capacities (tonnes per year) for LWR (World Nuclear Association, 2009).

Country	Year		
	2006	**2008**	**2012**
France	145	195	195
Japan	0	0	130
UK	40	40	40 +
Total for LWR	185	235	445

The feasibility of using MOX as SCWR is based on its thermal conductivity (see Figure 4.3 and Figure 4.4) and other thermophysical properties (see Table 4.1). The integral thermal conductivity can be used to describe gas release from the fuel (Olander, 1976). This parameter increases as temperature rises. At lower thermal conductivities, the integral thermal conductivity values are higher due to increased gas production (Figure 4.4).

The thermal conductivity of MOX reaches its minimum values within the range 1500°C – 2000°C (Figure 4.3). Beyond 2000°C, the thermal conductivity increases to about 4 W/m K. The thermal conductivity of MOX used in this analysis was calculated according to Equation (4.1) (Kirillov et al., 2007):

$$k_{MOX} = 8.9111 - 0.01393T + 1.1451 \times 10^{-5}T^2 - 4.2535 \times 10^{-9}T^3 + 6.072 \times 10^{-13}T^4 \quad (4.1)$$

where T is the temperature in Kelvin.

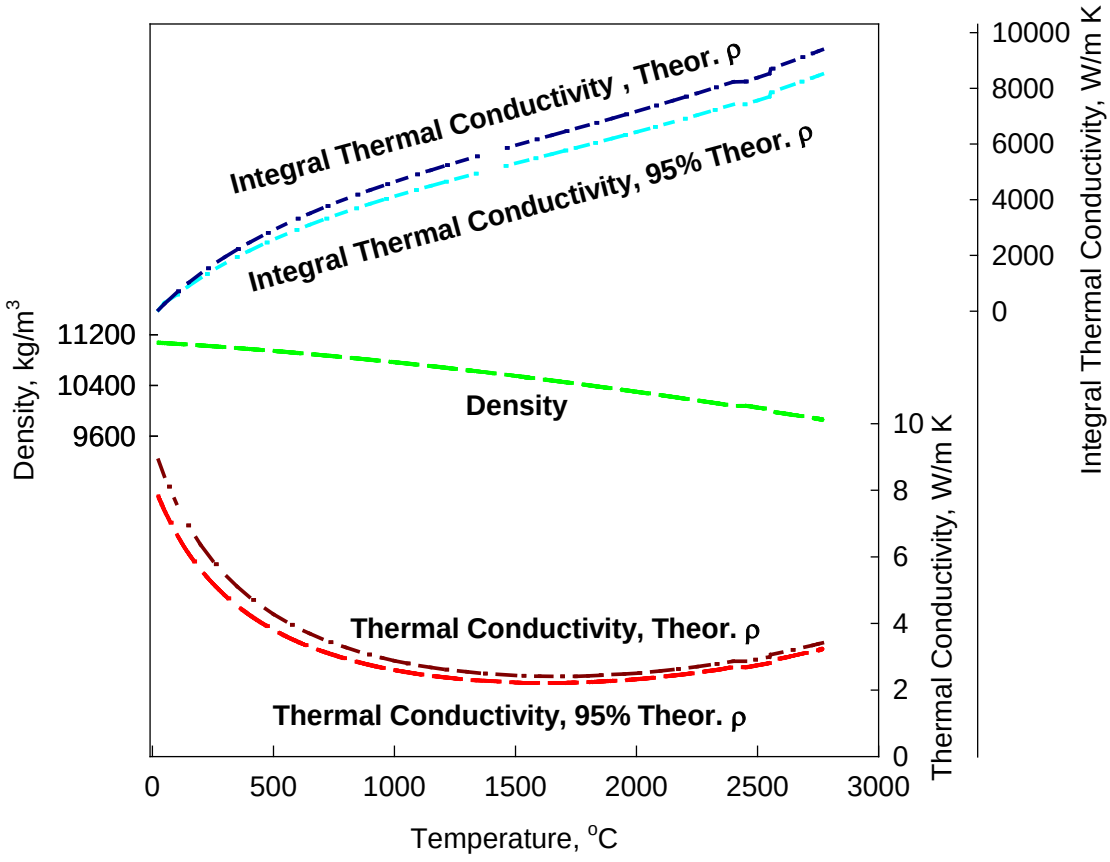

Figure 4.4. Thermophysical properties of MOX fuel of stoichiometric composition $(U_{0.8}Pu_{0.2})O_2$ in solid state (Kirillov et al., 2007).

4.4 Thorium dioxide

Thoria resources are from three to four times more abundant then that of uranium (Table 4.3) and involve less expensive mining operations (Gangulgy, 2005). Use of ThO_2 will supplement the depleting uranium reserves, which are currently used extensively for modern nuclear power reactors (Cochran and Tsoulfanidis, 1999). Therefore, thoria was selected as an alternative to UO_2.

In comparison with other candidate fuels, ThO_2 has the highest melting point (Table 4.1). Melting point is an important parameter in terms of fuel-pellet failures and fission-product release. Thoria's high melting point increases safety and durability during normal and abnormal reactor operation. Another important feature of ThO_2 fuel is its stability. Thoria is relatively inert due to its high chemical and radiation stabilities and is one of the most stable oxides (unlike UO_2 that oxidizes easily to UO_3 and U_3O_8) (Gangulgy, 2005).

Table 4.3. World known thorium resources (Greneche et al., 2007).

Country	Reserves (tonnes)
Australia	300 000
India	290 000
Norway	170 000
USA	160 000
Canada	100 000
South Africa	35 000
Brazil	16 000
Other countries	95 000
World total	**1 200 000**

Figure 4.5 shows a comparison of ThO_2 thermal conductivities from various sources. According to the latest source (Jain et al., 2006) the thermal conductivity of ThO_2 is higher than that of UO_2 within the operational range of SCWRs (Figure 4.3). Jain et al.'s thermal-conductivity correlation (Equation (4.2)) for thoria was used in the current calculations, because it is most recent source as well as originated from a a country that uses thoria in power reactors (India) (IAEA, 2005).

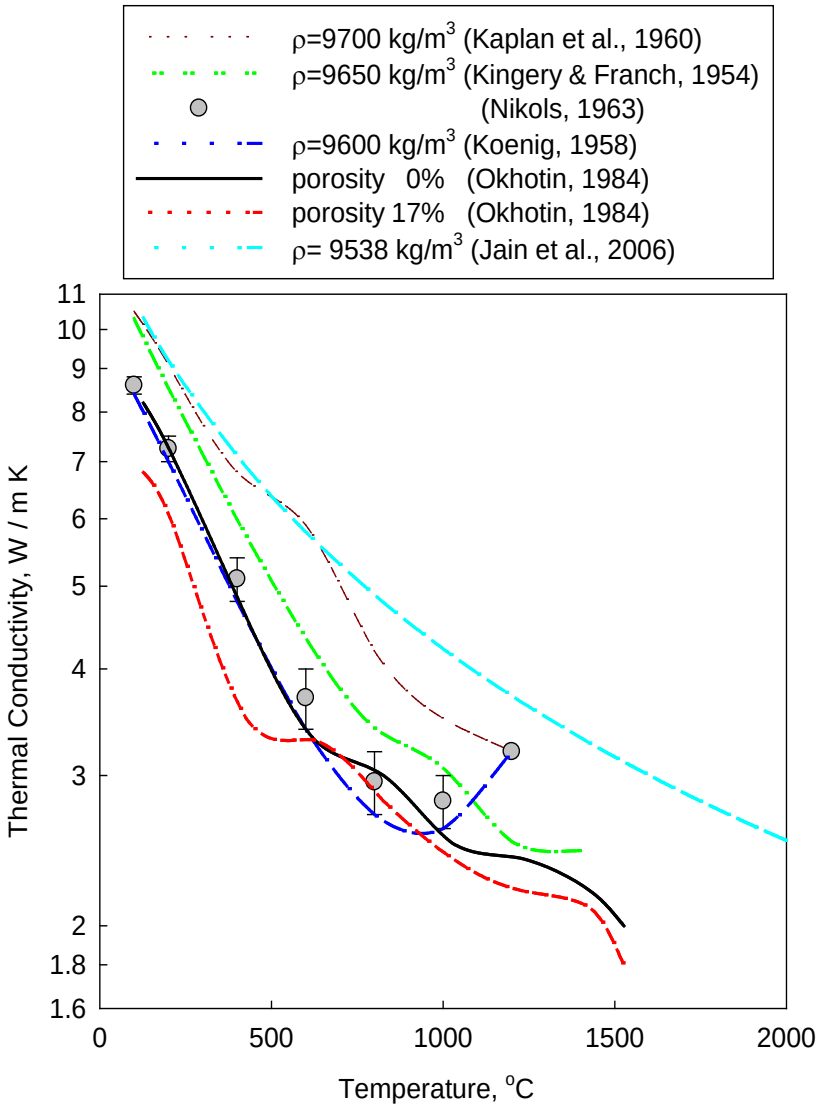

Figure 4.5. Comparison of thermal conductivities of thoria for various porosities and densities.

$$k_{ThO_2} = \frac{1}{0.0327+(1.603\times10^{-4}\mathrm{T})} \quad (4.2)$$

where *T* is the temperature in Kelvin.

Thoria is a fertile material. Fertile refers to isotopes that can be converted to fissile material by the capture of a neutron (Cochran and Tsoulfanidis, 1999). Once the fuel becomes fissile it is able to fission with slow (thermal) neutrons. Therefore, thoria reactors require external neutron source or "seed" fuel to produce fissionable fuel. Thoria fuel is in compliance with the Non-Proliferation Treaty as it decreases the production of Plutonium and other transuranics elements compared to those of irradiated UO_2 (IAEA, 2000).

The conversion of ^{232}Th into fissile ^{233}U liberates greater than 2.0 neutrons per neutron absorbed (Gangulgy, 2005). This occurs over a wide range of thermal-neutron spectrum unlike fissile products of UO_2 (^{235}U and ^{239}Pu). By combining the neutronic properties of flexible conversion of ^{232}Th with the increased neutron production from ^{233}U fissions it leads to higher fuel burn-ups.

Thoria is able to sustain a closed/breeder fuel cycle. Breeder fuel cycle includes used fuel reprocessing and recycling. In the breeder cycle, both weapons grade and civil plutonium can be added to fabricate (Th-Pu)O_2 to increase breeding gains (Lombardi et al., 2008) The breeder cycle can also burn (^{232}Th - ^{233}U)O_2, (depleted U-^{233}U)O_2 and (reprocessed U-^{233}U)O_2 (Gangulgy, 2005).

However, there are operational issues associated with Th-based fuels. During start-up an excess positive reactivity is required to instigate the fertilization of ^{232}Th. This positive reactivity can be achieved with use of an external neutron source or booster rods. The relatively long half-life of ^{233}Pa causes a small fraction of this isotope to undergo radiative capture and does not produce ^{233}U (Lombardi et al., 2008). Conversely, during long unit shut-down a build-up of ^{233}U occurs from the beta decay of ^{233}Pa.

Excess reactivity and flux distortions during operation can be compensated for by using: a multitude of control rods (varying reactivity worth), a burnable poison (such as boric acid) and transmutation fuel rods of ^{232}Th (then the ^{233}U can be reused in a closed-fuel cycle)(Sahin et al., 2008).

Irradiated ThO_2 has higher gamma-radiation fields than UO_2 due to "daughter" products of ^{232}U (^{212}Bi and ^{208}Tl) (Sahin et al., 2008). This would create a higher dose-risk for used fuel activities: handling, storage, reprocessing and refabrication. These dose-risks can be minimized by: remote and automated reprocessing and refabrication in heavily shielded hot-cells with an increase in the cost of fuel-cycle activities (Gangulgy, 2005).

The present production of ThO_2 is almost entirely as a by-product of rare-earth extraction from monazite sand (IAEA, 2005). Monazite is a mixed ThO_2 rare-earth uranium phosphate, is the most popular source of ThO_2 and is available in many countries inside beach or river sands along with heavy minerals such as ilmenite, rutile, monazite, zircon, sillimenite and garnet.

Also, thoria has another beneficial, such as increased in thermal conductivity compared to that of UO_2 fuel for SCWR temperature range. The use of thoria in SCWR applications might be important then current reactors because it is a non-uranium based fuel, uranium resources are being used with an accelerating trend.

4.5 Uranium nitride

Uranium nitride as a nuclear fuel considered in the current thesis because of its high actinide density (increases probability of fission with fast neutrons) along with the desired increased thermal conductivity and rising thermal conductivity trend. Also, the uranium nitride is a favorable fuel choice due to its high thermal conductivity, which is ten times higher than that of UO_2 at 1000°C (Figure 4.3). However, the drawback of using UN fuel use is that the decomposition products are reactive with nickel (a constituent in the Inconel sheath material) and requires a hafnium nitride (HfN) or thorium nitride (ThN) additives to become inert (Choi et al., 2006).

The UN fuel has a high melting temperature, which is described as a function of pressure within 10^{-8} Pa $\leq P_{N_2} \leq 7.5 \cdot 10^5$ Pa (Hayes, 1990):

$$T_m(K) = 3055 \cdot P_{N_2}^{0.02832} \tag{4.3}$$

where *P* is the pressure in Pascal.

However, at low pressures the UN fuel would decompose (Prins & Gordfunke, 1980):

$$UN(s) \rightarrow U(liq) + 0.5\ N_2(gas) \tag{4.4}$$

Uranium nitride has the lowest coefficient of linear expansion than the selected alternative fuels (see Table 4.1). Coefficient of thermal expansion is a material property that is indicative of the extent to which a material expands upon heating (Callister, 2003). One reason for UN having a smaller change in expansion is that it produces less fission-product gases.

The thermal conductivity of UN within temperatures from 273 K to 2300 K is calculated according to Equation (4.5) (Kirillov et al., 2007):

$$k_{UN} = 1.41\ T^{0.39} \tag{4.5}$$

where, *T* is the temperature in Kelvin.

Porosity (ε) has the most significant impact on thermal conductivity and is accounted for by Equation (4.6) (Kirillov et al., 2007):

$$k_{UN,\varepsilon} = 1.864\, e^{-2.14\varepsilon} T^{0.361} \quad (4.6)$$

where, ε is the porosity in volume fractions and T is the temperature in Kelvin.

The UN thermal conductivity decreases when porosity increases (Figure 4.6). Figure 4.7 shows various thermophysical properties of UN fuel versus temperature (Kirillov et al., 2007).

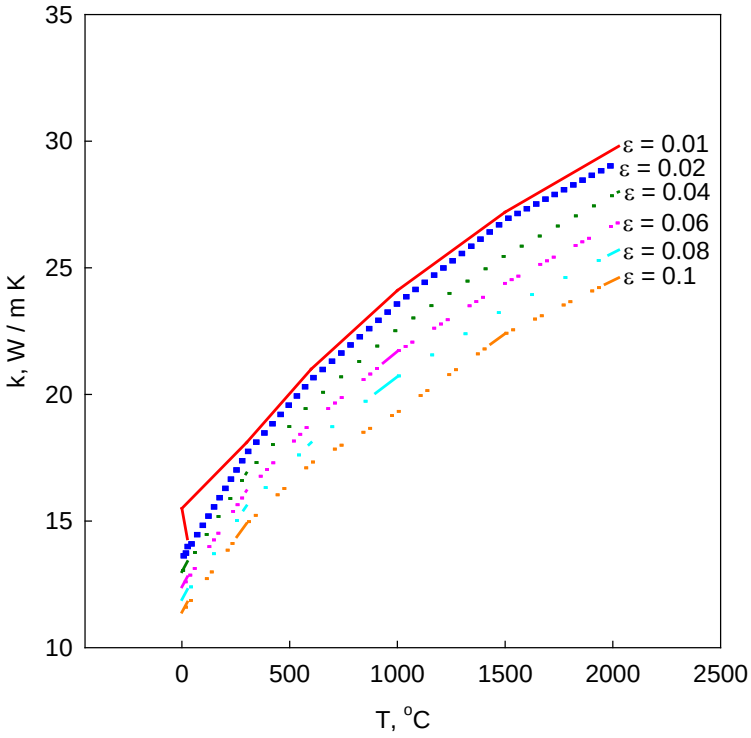

Figure 4.6. Effect of porosity on thermal conductivity of UN fuel (Kirillov et al., 2007).

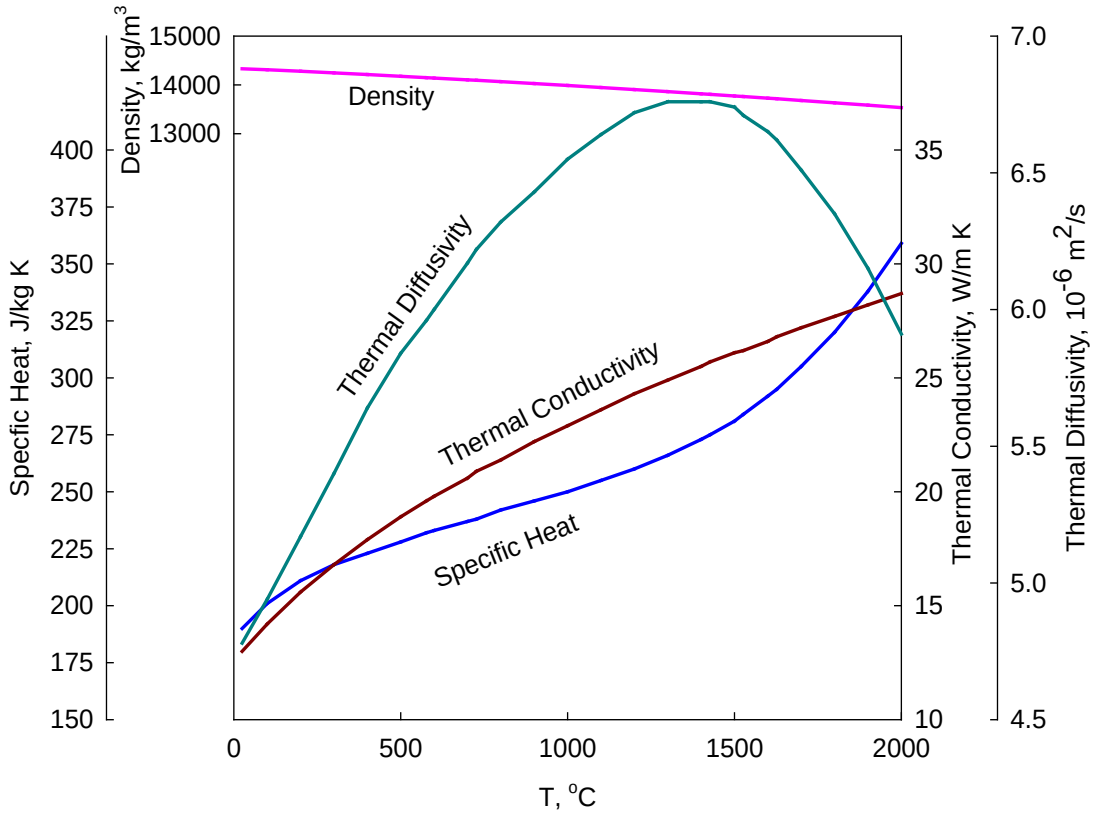

Figure 4.7. Selected thermophysical properties of UN fuel (Kirillov et al., 2007).

4.6 Carbide-based fuels

Uranium carbide consists of uranium and carbon and can exist in three separate forms: uranium monocarbide, commonly known as uranium carbide (UC), sesquicarbide (U_2C_3), and uranium dicarbide (UC_2). All forms exist as a hard refractive ceramic material. For SCWR application, it was decided to focus only on UC and UC_2 nuclear fuel. Currently, UC fuel is proposed to be used in high-temperature helium-gas cooled reactors. However, the compatibility of carbide based fuels and SCW needs to be investigated.

The chosen carbide based fuels are superior over all studied fuel options since its thermal conductivity is the highest. Both uranium carbide fuels (UC and UC_2) exhibit an "outstanding" thermal conductivity within the operating range of temperatures (1000 –

2000ºC) (Figure 4.3). On average, thermal conductivity of UC_2 fuel is about 7 times higher than that of UO_2, and UC thermal conductivity about 15 times higher than that of UO_2 fuel.

With both UC and UC_2 fuels there is a number factors beyond the this thesis in regards to cracking, swelling and irradiation which might affect the use of these fuels when considering them in application to SCWRs. Thus, it has been identified that swelling occurs from gas-bubble formation of UC fuel for temperatures above 700°C and burn-ups greater than 5×10^{20} fissions/cm^3 (Harrision, 1969).

4.6.1 Uranium carbide

The thermal-conductivity correlation for UC used for fuelcentreline calculations are based on Kirrilov et al. (2007):

$$k_{UC} = 30.4777 - 0.0223T + 1.6678 \times 10^{-5}T^2 - 1.8497 \times 10^{-10}T^3 + 3.1835 \times 10^{-14}T^4 \quad (4.7)$$

where T is the temperature in Kelvin.

4.6.2 Uranium dicarbide

For UC_2, the thermal conductivity has been determined by Chirkin (1968) and is defined as the following:

$$k_{UC_2} = 13.2712 - 2.8695 \times 10^{-3}T + 2.8423 \times 10^{-6}T^2 \quad (4.8)$$

where T is the temperature in Kelvin.

4.7 Axial Heat Flux Profiles

Both uniform and non-uniform Axial Heat Flux Profiles (AHFPs) were applied at average channel power. Uniform AHFP is representative of extreme flatting of the cosine AHFP with reactivity-control devices. The cosine AHFP is the conventional shape of heat flux during normal operation inside many reactors. The non-uniform AHFPs, such as: upstream-skewed cosine and downstream-skewed cosine, were analyzed since they demonstrate common channelized fuelling activities. The skewed-cosine AHFPs have been developed in the past decade. The upstream-skewed cosine occurs at the insertion of fresh fuel 2 bundles at a time (2-bundle shift), and a downstream-skewed cosine corresponds to the 8-bundle shift. In general, all these four AHFPs create an envelope for the most extreme cases.

Both uniform and non-uniform AHFPs were analyzed (Figure 4.8). The uniform AHFP was 967 kW/m^2 ($\dot{q}_{ave}$). The non-uniform AHFPs were fitted with 6th-degree polynomials with the minimum squared regression coefficient (r^2) of 0.9998. The cosine and upstream-skewed cosine AHFPs were are based on those presented by Leung (2008). The downstream-skewed cosine AHFP was produced as a mirror image of the upstream-skewed cosine AHFP.

The polynomials represent the power or heat flux ratio with respect to the axial position (Equations (4.9 – 4.11)). Equation (4.12) is used as a basis for all 3 non-uniform AHFPs. The polynomial coefficients are listed in Table 4.4. The channel power for each millimetre is found using Equations (3.13 – 3.16).

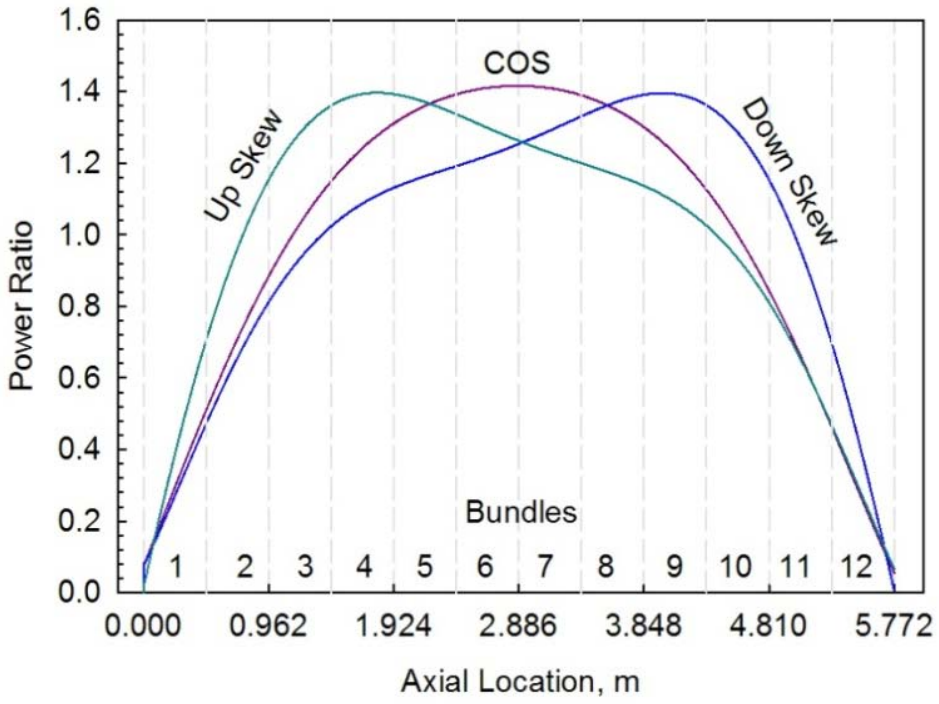

Figure 4.8. Non-uniform AHFPs (based on paper by Leung, 2008).

Table 4.4. Polynomial coefficients for Equation (4.12).

Cosine Profile	a_o	a_1	a_2	a_3	a_4	a_5	a_6	r^2
Normal	79.25	854.93	149.04	–291.25	108.03	–17.43	1.03	0.9998
Upstream	12.02	1552.15	–223.18	–341.85	166.29	–28.43	1.67	0.9999
Downstream	89.48	709.32	364.10	–517.40	200.23	–32.25	1.83	0.9998

$$Power\ Ratio = \dot{q}'_{loc} = \frac{\dot{q}_{loc}}{\dot{q}_{ave}} \tag{4.9}$$

$$\dot{q}_{ave} = \frac{\dot{Q}_{Ch}}{A_h} \tag{4.10}$$

$$A_h = \pi l_h (N_c D_c + N_{ir} D_{ir} + N_{mr} D_{mr} + N_{or} D_{or}) \quad (4.11)$$

$$\dot{q}'_{loc} = a_0 + a_1 x + a_2 x^2 + a_3 x^3 + a_4 x^4 + a_5 x^5 + a_6 x^6 \quad (4.12)$$

$$\dot{Q}_{loc_x} = p_h \int_0^x \dot{q}_{loc} dx \quad (4.13)$$

$$\dot{Q}_{loc_x} = p_h q_{ave} \int_0^x q'_{loc} dx \quad (4.14)$$

$$p_h = \pi (N_{ir} D_{ir} + N_{mr} D_{mr} + N_{or} D_{or}) \quad (4.15)$$

$$\int_0^x \dot{q}'_{loc} dx = a_0 \frac{1}{1} x + a_1 \frac{1}{2} x^2 + a_2 \frac{1}{3} x^3 + a_3 \frac{1}{4} x^4 + a_4 \frac{1}{5} x^5 + a_5 \frac{1}{6} x^6 + a_6 \frac{1}{7} x^7 \quad (4.16)$$

The area under the power-ratio curve (Figure 4.8) for the entire heated length is the total channel thermal power. The channel power was calculated through integration of the polynomial Equation (4.17). The results of this check showed that calculations of the channel powers for the three non-uniform AHFPs were within 5% of 8.5 MW_{th}.

$$\dot{Q}_{Ch} = p_h q_{ave} \int_0^{5.772} q'_{loc} dx = 8.5 \ - 5\% \text{ MW} \quad (4.17)$$

Equation (4.18) allows heat output at any axial location to be calculated. Power for each millimetre increment along the heated length was calculated with the following equations:

$$\dot{Q}_{loc.mm} = \dot{Q}_{loc.x+1} - \dot{Q}_{loc.x} \tag{4.18}$$

$$\dot{q}_{loc.x} = \frac{\dot{Q}_{loc.mm}}{A_{mm}} \tag{4.19}$$

$$A_{mm} = \pi(0.001\ \text{m})p_h \tag{4.20}$$

4.8 Fuel-Acceptance Criterion

The fuel centreline temperature must not exceed the industry accepted limit of 1850°C to be an suitable in SCWR applications. This temperature value was the averaged maximum fuel centreline temperature determined experimentally at Chalk River National Labs (Hastings et al., 1983). This temperature limit is also based on a conservative margin which is below by 1000°C of the melting point of UO_2 (see Table 4.1).

5 HEAT-TRANSFER CALCULATIONS

5.1 Methodology

The heat-transfer analysis will proceed as follows: 1) calculation of the heat-transfer rate per each millimeter based on the selected AHFPs, 2) calculation of the bulk-fluid-temperature profile based on the heat-balance method, 3) calculation of the HTC profile with the use of the modified Bishop et al. correlation (1964), 4) calculation of the inner-sheath-temperature profile, and 5) calculation of the fuel-centreline-temperature profile.

Thermophysical properties of the coolant at the sheath temperature and thermal conductivities of the sheath and fuel were calculated using an iterative method (see Appendices A and B for algorithms). In general, coolant properties were estimated based on a bulk-fluid temperature, i.e., an average coolant temperature within a cross section. All calculations were performed along the heated length of 5.772 m with a 1-mm increment along a bundle string.

5.2 Assumptions

The following assumptions were used in the current calculations: heat flux in the radial direction was uniform, the bundle-string length to be equal to the heated channel length (end-plates and end-caps of each bundle were not taken into consideration), the fuel thermal conductivity varies only with temperature, the contact resistance between a fuel pellet and sheath is negligible, and the coolant pressure is constant along the channel.

The generic PT-type SCWR parameters are: average channel power is 8.5 MW_{th}, the inlet temperature − 350°C, the outlet temperature − 625°C, the pressure − 25 MPa, and the coolant mass-flow rate − 4.4 kg/s.

5.3 Computer Software and Interfaces

The MATrix LABoratory (MATLAB) software was used to develop the computational code and the National Institute of Standards and Technology REference Fluid thermodynamic and transport Properties (NIST REFPROP) (Lemmon et al., 2007) was used to determine the thermophysical properties of SCW. The code is developed in three sections: bulk-fluid-temperature profiles, inner-sheath-temperature profiles and fuel-centreline-temperature profiles. Appendix A contains the code for a uniform AHFP of thoria fuel, and Appendix B contains the code for cosine AHFP for thoria.

5.4 Iterations

The abovementioned calculations for HTC and conduction through the sheath and fuel pellet required iterations. The iteration "stopping" criteria used in the temperature and thermal conductivity iterations were a differences of ± 0.5K and ± 0.05W/m K, respectively. Appendix A contains manual examples of iterations within the code to explain the process in details.

5.5 MATLAB Code Check

The MATLAB code was checked by: replication of previous results, comparison to a Microsoft Excel spreadsheet and a peer review. The primary analysis of these heat-transfer calculations was of UO_2 with the uniform AHFP by Pioro et al. (2008) (Figure 5.1). Figure 5.2 is the output of the current code. The fuel centreline temperature of the recent calculations did not exceed the industry accepted limit as the previous data. This discrepancy of fuel centreline temperature along the channel is due to that the latest results utilize a variable thermal conductivity (dependant on temperature) and a smaller fuel element OD (11.5 mm) versus a constant uniform thermal conductivity and a larger fuel element (13.5 mm).

The outer-temperature trends of the outer sheath are similar although the material type and sheath thickness of the previous study were unknown. The current model was based on an Inconel-600 sheath with a thickness of 0.430 mm.

Eleven data points along the fuel channel were compared against previous results and use of an Excel spreadsheet. The points of interest were selected as follows: channel inlet, channel outlet, metered increments, just below, in and above the pseudocritical point. The detailed comparison data of the selected points of interest between the previous results and the Excel spreadsheet is listed in Appendix C with the summary in Table 5.1.

It should be noted that in the previous studies the heat flux was 915 kW/m^2 compared to the current study heat flux of 967 kW/m^2. Therefore, the difference in HTC values might be due to this reason. Also some discrepancy can be caused by using the constant fuel conductivity versus the temperature-dependant thermal conductivity in the current study. The Excel spreadsheet was able to reproduce the MATLAB data with less than 0.04% difference. A peer review was also conducted for each millimeter increment along the channel for uniform and cosine AHFPs (Figure 5.3 and Figure 5.4).

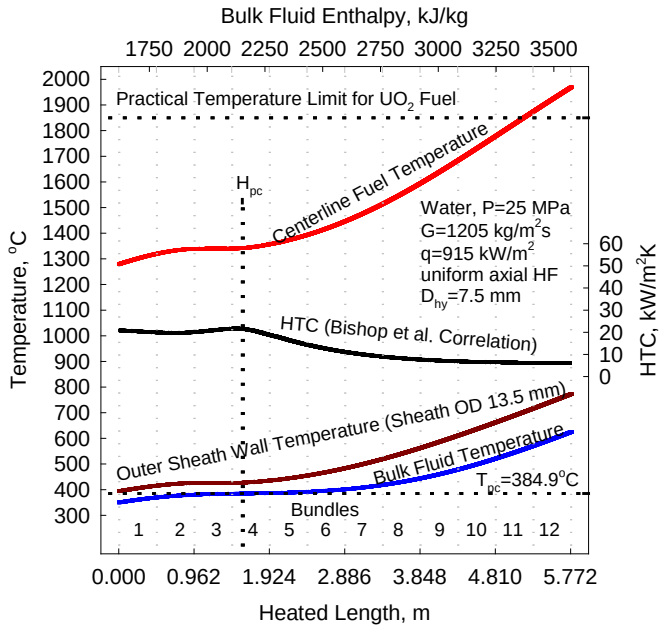

Figure 5.1. Temperature and HTC profiles for UO_2 with constant thermal conductivity along the heated length with uniform AHFP (Pioro et al., 2008).

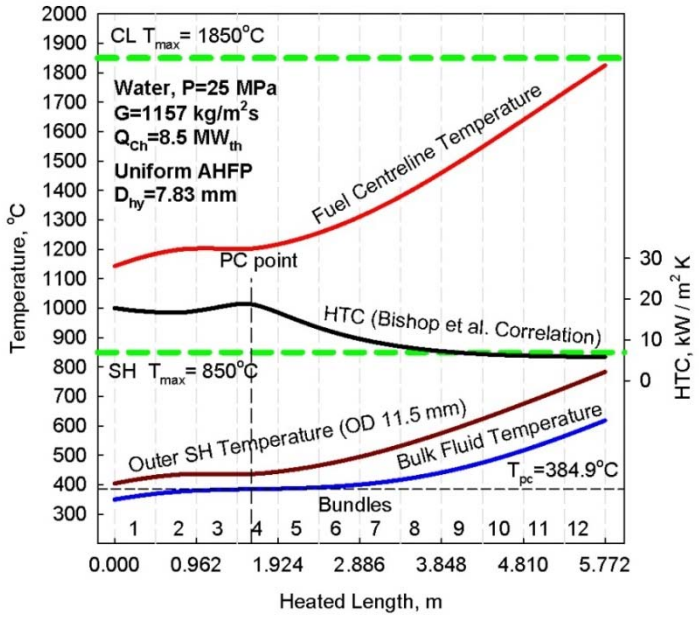

Figure 5.2. Temperature and HTC profiles for UO_2 fuel along heated length with uniform AHFP (these results are similar to Allison et al. (2009)).

Table 5.1. Summary of MATLAB data comparison between previous results, Excel spreadsheet and peer review.

		Bulk-Fluid Temperature	HTC	Outer-Sheath Temperature	Fuel Centreline Temperature
Previous Results					
Uniform AHFP	Max % Difference	0.6	14.4	2.6	24.6
	Distance, m	4.000	0.0	0.0	0.0
Excel Spreadsheet					
Uniform AHFP	Max % Difference	0.00	0.00	0.00	0.03
	Distance, m	–	–	–	4.000
Peer Review					
Uniform AHFP	Max % Difference	0.4	1.5	0.4	2.8
	Distance, m	5.772	0.151	5.772	3.949
Cosine AHFP	Max % Difference	3.7	7.6	4.3	14.7
	Distance, m	5.772	2.602	5.589	1.041

Both data sets for each output parameter are layered on the same graph to highlight the differences. Also, a summary of the maximum percent difference for the entire channel is provided in Table 5.1. The largest percent difference is between fuel centreline temperatures for both uniform and cosine AHFPs. These temperatures variation are due to the different calculation methods. The current results are based iterations conducted with "stopping" criterion of 0.05 W/m K for each of 5 radial increments. This is in comparison to the peer-review results, where iterations are performed only once, but over 500 radial increments. Overall, the temperature and HTC profiles of previous results and peer-review in terms of code results to the present are quite close with similar trends.

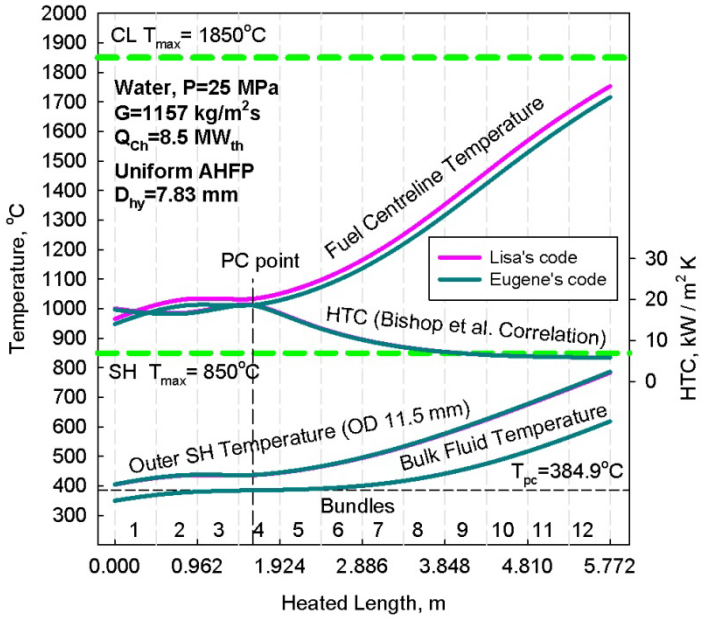

Figure 5.3. Peer-review results of temperature and HTC profiles for UO_2 fuel along heated length with uniform AHFP.

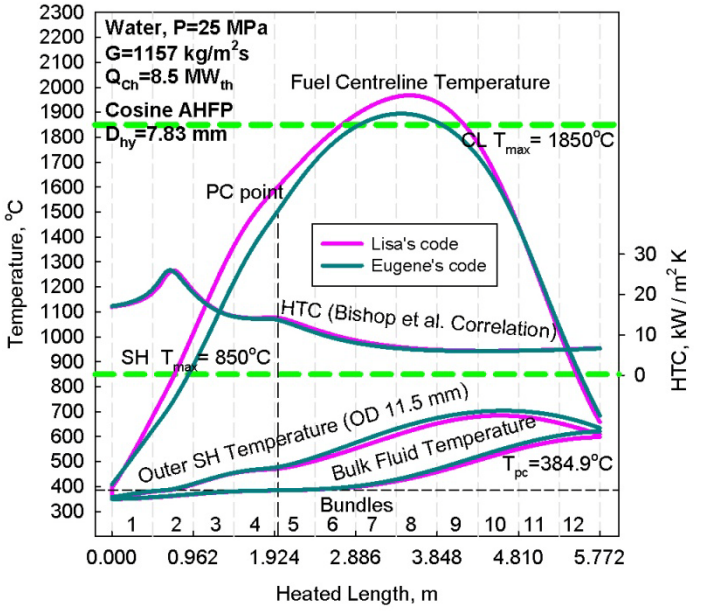

Figure 5.4. Peer-review results of temperature and HTC profiles for UO_2 fuel along heated length with cosine AHFP.

5.6 Bulk-Fluid Temperature

The initial step in this heat-transfer analysis is to determine the bulk-fluid temperature profile along the heated length, which was obtained based on the heat-balance method (Equation (5.1)). The inlet bulk-fluid enthalpy was obtained based on the inlet temperature of 350°C and constant pressure of 25 MPa.

$$h_x = \frac{\dot{Q}_{loc_{mm}}}{\dot{m}} + h_{x-1} \tag{5.1}$$

Based on h_x and constant pressure, the bulk-fluid temperature profile was determined using the NIST REFPROP (Lemmon et al., 2007).

5.7 Outer-Sheath Temperature

The outer-sheath temperature was obtained based on the corresponding bulk-fluid temperature (T_b), i.e., in the same axial position, and HTC. The HTC was calculated according to the modified Bishop et al. correlation (Equation (2.2)). Parameters required for this correlation are given in the following equations:

$$D_{hy} = \frac{4\,A_{flow}}{P_{wetted}} \tag{5.2}$$

$$A_{flow} = A_{pt} - A_{fuel\ bundle} \tag{5.3}$$

$$p_{wetted} = \pi(N_c D_c + N_{ir} D_{ir} + N_{mr} D_{mr} + N_{or} D_{or} + D_{pt}) \tag{5.4}$$

Where, N is the number of fuel rods (elements) per ring and D is the outer diameter of the fuel sheath in metres.

An alternative method to calculate hydraulic-equivalent diameter might be as the following (Muzychka & Yovanovich, 1998):

$$D_{hy} = \sqrt{A_{flow}} \tag{5.5}$$

This new method has been developed for non-circular ducts and is effective for multiple geometries. However, in nuclear-reactor thermal hydraulics the conventional hydraulic-equivalent diameter is used (Equation 5.2). Therefore, Equation 5.2 was used to calculated the hydraulic-equivalent diameter of the bundle geometry.

Calculating HTC via the modified Bishop et al. correlation requires iterations, because of the outer-sheath temperature ($T_{o,sh}$) and the bulk-fluid density based at the outer-sheath temperature ($\rho_{o,sh}$). Therefore, the starting point for iterations has been assumed as the following: $T_{o,sh} = T_b + 25$ K. Thus, the initial HTC value was calculated. Based on the following equation a new $T_{o,sh}$ value was calculated:

$$T_{o,sh} = \frac{\dot{q}}{HTC} + T_b \tag{5.6}$$

The new $T_{o,sh}$ was compared to the initial $T_{o,sh}$ value, and if the difference was greater than ±0.5 K then the arithmetic average between the two temperatures was inserted into the modified Bishop et al. correlation with the corresponding $h_{o,sh}$ and $\rho_{o,sh}$.

Finally, the $T_{o,sh}$ profile along the bundle-heated length was calculated based on the abovementioned iterations, and the maximum $T_{o,sh}$ value from this profile was compared to the design limit of 850°C.

5.8 Inner-Sheath Temperature

Inner-sheath temperatures were then calculated based on the heat conduction through the cylindrical sheath wall per millimetre increment (Cengel, 2007) as shown in the following equation:

$$\dot{Q}_{sh,x}\Big/_{0.001m} = 2\pi k_{sh}\frac{T_{i,sh}-T_{o,sh}}{\ln\left(r_{o,sh}/r_{i,sh}\right)} \tag{5.7}$$

Therefore, the inner-sheath temperature can be found according to:

$$T_{i,sh} = \frac{\dot{Q}_{sh,x}/_{0.0001m}\ln\left(\frac{r_{o,sh}}{r_{i,sh}}\right)}{2\pi k_{sh}} + T_{o_{sh}} \tag{5.8}$$

Equation (5.8) also requires iterations to be solved. In general, it must be calculated with the arithmetic average temperature of the sheath. Therefore, as the starting point a thermal conductivity of Inconel-600 (k_{sh}) at the known outer-sheath temperature was used. A new value for k_{sh} based on the arithmetic average of sheath temperatures; $T_{ave,sh} = ½(T_{o,sh} + T_{i,sh})$. The iteration "stopping" criterion was ±0.05 W/m K.

5.9 FuelCentreline Temperature

The following correlations were used for the fuel centreline temperature calculations per millimetre increment (Cengel, 2007). Equation 5.9 is suitable to find the maximum temperature within a solid for steady-state heat conduction with constant heat generation ($\dot{e}_{gen,mm}$) and constant thermal conductivity (k_{fuel}).

$$T_{fc,mm} = \frac{\dot{e}_{gen,mm} {r_{i,sh}}^2}{4\, k_{fuel}} + T_{i,sh,mm} \tag{5.9}$$

$$\dot{e}_{gen,mm} = \frac{\dot{Q}_{loc,mm}}{{D_{i,sh}}^2 \pi (0.001m)} \tag{5.10}$$

The heat generation was assumed to be uniform throughout the pellet. To increase accuracy of the calculated fuel centreline temperature, the fuel-pellet radius was divided into increments. Five increments of approximately 1 mm each were applied. Five increments were chosen, because of increasing the number increments the fuel centreline temperature varied only by hundredths of a degree Celsius. The fuel thermal conductivity was assumed to be constant within the radial increments. Iterations were applied to each increment to find the thermal conductivity of the fuel. The last increment determines the fuel centreline temperature. Equation (5.11) was used for fuel centreline temperature was calculated with radial increments. The fuel-centreline-temperature profile was compared to the industry accepted limit of 1850°C to determine viability of a fuel in SCWR applications.

$$T_{n-1,mm} = \frac{\dot{e}_{gen,mm} \left[{r_{i,sh,n}}^2 - {r_{i,sh,n-1}}^2 \right]}{4\, k_{fuel}} + T_{n,mm} \tag{5.11}$$

6 RESULTS

Each nuclear fuel was analyzed within a Inconel-600 43-element Variant 20 bundle with a centre unheated rod (20 mm OD) and the rest of the fuelled elements (11.5 mm OD) against each of the four AHFPs at average channel power. In all investigated cases, the sheath temperature remained below the design limit of 850°C.

The fuel centreline temperatures exceed the industry accepted limit for UO_2 fuel for both cosine and downstream-skewed cosine AHFPs (Figure 6.1 and Figure 6.3) and for MOX fuel for all AHFPs (Figure 6.4 – Figure 6.7). Uranium dioxide and MOX fuels may still be used in SCWRs, however, the fuel-bundle design might require a modification. Fuel centreline temperatures may be decreased by using smaller diameter pellets, hollow pellets or/and decreasing channel power. In terms of fuel supply, MOX is the most sustainable option, since it is formed from irradiated UO_2.

The remaining fuels (ThO_2, UN and UC_2) for all AHFPs (shown in Figure 6.8 –Figure 6.23) are deemed acceptable in SCWR applications by this thermal-hydraulic analysis as fuel centreline temperature constraints. In comparison to the rest of the fuels thoria is unique due to non-uranium basis.

The lowest fuel centreline temperatures occur with UC fuel at upstream-skewed cosine AHFP (see Figure 6.23). Within this scenario the UC fuel centreline temperatures does not exceed the sheath-temperature limit. Although, UC largely increases the safety margin by having a minimum fuel centreline temperature, there are limited data on operational performance, fabrication methods and irradiation behaviour.

The sheath and fuel centreline profiles vary drastically from uniform to non-uniform AHFPs. The non-uniform AHFPs have lower sheath and fuel centreline temperatures at the inlet and outlet of the channel. In contrast, for the uniform AHFP the maximum sheath and fuel centreline temperatures occurs only at the outlet of the channel. For the non-uniform AHFPs, the shapes of the outer-sheath and fuel centreline temperatures follow shapes of the corresponding power profiles. The non-uniform maximum sheath and fuel centreline temperatures at cosine and downstream-skewed AHFPs are located within the downstream end of the fuel channel.

It can be noticed from analyzing all the AHFPs that the upstream-skewed profile is more preferable in terms of lower sheath and fuel centreline temperatures. In opposite, the downstream-skewed profile is the least preferred.

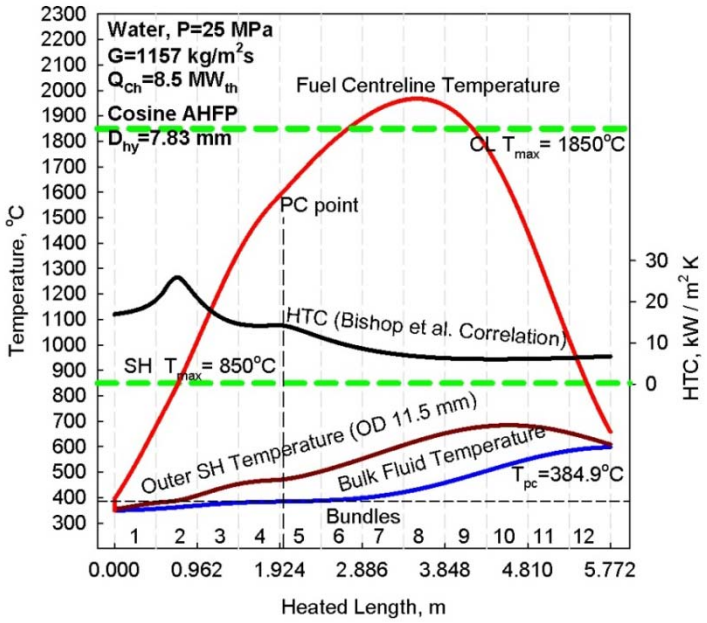

Figure 6.1. Temperature and HTC profiles for UO_2 fuel along heated length with cosine AHFP (Grande et al., 2011).

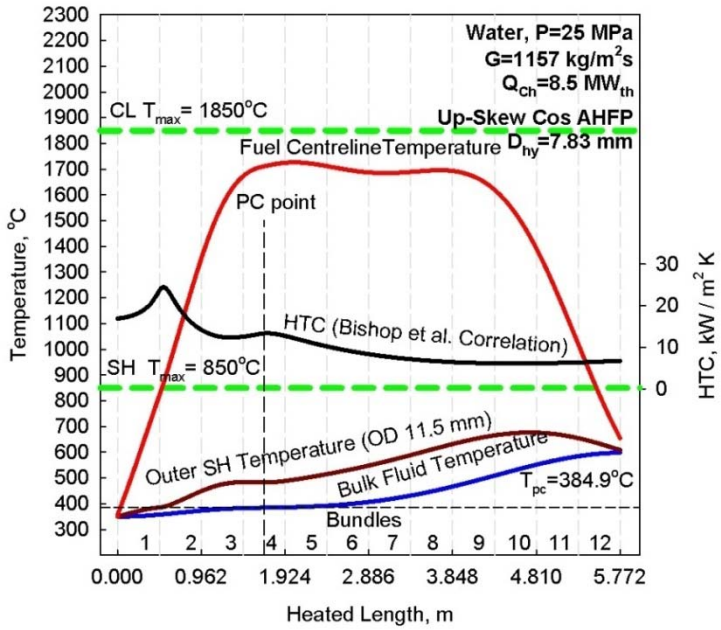

Figure 6.2. Temperature and HTC profiles for UO_2 fuel along heated length with upstream-skewed cosine AHFP (Grande et al., 2011).

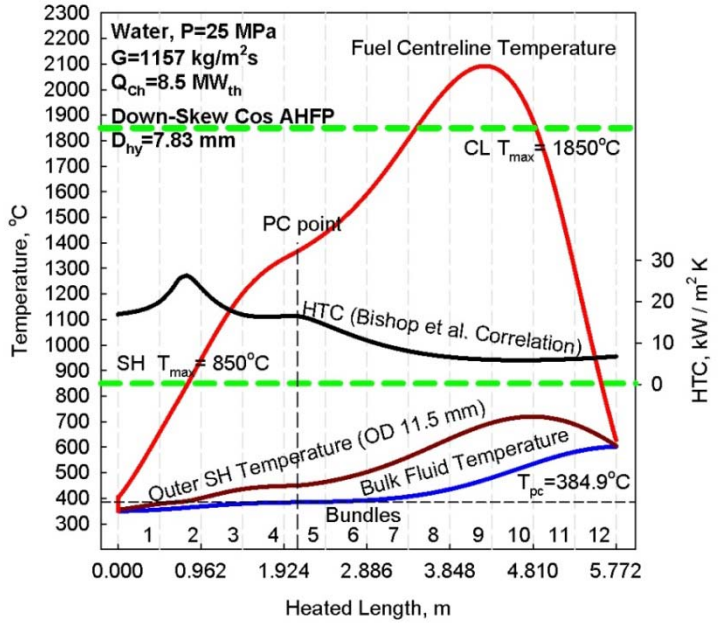

Figure 6.3. Temperature and HTC profiles for UO_2 fuel along heated length with downstream-skewed cosine AHFP (Grande et al., 2011).

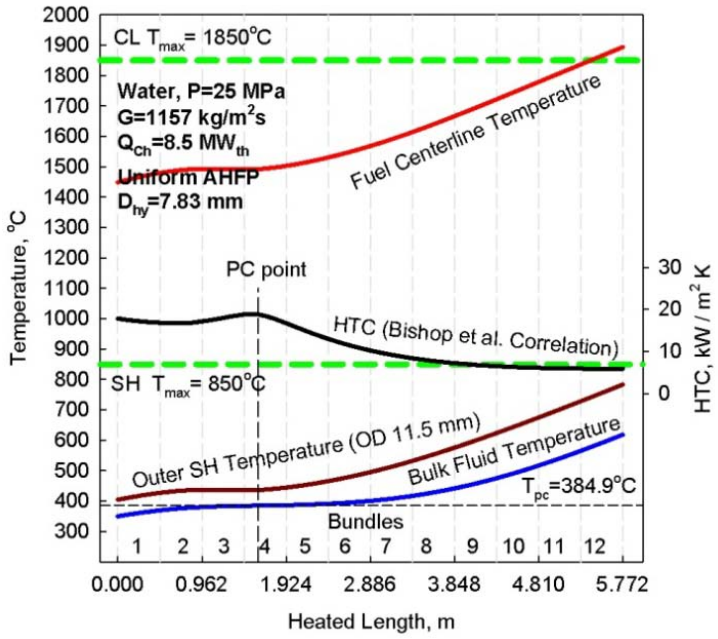

Figure 6.4. Temperature and HTC profiles for MOX fuel along heated length with uniform AHFP (Grande et al., 2010b).

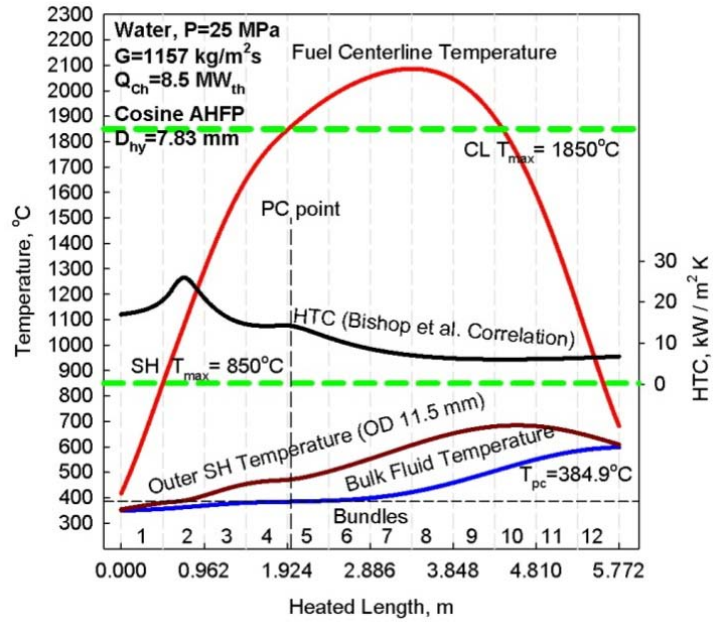

Figure 6.5. Temperature and HTC profiles for MOX fuel along heated length with cosine AHFP (Grande et al., 2010b).

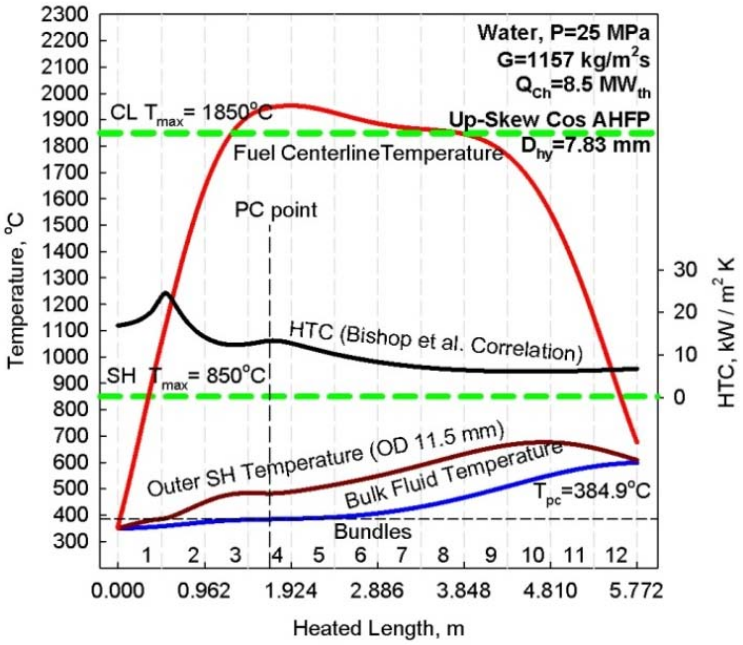

Figure 6.6. Temperature and HTC profiles for MOX fuel along heated length with upstream-skewed cosine AHFP (Grande et al., 2010b).

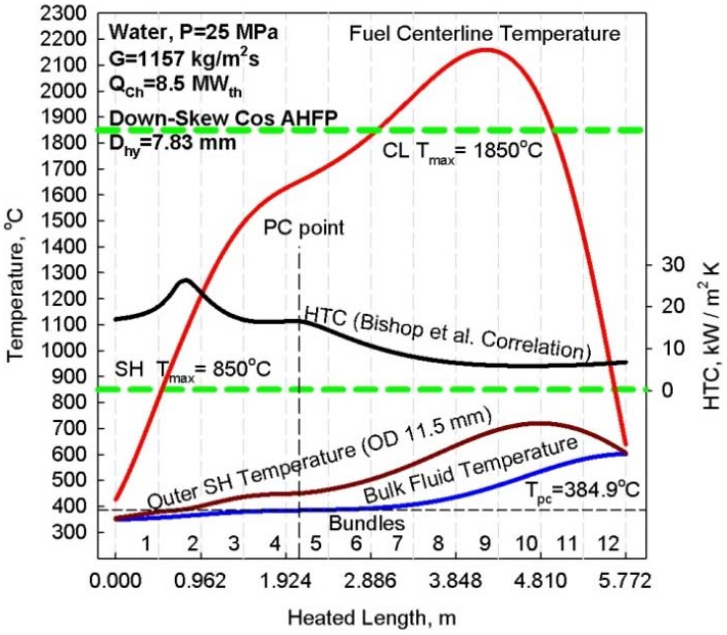

Figure 6.7. Temperature and HTC profiles for MOX fuel along heated length with downstream-skewed cosine AHFP (Grande et al., 2010b).

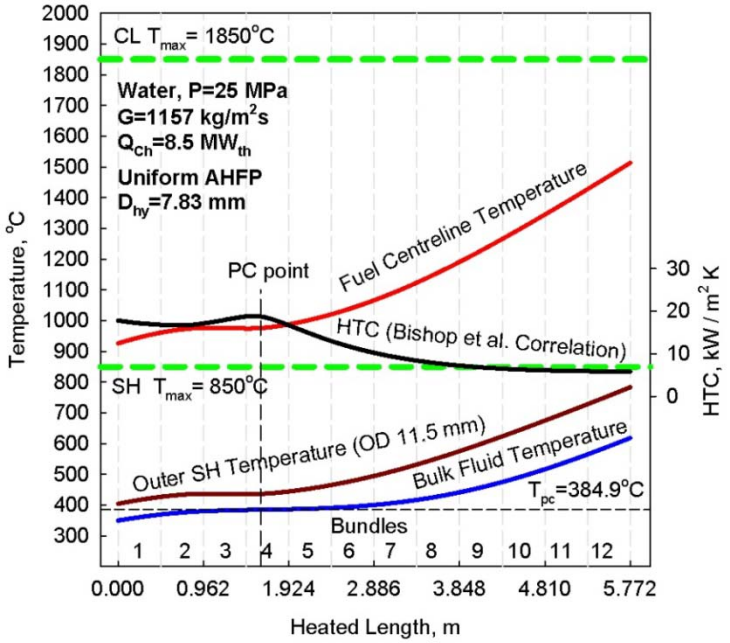

Figure 6.8. Temperature and HTC profiles for thoria fuel along heated length with uniform AHFP (Grande et al., 2009).

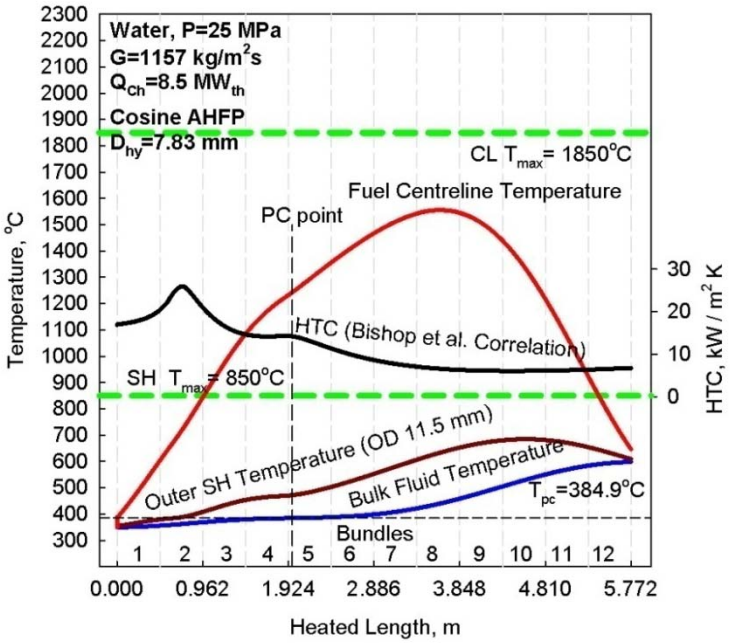

Figure 6.9. Temperature and HTC profiles for thoria fuel along heated length with cosine AHFP (Grande et al., 2009).

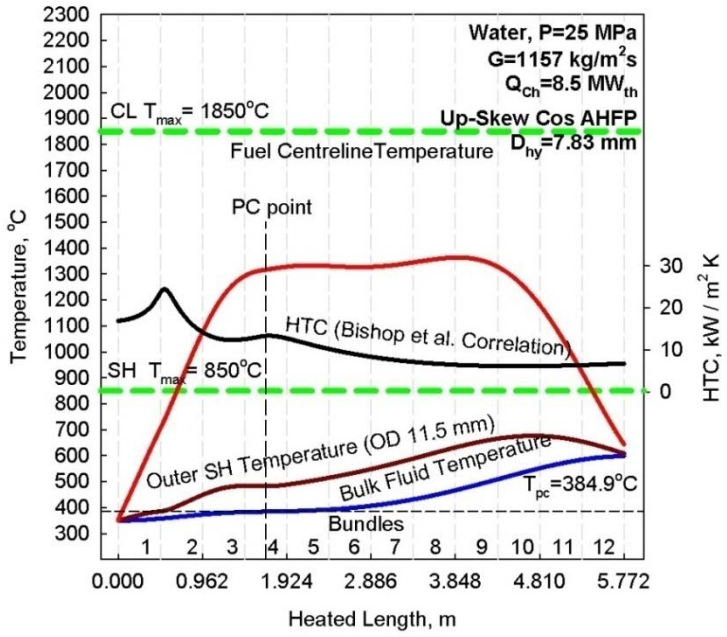

Figure 6.10. Temperature and HTC profiles for thoria fuel along heated length with upstream-skewed cosine AHFP (Grande et al., 2009).

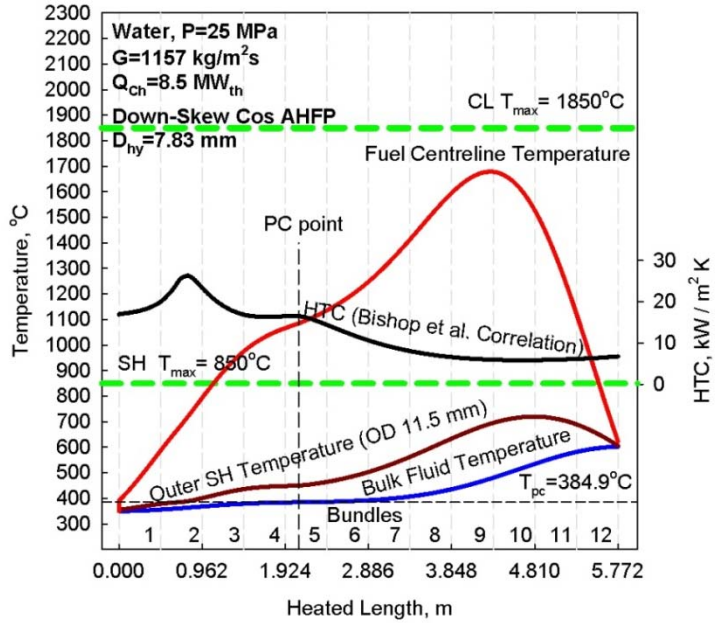

Figure 6.11. Temperature and HTC profiles for thoria fuel along heated length with downstream-skewed cosine AHFP (Grande et al., 2009).

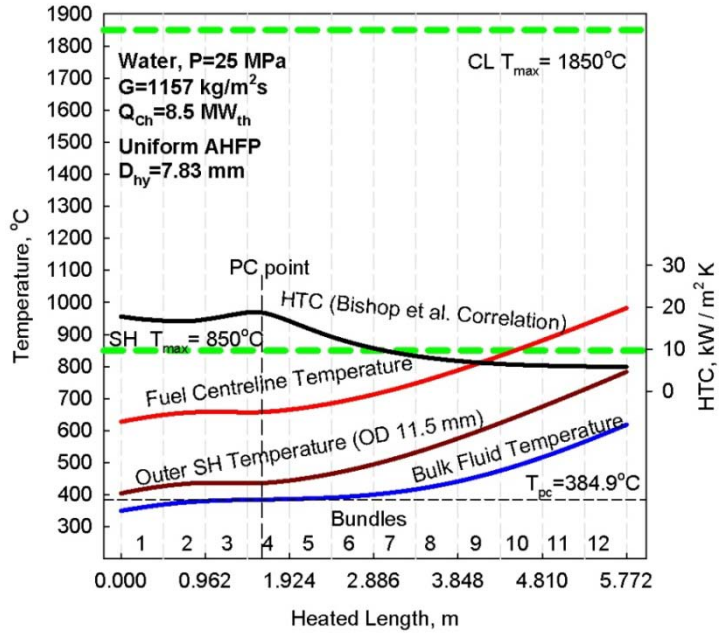

Figure 6.12. Temperature and HTC profiles for UC_2 fuel along heated length with uniform AHFP (Grande et al., 2011).

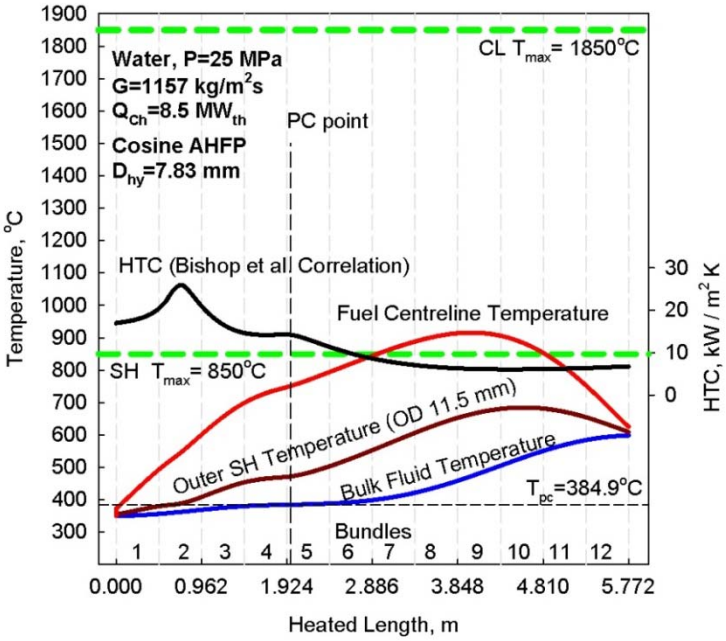

Figure 6.13 Temperature and HTC profiles for UC_2 fuel along heated length with cosine AHFP (Villamere et al., 2009).

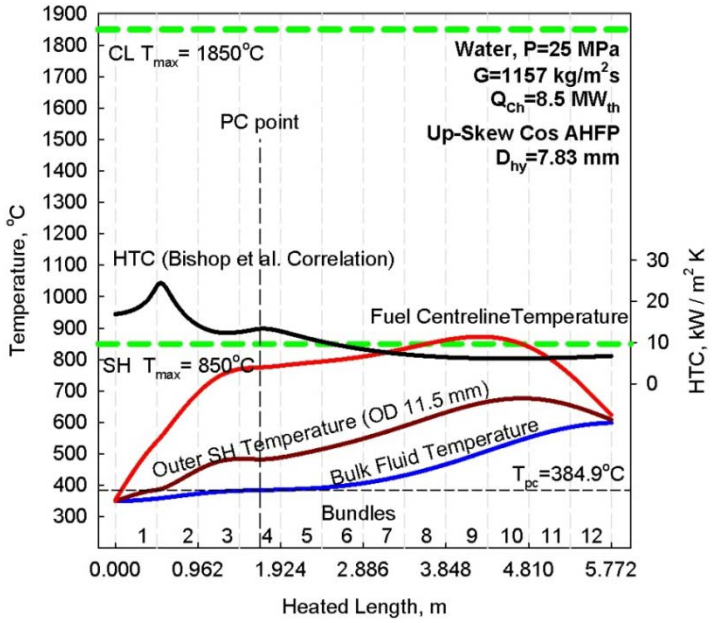

Figure 6.14. Temperature and HTC profiles for UC_2 fuel along heated length with upstream-skewed cosine AHFP (Grande et al., 2011).

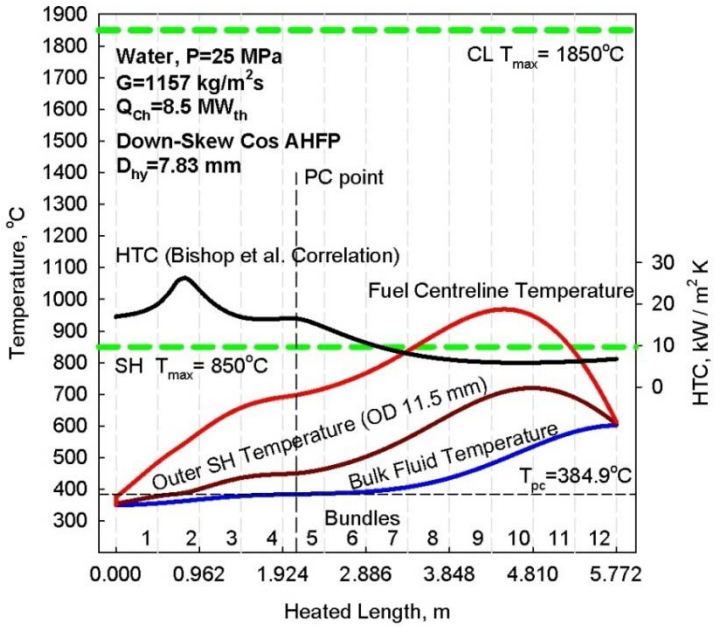

Figure 6.15. Temperature and HTC profiles for UC_2 fuel along heated length with downstream-skewed cosine AHFP (Grande et al., 2011).

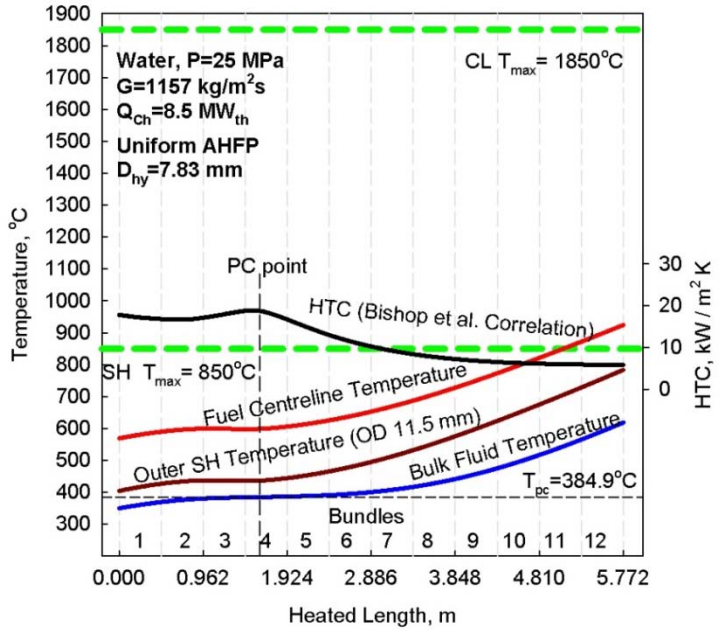

Figure 6.16. Temperature and HTC profiles for UN fuel along heated length with uniform AHFP (Grande et al., 2010c).

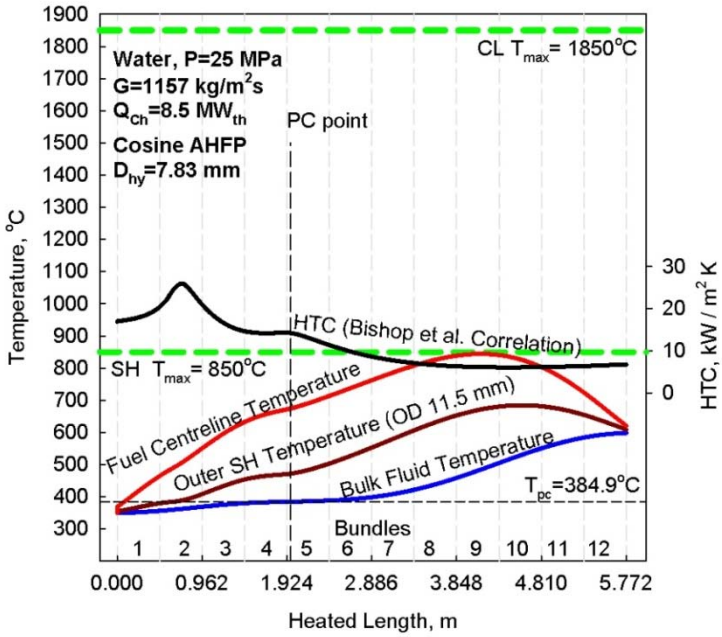

Figure 6.17. Temperature and HTC profiles for UN fuel along heated length with cosine AHFP.

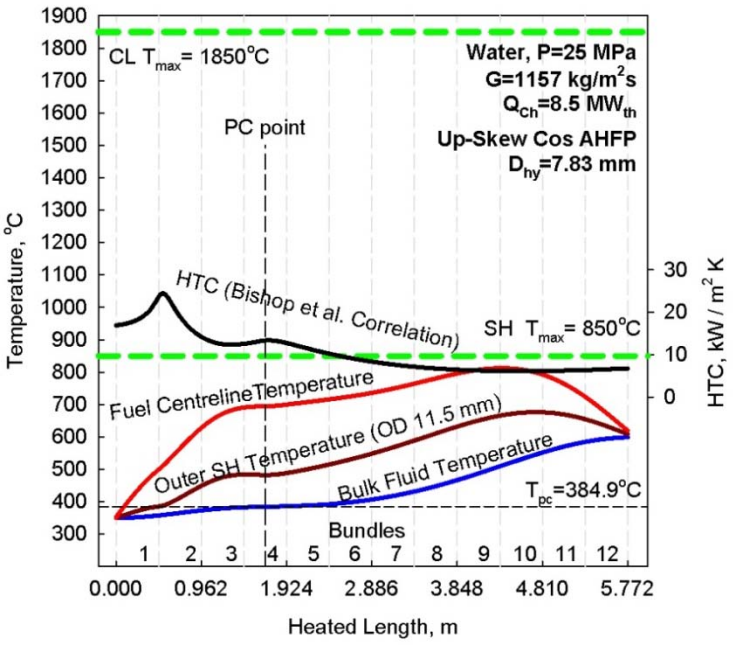

Figure 6.18. Temperature and HTC profiles for UN fuel along heated length with upstream-skewed cosine AHFP (Grande et al., 2010a).

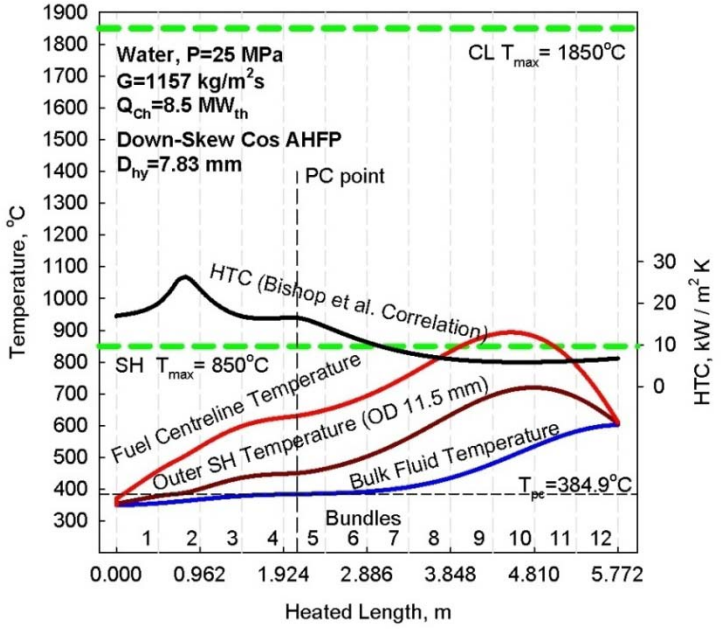

Figure 6.19. Temperature and HTC profiles for UN fuel along heated length with downstream-skewed cosine AHFP (Grande et al., 2010a).

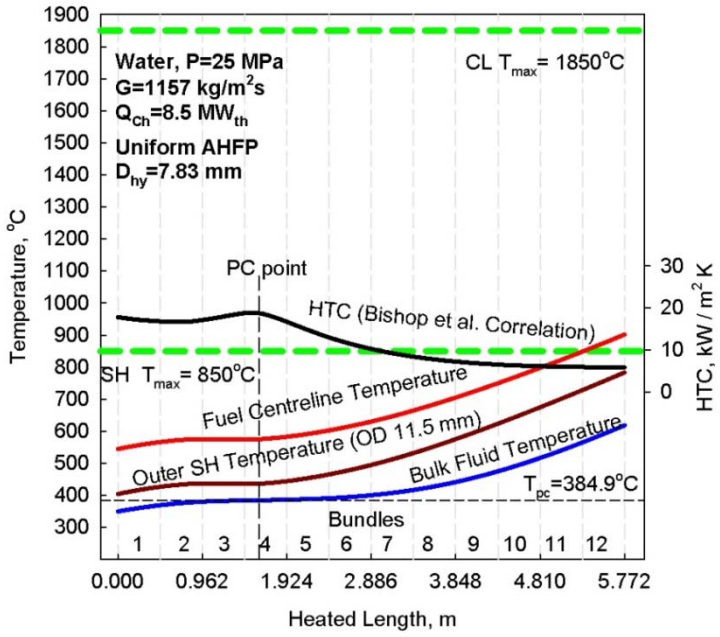

Figure 6.20. Temperature and HTC profiles for UC fuel along heated length with uniform AHFP (Grande et al., 2011).

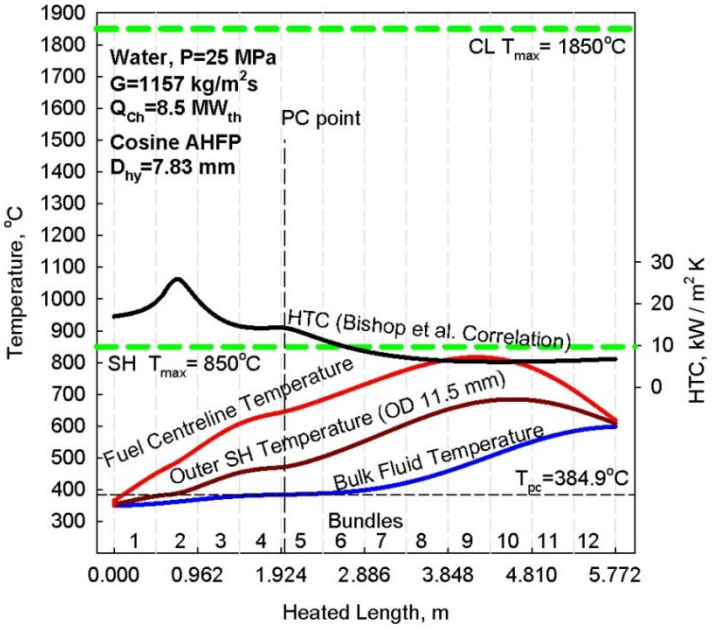

Figure 6.21. Temperature and HTC profiles for UC fuel along heated length with cosine AHFP (Grande et al., 2011).

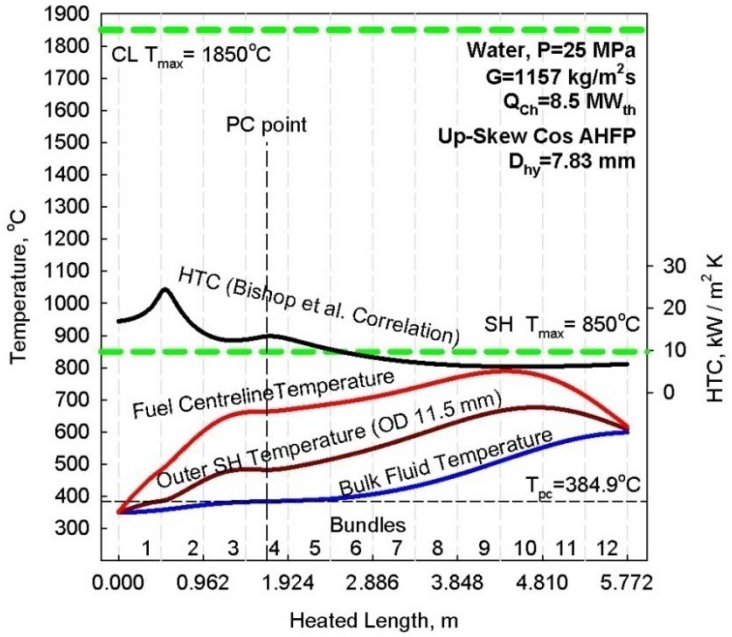

Figure 6.22. Temperature and HTC profiles for UC fuel along heated length with upstream-skewed cosine AHFP (Grande et al., 2011).

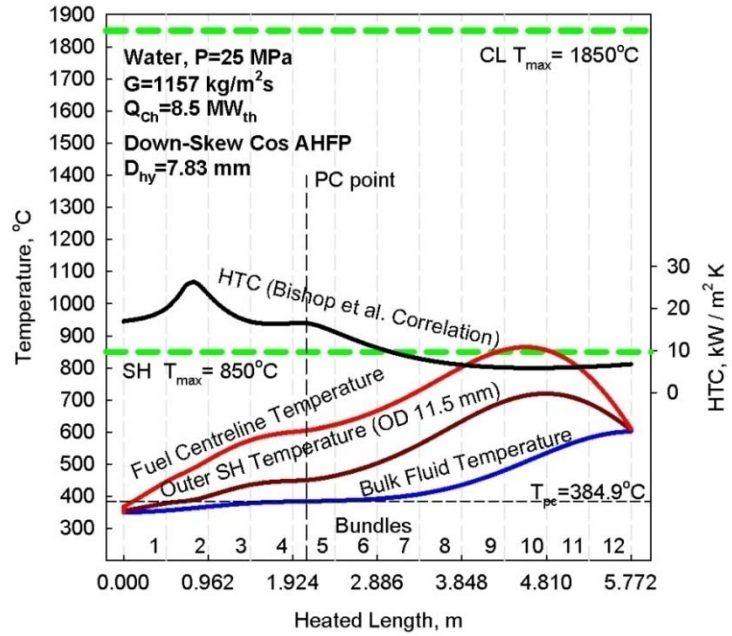

Figure 6.23. Temperature and HTC profiles for UC fuel along heated length with downstream-skewed cosine AHFP (Grande et al., 2011).

7 CONCLUSIONS

For all investigated cases the sheath design temperature limit of 850°C was not exceeded. The fuel centreline temperature industry limit of 1850°C was surpassed in the case of UO_2 fuel for some AHFPs (cosine and downstream-skewed cosine) and in the case of MOX fuel for all AHFPs (uniform, cosine, upstream-skewed cosine and downstream-skewed cosine). For UO_2 and MOX fuels to be suitable in SCWR applications bundle design might be modified and/or the channel power may be reduced. Thoria, UC_2, UN and UC are feasible SCWR nuclear fuels as their fuel centreline temperatures remain below the industry accepted limit of 1850°C. In addition, thoria offers an advantage of decreased dependency on uranium reserves. Uranium-nitride and carbide-based fuels are excellent options in SCWR applications compared to other fuels due to quite high thermal conductivity. However, some important properties of the new fuels gas release, swelling, cracking, and compatibility with SCW are not well known and require further investigation.

Inconel-600 seems to be the best sheath-material option compared to Inconel-718, stainless steel-304 and Zircaloys-2, because of higher mechanical strength at high pressures and temperatures.

8 FUTURE STUDIES

Future topics may include refining the computer code by removing some of the assumptions (i.e., accounting for changes in coolant pressure along the channel, acknowledging the effects of variations in fuel and sheath thermal conductivities due to neutron bombardment, and modeling of multiple channels). Additionally, with the construction of laboratory space in the new Energy Research Centre, it would be important to design and construct an experimental setup for supercritical water and modeling fluids, and to get experimental data not only in bare tubes, but also with bundle-flow geometries. Thermal-hydraulic analysis should be performed for the maximum channel power as the conservative approach compared to the average channel power. Due to this core-physics and neutronic calculations are essential for verifying AHFPs and cross-sectional power distribution in fuel channels.

9 REFERENCES

Allison, L., Grande, L., Villamere, B., Mikhael, S., Rodriguez-Prado, A., & Pioro, I. (2009). Uranium Carbide and Uranium Dicarbide in Axial Radial Uniform Heat Flux in SuperCritical Water-cooled nuclear Reactor. Proc. of ICONE 17 (p. 10). Brussels, Belgium: ASME.

Bishop, A., Sandberg, R., & Tong, L. (1964). Forced convection heat transfer to water at near-critical temperatures and super-critical pressures. Atomic Power Division. Pittsburgh, PA, USA: Westinghouse Electric Corporation.

Blumm, J., Lindemann, A., & Niedrig, B. (2005). Measurement of the thermophysical properties of an NPL thermal conductivity standard Inconel 600. Proc. of 17th European Conference on Thermophysical Properties, (pp. 621-626). Bratislava, Slovakia.

Boczar, P., Dyck, G., Chow, H., Sullivan, J., Cox, D., & Fehrenbach, P. (2002). CANDU advanced fuels and fuel cycles. 1 Proc. of 3th Pacific Basin Nuclear Conference, (p. 10). Shenzhen, China.

Bowman, A., Arnold, G., Witteman, W., & Wallace, T. (1966). Thermal expansion of uranium dicarbide and uranium sesquicarbide. J. of Nuclear Materials , 19, 111-112.

British Stainless Steel Association. (n.d.). Elevated temperature properties of stainless steels. Retrieved December 2, 2008, from http://www.bssa.org.uk/topics.php?article=139

Callister, W. (2003). Material Science and Engineering: An Introduction 6th Edition. USA: John Wiley and Sons, Inc.

Cengel, Y. (2007). Heat and mass transfer: a practicle approach 3rd Ed. New York, NY, USA: McGraw-Hill Companies Inc.

Chan, P., Alavi, P., Lau, J., Purdy, P., Rattan, D., Sejnoha, R., et al. (1999). An update on the design verification of CANFLEX fuel bundle. Proc. of 6th International CNS CANDU Fuel Conference (p. 6). Niagra Falls: CNS.

Chirkin, V. (1968). Thermophysical Properties of Materials for Nuclear Engineering, (In Russian). Moscow, Russia: Atomizdat Publ. House.

Choi, B., Ebbinghaus, J., Meie, T., & Ahn, J. (2006). Laboratory Directed Research and Development (LDRD) on mono-uranium nitride fuel development for SSTAR and space applications. Washington: U.S. Department of Energy.

Chow, C. K., & Khartabil, H. F. (2007). Conceptual Fuel Channel Designs for CANDU-SCWR. Nuclear Engineering and Technology, Special Issue on the 3RD International Symposium on SCWR, 40 (2), 8.

Cochran and Tsoulfanidis. (1999). The Nuclear Fuel Cycle: Analysis and Management; Second Edition. Illinois: American Nuclear Society.

DOE & GIF. (2002). A technology roadmap for Generation IV nuclear energy systems: Ten nations prepareing today for tomorrows energy needs . US DOE Nuclear Energy Research Advisory Committee and the Generation IV Internation Forum.

Duffey, R., & Hedges, K. (1999). Future CANDU reactor development. Proc. of ICONE 7 (p. 14). Tokyo, Japan: ASME.

Duffey, R. B., Pioro, I. L., & Sermet, A. K. (2008a). Advanced concepts for pressure-channel reactors: modularity, performance and safety. Journal of Power and Energy Systems , 112-121.

Duffey, R., Pioro, I., Zhou, T., Zirn, U., Kuran, S., Khartabil, H., et al. (2008b). Supercritical Water-Cooled Nuclear Reactors (SCWRs): Current and Future Concepts - Steam-Cycle Options. Proc. of ICONE 16 (p. 9). Florida, USA: ASME.

Fact-index. (n.d.). Thorium. Retrieved December 7, 2010, from http://www.fact-index.com//t/th/thorium.html

Gangulgy, C. (2005). The Thorium Fuel Cycle. Fissile Material Management Stragegies for Sustainable Nuclear Energy (pp. 769-804). Vienna, Austria: IAEA.

Grande, L., Villamere, B., Allison, L., Mikhael, S., Rodriguez-Prado, A., & Pioro, I. (2011). Thermal aspects of uranium carbide and uranium dicarbide fuels in supercritical water-cooled nuclear reactors. J. of Engineering for Gas Turbines and Power, 133, 7.

Grande, L., Peiman, W., Mikhael, S., Villamere, B., Rodriguez-Prado, A., Allison, L., et al. (2010a). Thermal aspects of using uranium nitride in supercritical water cooled nuclear reactors. Proc. of ICONE-18 (p. 8). Xi'an, China: ASME.

Grande, L., Peiman, W., Rodriguez-Prado, A., Villamere, B., Mikhael, S., Allison, L., et al. (2010b). Thermal aspects of using mixed oxide fuel in application to supercritical water-Cooled nuclear reactors. Proc. of 2nd Canada-China Joint Workshop on Supercritical Water-Cooled Reactors (CCSC 2010) (p. 11). Toronto, Canada: CNS.

Grande, L., Peiman, W., Villamere, B., Rodriguez-Prado, A., Mikhael, S., Allison, L., et al. (2010c). Thermal aspects of alternative fuels for use in supercritical water-cooled nuclear reactors. Proc. of 11th International Conference on CANDU fuel (p. 15). Niagra Falls, Ontario: CNS.

Grande, L., Rodriguez-Prado, A., Mikhael, S. V., Allison, L., & Pioro, I. (2010d). Thermal aspects of using uranium nitride, mixed oxide and thoria fuels as applied to supercritical water-cooled nuclear reactors. Proc. of 34th CNS/CAN Student Conference (p. 9). Montreal, Canada: CNS.

Grande, L., Villamere, B., Rodriguez-Prado, A., Mikhael, S., Allison, L., & Pioro, I. (2009). Thermal aspects of using thoria fuel in supercritical water-cooled nuclear reactors. Proc. of ICONE 17 (p. 10). Brussels, Belgium: ASME.

Greneche, D., Szymczak, W., Buchheit, J., Delpech, V. A., & Golfier, H. (2007). Rethinking the Thorium Fuel Cycle: An Industrial Point of View. Proc. of ICAPP 07. Nice, France: ICAPP.

Harrision, J. (1969). The irradiation-induced swelling of uranium carbide. J. of Nuclear Materials, 30, 319-323.

Hastings, I., Carter, T., DaSilva, R., Fehrenbach, P., Hardy, D., & Wood, J. (1983). CANDU fuel performance: influence of fabrication variables. IAEA/CNEA International Seminar on Heavy Water Fuel Technology (p. 13). San Carlos de Bariloche: IAEA.

Hayes, S. (1990). Material property correlations for uranium mononitride. I. Physical properties. Journal of Nuclear Materials , 171, 262-270.

IAEA Nuclear Fuel Cycle and Material Selection . (2005). Thorium fuel cycle - Potential benefits and challenges. Austria: IAEA.

IAEA Nuclear Power Technology Development Section. (2000). Thorium based fuel options for the generation of electricity: Developments in the 1990s. Vienna: IAEA.

IAEA. (2003). Status and Advances in MOX Fuel Technology. Vienna: IAEA.

Incorpera, F., Dewitt, D., Bergman, T., & Lavine, A. (2007). Fundementals of Heat and Mass Transfer; 6th edition. New Jersey: John Wiley & Sons, Inc.

International Bio-Analytical Industries, Inc. (n.d.). Retrieved December 8, 2010, from http://www.ibilabs.com/Uranium%20Carbide.htm

Jain, D., Pillai, C., Rao, B., Kulkarni, R., Ramdasan, E., & Sahoo, K. (2006). Thermal Diffusivity and Thermal Conductivity of Thoria-Lanthana Solid Solutions up to 10 mol.% $LaO_{1.5}$. J. of Nuclear Materials, 353, 35-41.

Kaplan, G.E. (Editor), 1960. Thorium, Its Resources, Chemistry and Technology (In Russian), Atomizdat Publ. House, Moscow, Russia.

Kingery, W.D. and Franch, J., 1954. Thermal Conductivity: X, Data for Several Pure Oxide Materials corrected to zero porosity, Journal of American Ceramic Society, Vol. 37, No. 2, Part II, p. 107.

Khartabil, H., Duffey, R., Spinks, N., & Diamond, W. (2005). The pressure-tube concept of Generation IV SuperCritical Water-cooled Reactor (SCWR): Overview and status. Proc. of ICAPP 05 (p.7) Paper No. 5564). Seoul, Korea: ICAPP.

Kirillov, P., Terent'eva, M., & Deniskina, N. (2007). Thermophysical Properties of Nuclear Engineering Materials, 2nd ed. revised and augmented. Atomizdat Publ. House, Moscow, Russia.

Koenig, J.H., 1958. New Development and Ceramics, Materials Design Engineering, Vol. 47, No. 5.

Kutz, M. (2006). Mechanical Engineers' handbook; 3rd edition. New Jersey: J. Wiley and Sons, Inc.

Lamarsh, J., & Baratta, A. (2001). Introduction to nuclear engineering; third editions. New Jersey: Prentice-Hall, Inc.

Lemmon, E., Huber, M., & McLinden, M. (2007). National Institute of Standards and Technology Reference Fluid Thermodynamic and Transport Properties— NIST REFPROP. Colorado: Department of Commerce.

Leshock, C. E., Kim, J., & Shin, Y. (2001). Plasma enhanced machining of Inconel 718: modeling of workpiece temperature with plasma heating and experimental results. International Journal of Machine Tools & Manufacture , 46 (14), 877-897.

Leung, L. (2008). Effect of CANDU bundle-geometry variation on dryout power. Proc. of ICONE 16. Paper #48827, p. 8. Orlando, Florida, USA: ASME.

Lombardi, C., Luzzi, L., Padovani, E., & Vettraino, F. (2008). Thoria and inert matrix fuels for a sustainable nuclear power. Progress in Nuclear Energy, 10.

Lucuta, P., Matzke, H., & Hastings, I. (1996). A pramagtic approach to modelling thermal conductivity of irradiated UO2 fuel: review and recommendations. J. of Nuclear Materials , 232, 166-180.

Matweb. (n.d.). Material Property Data. Retrieved December 2, 2008, from http://www.matweb.com/index.aspx

Mokry, S., Farah, A., King, K., Gupta, S., & Pioro, I. (2009). Development of supercritical waterheat-transfer correlation for vertical bare tubes. Proc. of International Conference Nuclear Energy for New Europe 2009, (p. 13). Bled, Slovenia.

Muzychka, Y., & Yovanovich, M. (1998). Modelling friction factors in non-circular ducts for developing laminar flow. 2nd AIAA Theoretical Fluid Mechanics Meeting (p. 12). Alburquerque, NM: AIAA.

Naidin, M., Pioro, I., Duffey, R., Mokry, S., Grande, L., Villamere, B, et al. (2009). SuperCritical Water-Cooled nuclear Reactors (SCWRs): Thermodynamic cycle options and thermal aspects of pressure-channel design. International Conference on Opportunities and Challenges for Water Cooled Reactors in the 21st Century. Book of Extended Synopses, pp. 134-155. Vienna, Austria: IAEA.

Naterer, G., Suppiah, S., Lewis, M., & Pioro, I. (2009). Recent Canadian advances in nuclear-based hydrogen production and the thermochemical Cu-Cl cycle. Int. J. of Hydrogen Energy (IJHE), 34, 2901-2917.

Naterer, G., Suppiah, S., Stolberg, L., & Pioro, I. (2010). Canada's program on nuclear hydrogen production and the thermochemical Cu-Cl Cycle. Int. J. of Hydrogen Energy (IJHE), 35, 1090- 10926.

Nikolz, P., (1963). Materials for nuclear reactors. Ceramic Combustion (In Russian), Atomizdat Publ. House, Moscow, Russia, p. 154.

Okhotin, A.S. (Editor), (1984). Thermal Conductivity of Solids, Energoatomizdat Publ. House, Moscow, Russia, 321.

Olander, D. (1976). Fundamental aspects of nuclear reactor fuel elements. National Technical Information Services.

Pioro, I., & Duffey, R. (2007). Heat transfer and hydraulic resistance at supercritcal pressures in power engineering applications. New York: ASME.

Pioro, I., Mokry, S., Peiman, W., Grande, L., & Saltanov, E. (2010). Supercritical water-cooled nuclear reactors: NPP layouts and thermal design options of pressure channels. Proc. of Pacific Basin Nuclear Conference (PBNC-2010), (p. 31). Cancun, Mexico.

Pioro, I., Khan, M., Hopps, V., Jacobs, C., R, P., Gopaul, S., et al. (2008). SCW Pressure Channel Nuclear Reactor. Some Design Features. JSME J. of Power and Energy Systems, 2 (2), 874-888.

Prins, G., & Gordfunke, E. (1980). Investigations of uranium carbonitrides. III. Nitrogen vapour pressure and thermodynamic properties. Journal of Nuclear Materials, 89, 221-228.

Sahin, S., Yalcun, S., Yildiz, K., Sahin, H., Acir, A., & Sahin, N. (2008). CANDU reactor as a minor actinide/thorium burner with uniform power density in the fuel bundle. Annals of Nuclear Energy, 35, 690-703.

Samuel, J., Harvel, G., & Pioro, I. (2010). Design concept and heat transfer anaylsis for a double pipe channel for SCWRs type reactors. Proc. of ICONE 18 (p. 8). Xi'an, China: ASME.

Special Metals. (n.d.). Inconel alloy 600. Retrieved December 2, 2008, from http://www.specialmetals.com/products/inconelalloy600.php

Trellue, H. (2006). Safety and neutronics: a comparison of MOX vs. UO_2 fuel. Progress in Nuclear Energy, 48, 135-145.

Villamere, B., Allison, L., Grande, L., Mikhael, S. R.-P., & Pioro, I. (2009). Thermal aspects for uranium carbide and uranium dicarbide fuels in supercritical water-cooled nuclear reactors. Proc. of ICONE 17 (p. 12). Brussels, Belgium: ASME.

World Nuclear Association. (2009, March). Mixed OXide (MOX) fuel. Retrieved March 26, 2009, from http://www.world-nuclear.org/info/inf29.html

Zhonsheng, X., & Boczar, P. (1999). CANDU fuel-cycle vision. China J. of Nuclear Power Engineering , 20, 18.

Appendix A - MATLAB Code for Uniform AHFP Analysis of Thoria

Bulk-fluid temperature profile

```
%%%%%%%%%%%%%%%%%%%%%%%%%%%%%%%%%%%%%%%%%%%%
%%%%%%%%%%%%%%%%%%%%%%%%%%%%%%%%%
%Calculating Tbulk for 5772 1mm intervals along the heated length of a    %
%fuel channel in a PT-type SCWR with 43 element 20 mm fuel    %
%bundle geometry with uniform AHFP.                              %
%%%%%%%%%%%%%%%%%%%%%%%%%%%%%%%%%%%%%%%%%%%%
%%%%%%%%%%%%%%%%%%%%%%%%%%%%%%%%%

clear;clc;
thermalPower = 2540 *10^6;  %Total thermal output of energy in W
massFlowRate = 1320 ;     %Total Flow rate in reactor in kg/s
numChannels = 300;         %Total number of channels in core
channelPower = thermalPower/numChannels;    %Power output of 1 channel
channelFlow = massFlowRate/numChannels;        %flow rate of 1 channel
inletTemperature = 623.15;     %Inlet Temperature of coolant in K
pressure = 25000;              %Pressure along channel assumed no drop(kPa)

%Enthalpy measured in J/kg
enthalpyBulkFluid(5773) = 0;
enthalpyBulkFluid(1) = refpropm('H','T',inletTemperature,'P',pressure,'water');

largeDiameter = 0.020; %center pin diameter(m)
largeElements = 1;      %center pin elements
smallDiameter = 0.0115; %outer rings have same diameter(m)
smallElements = 42;     %outer rings elements
innerPressureTubeDiameter = 0.1039; %measurement in meters
```

```
%calculates partial values because of multiple similar calculations for
%perimeter and area
pressureTubeArea = pi*innerPressureTubeDiameter^2/4;
pressureTubePerimeter = pi*innerPressureTubeDiameter;
largePerimeter = pi*largeDiameter*largeElements;
largeArea = pi*largeDiameter^2*largeElements/4;
smallPerimeter = pi*smallDiameter*smallElements;
smallArea = pi*smallDiameter^2*smallElements/4;
flowArea = pressureTubeArea - (largeArea+smallArea);
```

$$A_{flow} = A_{pt} - A_{fuel\ bundle}$$

```
wettedPerimeter = pressureTubePerimeter+largePerimeter+smallPerimeter;
massFlux = channelFlow/flowArea;
hydraulicDiameter = 4*flowArea/wettedPerimeter;
lenXsec = 0.001;
fullHeatLen = 5.772;    %full heated length of channel in m
crossSectionHeatedLength = 0.001:0.001:(fullHeatLen+0.001);
%This is the heated length which will be measured in (m)
%from 0.001 to 5.772 at 0.001m increments

fullHeatedArea = smallPerimeter*fullHeatLen;
%This calculates the full heated area of the fuel bundle

q = channelPower/fullHeatedArea;
%to determine the amount of power per area of fuel bundles in channel
```

$$\dot{q}_{ave} = \frac{\dot{Q}_{Ch}}{A_h}$$

```
%crossSectionHeatedArea = (largeHeatDiameter*crossSectionHeatedLength)...
%   +(smallHeatDiameter * crossSectionHeatedLength);
```

%Calculates the heated area of the cross section being observed

Memory allocation:

```
toGetCrossSection = 0;
crossSectionHeatedArea(5773) = 0;
bulkFluidTemperature(5773) = 0;
bulkFluidTemperature(1)=inletTemperature;
dynamicViscosity(5773) = 0;
dynamicViscosity(1) = refpropm('V','T',inletTemperature,'P',pressure,'water');
thermalConductivity(5773) = 0;
thermalConductivity(1) = refpropm('L','T',inletTemperature,'P',pressure,'water');
bulkFluidDensity(5773) = 0;
bulkFluidDensity(1) = refpropm('D','T',inletTemperature,'P',pressure,'water');
ReynoldsNumber(5773) = 0;
ReynoldsNumber(1) = massFlux*hydraulicDiameter/dynamicViscosity(1);
Q(5773) = 0;
heatFluxPermm(5773) = 0;

%Q = q*crossSectionHeatedArea;   %Power of the observed cross section
for i = 2:length(crossSectionHeatedLength)
   crossSectionHeatedArea(i-1) = (smallPerimeter...
      * crossSectionHeatedLength(i-1) - toGetCrossSection);
   toGetCrossSection = toGetCrossSection + crossSectionHeatedArea(i-1);
   Q(i-1) = q * crossSectionHeatedArea(i-1);
```

$$\dot{Q}_{loc.mm} = \dot{Q}_{loc.x+1} - \dot{Q}_{loc.x}$$

```
   heatFluxPermm(i-1) = Q(i-1) / (smallPerimeter*lenXsec);
```

$$\dot{q}_{loc.x} = \frac{\dot{Q}_{loc.mm}}{A_{mm}}$$

```
enthalpyBulkFluid(i) = (Q(i-1) / channelFlow) + enthalpyBulkFluid(i-1);
```

$$h_x = \frac{\dot{Q}_{loc_{mm}}}{\dot{m}} + h_{x-1}$$

```
    bulkFluidTemperature(i) = refpropm('T','H',enthalpyBulkFluid(i),'P',pressure,'water');
%Temperature measured in K
    dynamicViscosity(i) = refpropm('V','H',enthalpyBulkFluid(i),'P',pressure,'water');
    ReynoldsNumber(i) = massFlux*hydraulicDiameter/dynamicViscosity(i);
    thermalConductivity(i) = refpropm('L','H',enthalpyBulkFluid(i),'P',pressure,'water');
    bulkFluidDensity(i) = refpropm('D','H',enthalpyBulkFluid(i),'P',pressure,'water');
end
Q(5773) = q * crossSectionHeatedArea(5772);
heatFluxPermm(5773) = Q(5773) / (smallPerimeter*lenXsec);

tempWallEstimate(5773) = 0;
tempWallEst(5773) = 0;
tempWall(5773) = 0;
enthalpyWallEstimate(5773) = 0;
densityWallEstimate(5773) = 0;
avgPrandtlNumber(5773) = 0;
NusseltNumber(5773) = 0;
heatTransferCoef(5773) = 0;
PrandtlNumber(5773) = 0;
SpecificHeat(5773) = 0;
```

Iterations begin with an initial estimate for the bulk fluid at the next mm increment is 25 K greater than current location.

$$T_{o,sh} = T_b + 25\ K$$

For x = 0.001m

Iteration #1

$T_{o,sh,a} = 623.20\ K + 25\ K$

$T_{o,sh,a} = 648.20\ K$

```
for j = 1:length(bulkFluidTemperature)
   tempWallEstimate(j) = bulkFluidTemperature(j) + 25;
   tempDiff = tempWallEstimate(j) - bulkFluidTemperature(j);
   tempWall(j) = tempWallEstimate(j);
   tempWallEst(j) = tempWall(j);

   while (tempDiff > 0.5)
```

Stopping criteria is 0.5 K.

Iteration #1

Temp Diff = $T_{o,sh,a} - T_{o,sh,b}$

Temp Diff = 692.31 K - 648.20 K

Temp Diff = 44.11 K

This is greater than 0.5 K so proceed with iteration #2

Iteration #2

Temp Diff = $T_{o,sh,a} - T_{o,sh,b}$

Temp Diff = 688.82K – 670.23 K

Temp Diff = 18.59 K

This is greater than 0.5 K so proceed with iteration #3

Iteration #3

Temp Diff = $T_{o,sh,a}$ - $T_{o,sh,b}$

Temp Diff = 696.10 K – 679.55 K

Temp Diff = 16.55 K

This is greater than 0.5 K so proceed with iteration s until the stopping criteria is satisfied. The final wall temperature is 677.58 K when x is 0.001m.

To converge the iterations the proceeding bulk fluid estimate for next mm increment is the arithmetic average of current location.

```
tempWallEst(j) = (tempWallEst(j) + tempWall(j))/2;
```

Iteration #2

$T_{o,sh,a}$ = (692.31 K + 648.20)/2

$T_{o,sh,a}$ = 670.23 K

Iteration #3

$T_{o,sh,a}$ = (688.82K + 670.23 K)/2

$T_{o,sh,a}$ = 679.55 K

```
enthalpyWallEstimate(j) = refpropm('H', 'T',tempWallEst(j), 'P', pressure, 'water');
densityWallEstimate(j) = refpropm('D', 'T',tempWallEst(j), 'P', pressure, 'water');
avgSpecHeatConstPres = (enthalpyWallEstimate(j)-
enthalpyBulkFluid(j))/(tempWallEst(j)-bulkFluidTemperature(j));
avgPrandtlNumber(j) =
dynamicViscosity(j)*avgSpecHeatConstPres/thermalConductivity(j);
NusseltNumber(j) =
0.0069*ReynoldsNumber(j)^0.9*avgPrandtlNumber(j)^0.66*(densityWallEstimate(j)/bul
kFluidDensity(j))^0.43;
```

$$\mathbf{Nu}_x = 0.0069\mathbf{Re}_x^{0.9}\overline{\mathbf{Pr}_x}^{0.66}\left(\frac{\rho_w}{\rho_b}\right)_x^{0.43}$$

Iteration #1

Re = 94303.76

$\overline{\mathbf{Pr}}$ **=** 1.37

Nu = 231.95

Iteration #2

Re = 94303.76

$\overline{\mathbf{Pr}}$ **=**2.94

Nu = 244.27

Iteration #3

Re = 94303.76

$\overline{\mathbf{Pr}}$ **=** 2.76

Nu = 219.89

heatTransferCoef(j) = NusseltNumber(j)*thermalConductivity(j)/hydraulicDiameter;

tempWall(j) = q/heatTransferCoef(j) + bulkFluidTemperature(j);

$$T_{o,sh} = \frac{\dot{q}}{HTC} + T_b$$

For Iteration #1

HTC = 13987.88 W/m^2 K

$T_{o,sh,b}$ = 692.31 K

For Iteration #2

HTC = 1473.57 W/m^2 K

$T_{o,sh,b}$ = 688.82 K

For Iteration #3

HTC = 13260.62 W/m^2 K

$T_{o,sh,b}$ = 696.10 K

```
        tempDiff = tempWall(j) - tempWallEst(j);
    end
    enthalpyWallEstimate(j) = refpropm('H', 'T',tempWallEst(j), 'P', pressure, 'water');
    densityWallEstimate(j) = refpropm('D', 'T',tempWallEst(j), 'P', pressure, 'water');
    avgSpecHeatConstPres = (enthalpyWallEstimate(j)-
enthalpyBulkFluid(j))/(tempWallEst(j)-bulkFluidTemperature(j));
    avgPrandtlNumber(j) =
dynamicViscosity(j)*avgSpecHeatConstPres/thermalConductivity(j);
    SpecificHeat(j) = refpropm('C','T',bulkFluidTemperature(j),'P',pressure,'water');
    PrandtlNumber(j) = (SpecificHeat(j)*dynamicViscosity(j))/thermalConductivity(j);
    tempDiff = 0;
end
```

Conversion from Kelvin to Celcius.

```
BulkFluid=transpose(bulkFluidTemperature-273.15);
OuterSH=transpose(tempWall-273.15);
Bishop=transpose(heatTransferCoef/1000);
enthalpy=transpose(enthalpyBulkFluid);
xSecTemp=transpose(bulkFluidTemperature);
dynmcVis=transpose(dynamicViscosity);
thrmlCon=transpose(thermalConductivity);
blkFldDn=transpose(bulkFluidDensity);
entWlEst=transpose(enthalpyWallEstimate);
denWlEst=transpose(densityWallEstimate);
```

```
avgPrNum=transpose(avgPrandtlNumber);
avgSpHet=transpose(avgSpecHeatConstPres);
heatTrCo=transpose(heatTransferCoef);
wallTemp=transpose(tempWall);
walEsTmp=transpose(tempWallEst);
specHeat=transpose(SpecificHeat);
pranNumb=transpose(PrandtlNumber);
heatFlux=transpose(heatFluxPermm);

Output to tabs within an excel spreadsheet.
xlswrite('uniform.xlsx',BulkFluid,'BulkFluid','A1');
xlswrite('uniform.xlsx',Bishop,'Bishop','A1');
xlswrite('uniform.xlsx',OuterSH,'OuterSH','A1')
xlswrite('uniform.xlsx',enthalpy,'Enthalpies','A1');
xlswrite('uniform.xlsx',xSecTemp,'Temperatures','A1');
xlswrite('uniform.xlsx',dynmcVis,'DynamicViscosity','A1');
xlswrite('uniform.xlsx',thrmlCon,'ThermalConductivity','A1');
xlswrite('uniform.xlsx',blkFldDn,'BulkFluidDensity','A1');
xlswrite('uniform.xlsx',entWlEst,'EstimatedWallEnthalpy','A1');
xlswrite('uniform.xlsx',denWlEst,'EstimatedWallDensity','A1');
xlswrite('uniform.xlsx',avgPrNum,'AveragePrandtlNumber','A1');
xlswrite('uniform.xlsx',heatTrCo,'HeatTransferCoefficient','A1');
xlswrite('uniform.xlsx',wallTemp,'OuterSheathTemp','A1');
xlswrite('uniform.xlsx',walEsTmp,'WallEstimationSeconded','A1');
xlswrite('uniform.xlsx',specHeat,'SpecificHeat','A1');
xlswrite('uniform.xlsx',pranNumb,'PrandtlNumber','A1');
xlswrite('uniform.xlsx',heatFlux,'HeatFluxPermm','A1');
disp(flowArea)
disp(q)
disp(wettedPerimeter)
disp(massFlux)
```

```
disp(hydraulicDiameter)
disp(Q(1))
```

Outer-Sheath-Temperature Profile

```
%%%%%%%%%%%%%%%%%%%%%%%%%%%%%%%%%%%%%%%%%%%%%%%%%%%%%%%%%%%%%%%%%%%%%%%%%%%%%%%%%%%%%%%%%%%%%%%%%%
%Calculating Inner Sheath temperature for 5772 1mm intervals along the    %
%heated length of the fuel channel in PT-type SCWR reactor with       %
%43-element fuel bundle with 20 mm and Inconel-600 for the sheath material. %
%%%%%%%%%%%%%%%%%%%%%%%%%%%%%%%%%%%%%%%%%%%%%%%%%%%%%%%%%%%%%%%%%%%%%%%%%%%%%%%%%%%%%%%%%%%%%%%%%%

clear;clc;
thermalPower = 2540 *10^6;  %Total thermal output of energy in W
numChannels = 300;          %Total number of channels in core
channelPower = thermalPower/numChannels;    %Power output of 1 channel
```

Read in bulk-fluid-temperature profiles.

```
tempOuterSheath = xlsread ('uniform.xlsx','OuterSheathTemp');
heatFluxPerMilli = xlsread('uniform.xlsx','HeatFluxPermm');
```

Thermal conductivity of Inconel-600

$$k = 14.2214 + 0.01625\,T$$

```
thermalConductivity = 14.22143291+(0.01624506*tempOuterSheath);
```

```
largeDiameter = 0.020; %center pin diameter(m)
largeElements = 1;      %center pin
smallDiameter = 0.0115; %outer elements diameter(m)
smallElements = 42;     %number of outer elements

largeOuterRadius = largeDiameter/2;
largeInnerRadius = largeOuterRadius - 0.000747837036;
smallOuterRadius = smallDiameter/2;

Sheath thickness is 43 mm

smallInnerRadius = smallOuterRadius - 0.000430006296;

largePerimeter = pi*largeDiameter;
largeArea = pi*largeDiameter^2/4;
smallPerimeter = pi*smallDiameter;
smallArea = pi*smallDiameter^2/4;

lenXSec = 0.001;
fullHeatLen = 5.772;    %full heated length of channel in m
crossSectionLength = 0.001:0.001:(fullHeatLen+0.001);

%This calculates the full heated area of the fuel bundle
fullHeatedArea = smallPerimeter*smallElements*fullHeatLen;
givenKMO(5773) = 0;
calculatedKMO(5773) = 0;
deltaKMO(5773) = 0;
tempInnerSheathMO(5773)=0;

q = channelPower/fullHeatedArea;
```

$$\dot{q}_{ave} = \frac{\dot{Q}_{Ch}}{A_h}$$

powerPerSheathIMO = q *(smallOuterRadius*2*pi*lenXSec);

for j = 1:length(crossSectionLength)
  givenKMO(j) = thermalConductivity(j);
  calculatedKMO(j) = thermalConductivity(j);
  deltaKMO(j) = 1;

The stopping criteria for the sheath thermal conductivity is 0.05 W/m K

  while (deltaKMO(j) > 0.05)
    givenKMO(j) = calculatedKMO(j);
    tempInnerSheathMO(j) = (powerPerSheathIMO*log(smallOuterRadius/smallInnerRadius))/(2*pi*lenXSec*givenKMO(j))+tempOuterSheath(j);

$$T_{i,sh} = \frac{\dot{Q}_{sh,x} \ln\left(\frac{r_{o,sh}}{r_{i,sh}}\right)}{2\pi k_{sh}} + T_{o_{sh}}$$

The iterations begin by solving for inner sheath temperature ($T_{i,sh}$) when the thermal conductivity (k) is just based on the known outer sheath temperature (which corresponds to the temperature of the bulk fluid at the wall found by previous code).

When:
x = 0.0001 m
$T_{o,sh}$ = 677.53 K
k_a= 25.23 W/m K

Then:
$T_{i,sh}$ = 694.65 K

Then *k* is calculated based on the arithmetic average of the inner and outer sheath temperatures. Then $T_{i,sh}$ is calculated again. The differences of thermal fuel conductivity on based on the average sheath temperatures are compared to initial thermal conductivity value. If the difference is > 0.05 W/m K then iterations continues.

```
avgTempMO = (tempOuterSheath(j)+tempInnerSheathMO(j))/2;
calculatedKMO(j) = 14.22143291+(0.01624506*avgTempMO);
```

Iteration #1

k_b = 14.2214+0.01625 ((677.53 K +694.65 K)/2)

k_b = 25.37 W/m K

then $T_{i,sh}$ = 694.56 K

Compare sheath thermal conductivies:

$k_b - k_a > 0.05$ W/m K

25.37 W/m K - 25.23 W/m K > 0.05 W/m K

0.14 W/m K > 0.05 W/m K then proceed with Iteration #2 with $k_a = k_b$

Iteration #2

k_b = 14.2214+0.01625 ((677.53 K +694.56 K)/2)

k_b = 25.37 W/m K

then $T_{i,sh}$ = 694.56 K

Compare sheath thermal conductivies:

$k_b - k_a > 0.05$ W/m K

25.37 W/m K - 25.37 W/m K > 0.05 W/m K

0.00 W/m K < 0.05 W/m K then $T_{i,sh}$ = 694.56 K when x = 0.001 m

```
        deltaKMO(j) = abs(givenKMO(j) - calculatedKMO(j));
    end
end

InnerSheathMO = transpose(tempInnerSheathMO);
calcKMO = transpose(calculatedKMO);
changeOfKMO = transpose(deltaKMO);

Outputs inner-sheath-temperature profile to tabs within an excel file.
xlswrite('uni_SH.xlsx',calcKMO,'CalculatedThermalConductivities','A1');
xlswrite('uni_SH.xlsx',InnerSheathMO,'InnerSheathTemperatures','A1');
xlswrite('uni_SH.xlsx',changeOfKMO,'ChangeInThermalConductivity','A1');

disp(q)
```

Fuel-Centreline-Temperature Profile

```
%%%%%%%%%%%%%%%%%%%%%%%%%%%%%%%%%%%%%%%%%%%%%%%%%%%%%%%%%%%%%%%%%%%%%%%%%%%%
%Calculating the centerline fuel temperature for 5772 1mm intervals along %
%the heated length of a PT-type reactor with   %
%43-element fuel bundle with 20mm, Inconel 600 for the sheath material, and%
%the fuel being ThO2                                                      %
%%%%%%%%%%%%%%%%%%%%%%%%%%%%%%%%%%%%%%%%%%%%%%%%%%%%%%%%%%%%%%%%%%%%%%%%%%%%

clear;clc;
%Inputs
```

```
thermalPower = 2540 *10^6;  %Total thermal output of energy in W
numChannels = 300;          %Total number of channels in core
smallDiameter = 0.0115; %outer rings diameter(m)
smallElements = 42;     %outer rings elements
lenXSec = 0.001;
fullHeatLen = 5.772;    %full heated length of channel in m

%Calculations from previous programs used as inputs in this program
tempInnerSheath = xlsread('uni_SH.xlsx','InnerSheathTemperatures');

%Calculations
channelPower = thermalPower/numChannels;    %Power output of 1 channel
smallOuterRadius = smallDiameter/2;
smallInnerRadius = smallOuterRadius - 0.000430006296;

Dividing the fuel-element radius into 5 increments.

smRadiusFive = smallInnerRadius;
smRadiusFour = smallInnerRadius-(1/5*smallInnerRadius);
smRadiusThree = smallInnerRadius-(2/5*smallInnerRadius);
smRadiusTwo = smallInnerRadius-(3/5*smallInnerRadius);
smRadiusOne = smallInnerRadius-(4/5*smallInnerRadius);
smRadiusZero = smallInnerRadius-(5/5*smallInnerRadius);
smallPerimeter = pi*smallDiameter;
smallArea = pi*smallDiameter^2/4;
crossSectionLength = 0.001:0.001:(fullHeatLen+0.001);
fullHeatedArea = smallPerimeter*smallElements*fullHeatLen; % full heated area of
channel

q = channelPower/fullHeatedArea;
powerPerSheathIMO = q * (smallOuterRadius*2*pi*lenXSec);
```

heatGenRateIMO = powerPerSheathIMO/(smallInnerRadius^2*pi*lenXSec);

$$\dot{e}_{gen,mm} = \frac{\dot{Q}_{loc,mm}}{D_{i,sh}{}^2 \pi (0.001m)}$$

```
%Allocations of memory
smSurfaceTempOne(5773) = 0;
smSurfaceTempTwo(5773) = 0;
smSurfaceTempThree(5773) = 0;
smSurfaceTempFour(5773) = 0;
smSurfaceTempFive(5773) = 0;
thermalConductivityFuelIMO(5773) = 0;
givenKIMOFuel(5773) = 0;
calcFuelKOne(5773) = 0;
calcFuelKTwo(5773) = 0;
calcFuelKThr(5773) = 0;
calcFuelKFou(5773) = 0;
calcFuelKFiv(5773) = 0;
deltaKIMOFuel(5773) = 0;
tempCenterlineIMO(5773)=0;

for i = 1:1:length(crossSectionLength)

   % thermal conductivity of thoria
   thermalConductivityFuelIMO(i) = 1/(0.0327 + (1.603*10^-4*tempInnerSheath(i)));

   givenKIMOFuel(i) = thermalConductivityFuelIMO(i);
   calcFuelKOne(i) = thermalConductivityFuelIMO(i);
   deltaKIMOFuel(i) = 1;
```

Thermal conductivity iteration stopping criteria is 0.05 K for first increment.

```
   while (deltaKIMOFuel(i) > 0.05)
```

```
    givenKIMOFuel(i) = calcFuelKOne(i);
    smSurfaceTempOne(i) = tempInnerSheath(i) +
((heatGenRateIMO*(smRadiusFive^2-smRadiusFour^2))/(4*givenKIMOFuel(i)));
```

$$T_{n-1} = \frac{\dot{e}_{gen,mm}\left[{r_{i,sh,n}}^2 - {r_{i,sh,n-1}}^2\right]}{4\,k_{fuel}} + T_n$$

The iterations begin by solving for fuel pellet temperature for each of the radial increments. The last increment determines the fuel centreline temperature. The first increment starts at the surface pellet (T_5) and is equal to $T_{i,sh}$ (694.56 K), T_4 is unknown. The thermal conductivity of the fuel (k_{fuel}) is determined initially based on T_5.

```
    avgTempCenterlineIMO = (tempInnerSheath(i)+smSurfaceTempOne(i))/2;

    %% thermal conductivity of thoria
    calcFuelKOne(i) = 1/(0.0327 + (1.603*10^-4*avgTempCenterlineIMO));

    deltaKIMOFuel(i) = abs(givenKIMOFuel(i) - calcFuelKOne(i));
    end
```

When:

x = 0.0001 m

T_5 = 694.56 K

k_a= 6.94 W/m K

Then:

T_4 = 838.67 K

Then k_{fuel} is calculated based on the arithmetic average of the inner and outer sheath temperatures. Then T_4 is calculated again. The differences of thermal fuel conductivity on based on the average sheath temperatures are compared to initial thermal conductivity value. If the difference is > 0.05 W/m K then iterations continues.

Iteration #1

k_b = 1/(0.0327 + (1.603*10^-4* (694.56 K +838.67 K)/2)

k_b = 6.43 W/m K

then T_4 = 850.23 K

Compare sheath thermal conductivies:

$k_a - k_b$ > 0.05 W/m K

6.94 W/m K - 6.43 W/m K > 0.05 W/m K

0.52 W/m K > 0.05 W/m K then proceed with Iteration #2 with $k_a = k_b$

Iteration #2

k_b = 1/(0.0327 + (1.603*10^-4* (694.56 K +850.23 K)/2)

k_b = 6.39 W/m K

then T_4= 851.17 K

Compare sheath thermal conductivies:

$k_a - k_b$ > 0.05 W/m K

6.43 W/m K – 6.39 W/m K > 0.05 W/m K

0.04 W/m K < 0.05 W/m K then T_4= 851.17 K when x = 0.001 m

- deltaKIMOFuel(i) = 1;
- smSurfaceTempOne(i) = tempInnerSheath(i) + ((heatGenRateIMO*(smRadiusFive^2-smRadiusFour^2))/(4*calcFuelKOne(i)));

- calcFuelKTwo(i) = calcFuelKOne(i);

Thermal conductivity iteration stopping criteria is 0.05 K for second increment.

```
while (deltaKIMOFuel(i) > 0.05)
    givenKIMOFuel(i) = calcFuelKTwo(i);
    smSurfaceTempTwo(i) = smSurfaceTempOne(i) +
((heatGenRateIMO*(smRadiusFour^2-smRadiusThree^2))/(4*givenKIMOFuel(i)));

    avgTempCenterlineIMO = (smSurfaceTempTwo(i)+smSurfaceTempOne(i))/2;

    %% thermal conductivity of thoria
    calcFuelKTwo(i) = 1/(0.0327 + (1.603*10^-4*avgTempCenterlineIMO));

    deltaKIMOFuel(i) = abs(givenKIMOFuel(i) - calcFuelKTwo(i));
end
deltaKIMOFuel(i) = 1;
smSurfaceTempTwo(i) = smSurfaceTempOne(i) +
((heatGenRateIMO*(smRadiusFour^2-smRadiusThree^2))/(4*calcFuelKTwo(i)));
```

$$T_{n-1} = \frac{\dot{e}_{gen,mm}\left[{r_{i,sh,n}}^2 - {r_{i,sh,n-1}}^2\right]}{4\,k_{fuel}} + T_n$$

```
calcFuelKThr(i) = calcFuelKTwo(i);
```

Thermal conductivity iteration stopping criteria is 0.05 K for third increment.

```
   while (deltaKIMOFuel(i) > 0.05)
      givenKIMOFuel(i) = calcFuelKThr(i);
      smSurfaceTempThree(i) = smSurfaceTempTwo(i) +
((heatGenRateIMO*(smRadiusThree^2-smRadiusTwo^2))/(4*givenKIMOFuel(i)));


      avgTempCenterlineIMO = (smSurfaceTempThree(i)+smSurfaceTempTwo(i))/2;

          %% thermal conductivity of thoria
      calcFuelKThr(i) = 1/(0.0327 + (1.603*10^-4*avgTempCenterlineIMO));

      deltaKIMOFuel(i) = abs(givenKIMOFuel(i) - calcFuelKThr(i));
   end
   deltaKIMOFuel(i) = 1;
   smSurfaceTempThree(i) = smSurfaceTempTwo(i) +
((heatGenRateIMO*(smRadiusThree^2-smRadiusTwo^2))/(4*calcFuelKThr(i)));
```

$$T_{n-1} = \frac{\dot{e}_{gen,mm}\left[{r_{i,sh,n}}^2 - {r_{i,sh,n-1}}^2\right]}{4\ k_{fuel}} + T_n$$

```
   calcFuelKFou(i) = calcFuelKThr(i);
```

Thermal conductivity iteration stopping criteria is 0.05 K for fourth increment.

```
   while (deltaKIMOFuel(i) > 0.05)
      givenKIMOFuel(i) = calcFuelKFou(i);
      smSurfaceTempFour(i) = smSurfaceTempThree(i) +
((heatGenRateIMO*(smRadiusTwo^2-smRadiusOne^2))/(4*givenKIMOFuel(i)));

      avgTempCenterlineIMO = (smSurfaceTempFour(i)+smSurfaceTempThree(i))/2;
```

```
        %% thermal conductivity of thoria
        calcFuelKFou(i) = 1/(0.0327 + (1.603*10^-4*avgTempCenterlineIMO));

        deltaKIMOFuel(i) = abs(givenKIMOFuel(i) - calcFuelKFou(i));
    end
    deltaKIMOFuel(i) = 1;
    smSurfaceTempFour(i) = smSurfaceTempThree(i) +
((heatGenRateIMO*(smRadiusTwo^2-smRadiusOne^2))/(4*calcFuelKFou(i)));
    calcFuelKFiv(i) = calcFuelKFou(i);
```

$$T_{n-1} = \frac{\dot{e}_{gen,mm}\left[r_{i,sh,n}{}^2 - r_{i,sh,n-1}{}^2\right]}{4\,k_{fuel}} + T_n$$

Thermal conductivity iteration stopping criteria is 0.05 K for fifth increment.

```
    while (deltaKIMOFuel(i) > 0.05)
        givenKIMOFuel(i) = calcFuelKFiv(i);
        smSurfaceTempFive(i) = smSurfaceTempFour(i) +
((heatGenRateIMO*(smRadiusOne^2-smRadiusZero^2))/(4*givenKIMOFuel(i)));

        avgTempCenterlineIMO = (smSurfaceTempFive(i)+smSurfaceTempFour(i))/2;

        %% thermal conductivity of thoria
        calcFuelKFiv(i) = 1/(0.0327 + (1.603*10^-4*avgTempCenterlineIMO));

        deltaKIMOFuel(i) = abs(givenKIMOFuel(i) - calcFuelKFiv(i));
    end
    smSurfaceTempFive(i) = smSurfaceTempFour(i) +
((heatGenRateIMO*(smRadiusOne^2-smRadiusZero^2))/(4*calcFuelKFiv(i)));
```

$$T_{n-1} = \frac{\dot{e}_{gen,mm}\left[{r_{i,sh,n}}^2 - {r_{i,sh,n-1}}^2\right]}{4\,k_{fuel}} + T_n$$

```
    tempCenterlineIMO(i) = smSurfaceTempFive(i);
end

smSurTempOne = transpose(smSurfaceTempOne);
smSurTempTwo = transpose(smSurfaceTempTwo);
smSurTempThree = transpose(smSurfaceTempThree);
smSurTempFour = transpose(smSurfaceTempFour);
smSurTempFive = transpose(smSurfaceTempFive);
fuelkone = transpose(calcFuelKOne);
fuelktwo = transpose(calcFuelKTwo);
fuelkthr = transpose(calcFuelKThr);
fuelkfou = transpose(calcFuelKFou);
fuelkfiv = transpose(calcFuelKFiv);
centerlineIMO = transpose(tempCenterlineIMO-273.15);
changeOfKIMOFuel = transpose(deltaKIMOFuel);

Outputs fuel-centreline-temperature profile to tabs within an excel spreadsheet
xlswrite('ThO2_uni_FC.xlsx',smSurTempOne,'SmallPinSurfaceTempOne','A1');
xlswrite('ThO2_uni_FC.xlsx',smSurTempTwo,'SmallPinSurfaceTempTwo','A1');
xlswrite('ThO2_uni_FC.xlsx',smSurTempThree,'SmallPinSurfaceTempThree','A1');
xlswrite('ThO2_uni_FC.xlsx',smSurTempFour,'SmallPinSurfaceTempFour','A1');
xlswrite('ThO2_uni_FC.xlsx',smSurTempFive,'SmallPinSurfaceTempFive','A1');
xlswrite('ThO2_uni_FC.xlsx',fuelkone,'ThermCondSurface1','A1');
xlswrite('ThO2_uni_FC.xlsx',fuelktwo,'ThermCondSurface2','A1');
xlswrite('ThO2_uni_FC.xlsx',fuelkthr,'ThermCondSurface3','A1');
xlswrite('ThO2_uni_FC.xlsx',fuelkfou,'ThermCondSurface4','A1');
xlswrite('ThO2_uni_FC.xlsx',fuelkfiv,'ThermCondSurface5','A1');
xlswrite('ThO2_uni_FC.xlsx',centerlineIMO,'IMOCenterlineTemperatures','A1');
```

```
xlswrite('ThO2_uni_FC.xlsx',changeOfKIMOFuel,'IMOChangeInThermalConductivity','
A1');

disp(q)
disp(length(crossSectionLength))
```

Appendix B - MATLAB Code for Cosine AHFP Analysis of Thoria

Bulk-Fluid-Temperature Profile

```
%%%%%%%%%%%%%%%%%%%%%%%%%%%%%%%%%%%%%%%%%%%%%%%%%%%
%%%%%%%%%%%%%%%%%%%%%%%%%%%%%%%%%%%%%%
% Calculating Tbulk for 5772 1mm intervals along the heated length of a    %
%fuel channel in a PT-type SCWR with 43 element 20 mm fuel    %
%bundle geometry with cosine AHFP.                                %
                          %
%%%%%%%%%%%%%%%%%%%%%%%%%%%%%%%%%%%%%%%%%%%%%%%%%%%
%%%%%%%%%%%%%%%%%%%%%%%%%%%%%%%%%%%%%%

clear;clc;
%Inputs
thermalPower = 2540 *10^6;  %Total thermal output of energy in W
massFlowRate = 1320 ;     %Total Flow rate in reactor in kg/s
numChannels = 300;         %Total number of channels in core
inletTemperature = 623.15;     %Inlet Temperature of coolant in K
pressure = 25000;             %Pressure along channel assumed no drop(kPa)
largeDiameter = 0.020;  %center pin diameter in m
largeElements = 1;      %center number of elements
smallDiameter = 0.0115; %inner, middle, and outer ring diameter in m
smallElements = 42;     %inner, middle, and outer number of rings
innerPressureTubeDiameter = 0.1039;
fullHeatLen = 5.772;    %full heated length of channel in m
lenXSec = 0.001;

%calculated values based off inputs
channelPower = thermalPower/numChannels;    %Power output of 1 channel
channelFlow = massFlowRate/numChannels;        %flow rate of 1 channel
```

pressureTubeArea = pi*innerPressureTubeDiameter^2/4;

pressureTubePerimeter = pi*innerPressureTubeDiameter;

largePerimeter = pi*largeDiameter*largeElements;

largeArea = pi*largeDiameter^2*largeElements/4;

smallPerimeter = pi*smallDiameter*smallElements;

smallArea = pi*smallDiameter^2*smallElements/4;

flowArea = pressureTubeArea - (largeArea+smallArea);

$$A_{flow} = A_{pt} - A_{fuel\ bundle}$$

wettedPerimeter = pressureTubePerimeter+largePerimeter+smallPerimeter;

$$p_{wetted} = \pi\left(N_c D_c + N_{ir} D_{ir} + N_{mr} D_{mr} + N_{or} D_{or} + D_{pt}\right)$$

massFlux = channelFlow/flowArea;

hydraulicDiameter = 4*flowArea/wettedPerimeter;

$$D_{hy} = \frac{4\ A_{flow}}{P_{wetted}}$$

crossSectionHeatedLength = 0.001:0.001:(fullHeatLen+0.001);

fullHeatedArea = smallPerimeter*fullHeatLen;

heatFluxPermm(5773) = 0;

heatFluxChannel = channelPower/fullHeatedArea;

Cosine 6th degree polynomial coefficients.

%%%Cosine%%%

a6 = 1.034737548; a5 = -17.492065458; a4 = 108.026091454174; a3 = -291.249861406696; a2 = 149.037875985652/3000; a1 = 854.931825569044/2000; a0 = 79.2530215467826;

powerCosineEquation(5773) = 0;

count = 2;

```
toGetCrossSection = 0;
for i = 0.001:0.001:(fullHeatLen+0.001)
   powerCosineEquation(count) = a6*i^7 + a5*i^6 + a4*i^5 + a3*i^4 + a2*i^3 + a1*i^2
+ a0*i^1 - toGetCrossSection;
```

$$\int_0^x \dot{q}'_{loc} dx = a_0 \frac{1}{1} x + a_1 \frac{1}{2} x^2 + a_2 \frac{1}{3} x^3 + a_3 \frac{1}{4} x^4 + a_4 \frac{1}{5} x^5 + a_5 \frac{1}{6} x^6 + a_6 \frac{1}{7} x^7$$

```
   toGetCrossSection = toGetCrossSection + powerCosineEquation(count);
   count = count + 1;
end

%Enthalpy measured in J/kg
enthalpyBulkFluid(5773) = 0;
enthalpyBulkFluid(1) = refpropm('H','T',inletTemperature,'P',pressure,'water');
bulkFluidTemperature(5773) = 0;
bulkFluidTemperature(1)=inletTemperature;
dynamicViscosity(5773) = 0;
dynamicViscosity(1) = refpropm('V','T',inletTemperature,'P',pressure,'water');
thermalConductivity(5773) = 0;
thermalConductivity(1) = refpropm('L','T',inletTemperature,'P',pressure,'water');
bulkFluidDensity(5773) = 0;
bulkFluidDensity(1) = refpropm('D','T',inletTemperature,'P',pressure,'water');
ReynoldsNumber(5773) = 0;
ReynoldsNumber(1) = massFlux*hydraulicDiameter/dynamicViscosity(1);
Q(5773) = 0;
tempWallEstimate(5773) = 0;
tempWallEst(5773) = 0;
tempWall(5773) = 0;
enthalpyWallEstimate(5773) = 0;
densityWallEstimate(5773) = 0;
```

```
avgPrandtlNumber(5773) = 0;
NusseltNumber(5773) = 0;
heatTransferCoef(5773) = 0;
SpecificHeat(5773) = 0;
avgSpecHeatConstPres(5773) = 0;
PrandtlNumber(5773) = 0;

for i = 2:length(crossSectionHeatedLength)
   Q(i-1) = smallPerimeter*heatFluxChannel*powerCosineEquation(i-1);
```

$$\dot{Q}_{loc_x} = p_h q_{ave} \int_0^x q'_{loc} dx$$

```
   heatFluxPermm(i-1) = Q(i-1)/(smallPerimeter*lenXSec);
```

$$\dot{q}_{loc.x} = \frac{\dot{Q}_{loc.mm}}{A_{mm}}$$

```
   enthalpyBulkFluid(i) = (Q(i-1) / channelFlow) + enthalpyBulkFluid(i-1);
```

$$h_x = \frac{\dot{Q}_{loc_{mm}}}{\dot{m}} + h_{x-1}$$

```
   bulkFluidTemperature(i) = refpropm('T','H',enthalpyBulkFluid(i),'P',pressure,'water');
%Temperature measured in K
   dynamicViscosity(i) = refpropm('V','H',enthalpyBulkFluid(i),'P',pressure,'water');
   ReynoldsNumber(i) = massFlux*hydraulicDiameter/dynamicViscosity(i);
   thermalConductivity(i) = refpropm('L','H',enthalpyBulkFluid(i),'P',pressure,'water');
   bulkFluidDensity(i) = refpropm('D','H',enthalpyBulkFluid(i),'P',pressure,'water');
end
Q(5773) = smallPerimeter*heatFluxChannel*powerCosineEquation(5773);
heatFluxPermm(5773) = Q(5773)/(smallPerimeter*lenXSec);

for j = 1:length(bulkFluidTemperature)
```

Iterations begin with an initial estimate for the bulk fluid at the next mm increment is 25 K greater than current location.

$T_{o,sh} = T_b + 25$ K

```
tempWallEstimate(j) = bulkFluidTemperature(j) + 25;
tempDiff = tempWallEstimate(j) - bulkFluidTemperature(j);
tempWall(j) = tempWallEstimate(j);
tempWallEst(j) = tempWallEstimate(j);
```

Stopping criteria is 0.5 K.

```
while (tempDiff > 0.5)
    tempWallEst(j) = (tempWallEst(j) + tempWall(j))/2;
    enthalpyWallEstimate(j) = refpropm('H', 'T',tempWallEst(j), 'P', pressure, 'water');
    densityWallEstimate(j) = refpropm('D', 'T',tempWallEst(j), 'P', pressure, 'water');
    avgSpecHeatConstPres(j) = (enthalpyWallEstimate(j)-
enthalpyBulkFluid(j))/(tempWallEst(j)-bulkFluidTemperature(j));
    avgPrandtlNumber(j) =
dynamicViscosity(j)*avgSpecHeatConstPres(j)/thermalConductivity(j);
    NusseltNumber(j) =
0.0069*ReynoldsNumber(j)^0.9*avgPrandtlNumber(j)^0.66*(densityWallEstimate(j)/bul
kFluidDensity(j))^0.43;
```

$$\mathbf{Nu}_x = 0.0069\mathbf{Re}_x^{0.9}\overline{\mathbf{Pr}_x}^{0.66}\left(\frac{\rho_w}{\rho_b}\right)_x^{0.43}$$

```
    heatTransferCoef(j) = NusseltNumber(j)*thermalConductivity(j)/hydraulicDiameter;
    tempWall(j) = heatFluxPermm(j)/heatTransferCoef(j) + bulkFluidTemperature(j);
```

$$T_{o,sh} = \frac{\dot{q}}{HTC} + T_b$$

```
    SpecificHeat(j) = refpropm('C','T',bulkFluidTemperature(j),'P',pressure,'water');
    PrandtlNumber(j) = (SpecificHeat(j)*dynamicViscosity(j))/thermalConductivity(j);
```

```
        tempDiff = abs(tempWall(j) - tempWallEst(j));
    end
    enthalpyWallEstimate(j) = refpropm('H', 'T',tempWall(j), 'P', pressure, 'water');
    densityWallEstimate(j) = refpropm('D', 'T',tempWall(j), 'P', pressure, 'water');
    avgSpecHeatConstPres(j) = (enthalpyWallEstimate(j)-
enthalpyBulkFluid(j))/(tempWall(j)-bulkFluidTemperature(j));
    avgPrandtlNumber(j) =
dynamicViscosity(j)*avgSpecHeatConstPres(j)/thermalConductivity(j);
   tempDiff = 0;
end

enthalpy=transpose(enthalpyBulkFluid);
xSecTemp=transpose(bulkFluidTemperature);
dynmcVis=transpose(dynamicViscosity);
thrmlCon=transpose(thermalConductivity);
blkFldDn=transpose(bulkFluidDensity);
entWlEst=transpose(enthalpyWallEstimate);
denWlEst=transpose(densityWallEstimate);
avgPrNum=transpose(avgPrandtlNumber);
heatTrCo=transpose(heatTransferCoef);
wallTemp=transpose(tempWall);
walEsTmp=transpose(tempWallEst);
QPowered=transpose(Q);
cosinePo=transpose(powerCosineEquation);
crossSec=transpose(toGetCrossSection);
heatFlux=transpose(heatFluxPermm);
specheat=transpose(SpecificHeat);
avgspcht=transpose(avgSpecHeatConstPres);
pranumbr=transpose(PrandtlNumber);
```

Output to tabs within an excel spreadsheet.

```
xlswrite('Cosine.xlsx',enthalpy,'Enthalpies','A1');
xlswrite('Cosine.xlsx',xSecTemp,'Temperatures','A1');
xlswrite('Cosine.xlsx',dynmcVis,'DynamicViscosity','A1');
xlswrite('Cosine.xlsx',thrmlCon,'ThermalConductivity','A1');
xlswrite('Cosine.xlsx',blkFldDn,'BulkFluidDensity','A1');
xlswrite('Cosine.xlsx',entWlEst,'EstimatedWallEnthalpy','A1');
xlswrite('Cosine.xlsx',denWlEst,'EstimatedWallDensity','A1');
xlswrite('Cosine.xlsx',avgPrNum,'AveragePrandtlNumber','A1');
xlswrite('Cosine.xlsx',heatTrCo,'HeatTransferCoefficient','A1');
xlswrite('Cosine.xlsx',wallTemp,'OuterSheathTemp','A1');
xlswrite('Cosine.xlsx',walEsTmp,'WallEstimationSeconded','A1');
xlswrite('Cosine.xlsx',QPowered,'PowerPerMillimeter')
xlswrite('Cosine.xlsx',cosinePo,'TotalPowerCrossSection')
xlswrite('Cosine.xlsx',crossSec,'SubtractedCrossSectionPower')
xlswrite('Cosine.xlsx',heatFlux,'HeatFlux')
xlswrite('Cosine.xlsx',specheat,'SpecificHeat')
xlswrite('Cosine.xlsx',avgspcht,'AverageSpecificHeat')
xlswrite('Cosine.xlsx',pranumbr,'PrandtlNumber')
disp(flowArea)
disp(wettedPerimeter)
disp(massFlux)
disp(hydraulicDiameter)
disp(heatFluxChannel)

disp(flowArea)
disp(wettedPerimeter)
disp(massFlux)
disp(hydraulicDiameter)
disp(heatFluxChannel)
```

Outer-Sheath-Temperature Profile

```
%%%%%%%%%%%%%%%%%%%%%%%%%%%%%%%%%%%%%%%%%%%%%%%%%%%%%%%%%%%%%%%%%%%%%%%%%%%%%%
%Calculating Inner Sheath temperature for 5772 1mm intervals along the    %
%heated length of the fuel channel in PT-type SCWR reactor with       %
%43-element fuel bundle with 20 mm and Inconel-600 for the sheath material. %
%%%%%%%%%%%%%%%%%%%%%%%%%%%%%%%%%%%%%%%%%%%%%%%%%%%%%%%%%%%%%%%%%%%%%%%%%%%%%%

clear;clc;
thermalPower = 2540 *10^6;  %Total thermal output of energy in W
numChannels = 300;          %Total number of channels in core
channelPower = thermalPower/numChannels;    %Power output of 1 channel
```

Read in bulk-fluid-temperature profiles.

```
tempOuterSheath = xlsread ('Cosine.xlsx','OuterSheathTemp');
heatFluxPerMilli = xlsread ('Cosine.xlsx','HeatFlux');
largeDiameter = 0.020; %center pin diameter(m)
largeElements = 1;      %center pin elements
smallDiameter = 0.0115; %outer rings diameter(m)
smallElements = 42;     %outer rings have 35 elements
lenXSec = 0.001;
fullHeatLen = 5.772;    %full heated length of channel in m
```

Thermal conductivity of Inconel-600

$$k = 14.2214 + 0.01625\,T$$

```
thermalConductivity = 14.22143291+(0.01624506*tempOuterSheath);
largeOuterRadius = largeDiameter/2;
largeInnerRadius = largeOuterRadius - 0.000747837036;
```

```
smallOuterRadius = smallDiameter/2;
```

Sheath thickness is 43 mm

```
smallInnerRadius = smallOuterRadius - 0.000430006296;
largePerimeter = pi*largeDiameter;
largeArea = pi*largeDiameter^2/4;
smallPerimeter = pi*smallDiameter;
smallArea = pi*smallDiameter^2/4;
crossSectionLength = 0.001:0.001:(fullHeatLen+0.001);

% %This calculates the full heated area of the fuel bundle

givenKIMO(5773) = 0;
calculatedKIMO(5773) = 0;
deltaKIMO(5773) = 0;
tempInnerSheathIMO(5773)=0;
powerPerSheathIMO = heatFluxPerMilli *(smallOuterRadius*2*pi*lenXSec);

for j = 1:length(crossSectionLength)
    givenKIMO(j) = thermalConductivity(j);
    calculatedKIMO(j) = thermalConductivity(j);
    deltaKIMO(j) = 1;
```

The stopping criteria for the the sheath thermal conductivity is 0.05 W/m K

```
    while (deltaKIMO(j) > 0.05)
        givenKIMO(j) = calculatedKIMO(j);
        tempInnerSheathIMO(j) =
(powerPerSheathIMO(j)*log(smallOuterRadius/smallInnerRadius))/(2*pi*lenXSec*give
nKIMO(j))+tempOuterSheath(j);
```

$$T_{i,sh} = \frac{\dot{Q}_{sh,x} \ln\left(\frac{r_{o,sh}}{r_{i,sh}}\right)}{2\pi k_{sh}} + T_{o_{sh}}$$

The arithmetic average is used converge the iterations between the outer and inner sheath.

```
        avgTempIMO = (tempOuterSheath(j)+tempInnerSheathIMO(j))/2;
        calculatedKIMO(j) = 14.22143291+(0.01624506*avgTempIMO);
        deltaKIMO(j) = abs(givenKIMO(j) - calculatedKIMO(j));
    end
    tempInnerSheathIMO(j) =
(powerPerSheathIMO(j)*log(smallOuterRadius/smallInnerRadius))/(2*pi*lenXSec*calcu
latedKIMO(j))+tempOuterSheath(j);
end

InnerSheathIMO = transpose(tempInnerSheathIMO);
calcKIMO = transpose(calculatedKIMO);
changeOfKIMO = transpose(deltaKIMO);

Outputs inner-sheath-temperature profile to tabs within an excel file
xlswrite('Cosine_Sheath.xlsx',calcKIMO,'CalculatedThermalConductivities','A1');
xlswrite('Cosine_Sheath.xlsx',InnerSheathIMO,'InnerSheathTemperatures','B1');
xlswrite('Cosine_Sheath.xlsx',changeOfKIMO,'ChangeInThermalConductivity','A1');
xlswrite('Cosine_Sheath.xlsx',powerPerSheathIMO,'SheathPowerPerMillimeter','A1');

disp(smallArea)
```

Fuel-Centreline-Temperature Profile

```
%%%%%%%%%%%%%%%%%%%%%%%%%%%%%%%%%%%%%%%%%%%%%%%%%%%%%%%%%%%%%%%%%%%%%%%%%%%%%%%%%%
%calculating the centerline fuel temperature for 5772 1mm intervals along %
%the heated length of a PT-type reactor with   %
%43-element fuel bundle with 20mm, Inconel 600 for the sheath material, and%
%the fuel being ThO2                                            %
%%%%%%%%%%%%%%%%%%%%%%%%%%%%%%%%%%%%%%%%%%%%%%%%%%%%%%%%%%%%%%%%%%%%%%%%%%%%%%%%%%

clear;clc;
%Inputs
thermalPower = 2540 *10^6;  %Total thermal output of energy in W
numChannels = 300;          %Total number of channels in core
smallDiameter = 0.0115; %outer rings diameter(m)
smallElements = 42;     %outer rings elements
lenXSec = 0.001;
fullHeatLen = 5.772;    %full heated length of channel in m

%Calculations from previous programs used as inputs in this program
powerPerSheathIMO = xlsread('Cosine_Sheath.xlsx','SheathPowerPerMillimeter');
tempInnerSheath = xlsread('Cosine_Sheath.xlsx','InnerSheathTemperatures');



%Calculations
channelPower = thermalPower/numChannels;    %Power output of 1 channel
smallOuterRadius = smallDiameter/2;
smallInnerRadius = smallOuterRadius - 0.000430006296;
```

Dividing the fuel-element radius into 5 increments.

```
smRadiusFive = smallInnerRadius;
smRadiusFour = smallInnerRadius-(1/5*smallInnerRadius);
smRadiusThree = smallInnerRadius-(2/5*smallInnerRadius);
smRadiusTwo = smallInnerRadius-(3/5*smallInnerRadius);
smRadiusOne = smallInnerRadius-(4/5*smallInnerRadius);
smRadiusZero = smallInnerRadius-(5/5*smallInnerRadius);
smallPerimeter = pi*smallDiameter;
smallArea = pi*smallDiameter^2/4;
crossSectionLength = 0.001:0.001:(fullHeatLen+0.001);
fullHeatedArea = smallPerimeter*smallElements*fullHeatLen; % full heated area of q =
channelPower/fullHeatedArea;
heatGenRateIMO = powerPerSheathIMO/(smallInnerRadius^2*pi*lenXSec);
```

$$\dot{e}_{gen,mm} = \frac{\dot{Q}_{loc,mm}}{{D_{i,sh}}^2 \pi (0.001m)}$$

```
%Allocations of memory
smSurfaceTempOne(5773) = 0;
smSurfaceTempTwo(5773) = 0;
smSurfaceTempThree(5773) = 0;
smSurfaceTempFour(5773) = 0;
smSurfaceTempFive(5773) = 0;
thermalConductivityFuelIMO(5773) = 0;
givenKIMOFuel(5773) = 0;
calcFuelKOne(5773) = 0;
calcFuelKTwo(5773) = 0;
calcFuelKThr(5773) = 0;
calcFuelKFou(5773) = 0;
calcFuelKFiv(5773) = 0;
deltaKIMOFuel(5773) = 0;
tempCenterlineIMO(5773)=0;
```

```
for i = 1:1:length(crossSectionLength)

%     thermal conductivity of thoria
   thermalConductivityFuelIMO(i) = 1/(0.0327 + (0.0001603*tempInnerSheath(i)));

   givenKIMOFuel(i) = thermalConductivityFuelIMO(i);
   calcFuelKOne(i) = thermalConductivityFuelIMO(i);
   deltaKIMOFuel(i) = 1;
   while (deltaKIMOFuel(i) > 0.05)
      givenKIMOFuel(i) = calcFuelKOne(i);
      smSurfaceTempOne(i) = tempInnerSheath(i) +
((heatGenRateIMO(i)*(smRadiusFive^2-smRadiusFour^2))/(4*givenKIMOFuel(i)));
```

$$T_{n-1} = \frac{\dot{e}_{gen,mm}\left[{r_{i,sh,n}}^2 - {r_{i,sh,n-1}}^2\right]}{4\,k_{fuel}} + T_n$$

```
      avgTempCenterlineIMO = (tempInnerSheath(i)+smSurfaceTempOne(i))/2;

%        thermal conductivity of thoria
      calcFuelKOne(i) = 1/(0.0327 + (0.0001603*avgTempCenterlineIMO));

      deltaKIMOFuel(i) = abs(givenKIMOFuel(i) - calcFuelKOne(i));
   end
   deltaKIMOFuel(i) = 1;
   smSurfaceTempOne(i) = tempInnerSheath(i) +
((heatGenRateIMO(i)*(smRadiusFive^2-smRadiusFour^2))/(4*calcFuelKOne(i)));
   calcFuelKTwo(i) = calcFuelKOne(i);

Thermal conductivity is 0.05 K for second increment.

   while (deltaKIMOFuel(i) > 0.05)
```

```
        givenKIMOFuel(i) = calcFuelKTwo(i);
        smSurfaceTempTwo(i) = smSurfaceTempOne(i) +
((heatGenRateIMO(i)*(smRadiusFour^2-smRadiusThree^2))/(4*givenKIMOFuel(i)));

        avgTempCenterlineIMO = (smSurfaceTempTwo(i)+smSurfaceTempOne(i))/2;

%       thermal conductivity of thoria
        calcFuelKTwo(i) = 1/(0.0327 + (0.0001603*avgTempCenterlineIMO));

        deltaKIMOFuel(i) = abs(givenKIMOFuel(i) - calcFuelKTwo(i));
    end
    deltaKIMOFuel(i) = 1;
    smSurfaceTempTwo(i) = smSurfaceTempOne(i) +
((heatGenRateIMO(i)*(smRadiusFour^2-smRadiusThree^2))/(4*calcFuelKTwo(i)));
```

$$T_{n-1} = \frac{\dot{e}_{gen,mm}\left[{r_{i,sh,n}}^2 - {r_{i,sh,n-1}}^2\right]}{4\,k_{fuel}} + T_n$$

```
    calcFuelKThr(i) = calcFuelKTwo(i);
```

Thermal conductivity is 0.05 K for third increment.

```
    while (deltaKIMOFuel(i) > 0.05)
        givenKIMOFuel(i) = calcFuelKThr(i);
        smSurfaceTempThree(i) = smSurfaceTempTwo(i) +
((heatGenRateIMO(i)*(smRadiusThree^2-smRadiusTwo^2))/(4*givenKIMOFuel(i)));
        avgTempCenterlineIMO = (smSurfaceTempThree(i)+smSurfaceTempTwo(i))/2;

%       thermal conductivity of thoria
        calcFuelKThr(i) = 1/(0.0327 + (0.0001603*avgTempCenterlineIMO));

        deltaKIMOFuel(i) = abs(givenKIMOFuel(i) - calcFuelKThr(i));
```

```
    end
    deltaKIMOFuel(i) = 1;
    smSurfaceTempThree(i) = smSurfaceTempTwo(i) +
((heatGenRateIMO(i)*(smRadiusThree^2-smRadiusTwo^2))/(4*calcFuelKThr(i)));
    calcFuelKFou(i) = calcFuelKThr(i);
```

Thermal conductivity is 0.05 K for fourth increment.

```
    while (deltaKIMOFuel(i) > 0.05)
        givenKIMOFuel(i) = calcFuelKFou(i);
        smSurfaceTempFour(i) = smSurfaceTempThree(i) +
((heatGenRateIMO(i)*(smRadiusTwo^2-smRadiusOne^2))/(4*givenKIMOFuel(i)));
        avgTempCenterlineIMO = (smSurfaceTempFour(i)+smSurfaceTempThree(i))/2;

%       thermal conductivity of thoria
        calcFuelKFou(i) = 1/(0.0327 + (0.0001603*avgTempCenterlineIMO));

        deltaKIMOFuel(i) = abs(givenKIMOFuel(i) - calcFuelKFou(i));
    end
    deltaKIMOFuel(i) = 1;
    smSurfaceTempFour(i) = smSurfaceTempThree(i) +
((heatGenRateIMO(i)*(smRadiusTwo^2-smRadiusOne^2))/(4*calcFuelKFou(i)));
```

$$T_{n-1} = \frac{\dot{e}_{gen,mm}\left[{r_{i,sh,n}}^2 - {r_{i,sh,n-1}}^2\right]}{4\,k_{fuel}} + T_n$$

```
    calcFuelKFiv(i) = calcFuelKFou(i);
```

Thermal conductivity is 0.05 K for fifth increment.

```
    while (deltaKIMOFuel(i) > 0.05)
        givenKIMOFuel(i) = calcFuelKFiv(i);
```

```
        smSurfaceTempFive(i) = smSurfaceTempFour(i) +
((heatGenRateIMO(i)*(smRadiusOne^2-smRadiusZero^2))/(4*givenKIMOFuel(i)));
        avgTempCenterlineIMO = (smSurfaceTempFive(i)+smSurfaceTempFour(i))/2;

%       thermal conductivity of thoria
        calcFuelKFiv(i) = 1/(0.0327 + (0.0001603*avgTempCenterlineIMO));

        deltaKIMOFuel(i) = abs(givenKIMOFuel(i) - calcFuelKFiv(i));
    end
    smSurfaceTempFive(i) = smSurfaceTempFour(i) +
((heatGenRateIMO(i)*(smRadiusOne^2-smRadiusZero^2))/(4*calcFuelKFiv(i)));
    tempCenterlineIMO(i) = smSurfaceTempFive(i);
```

$$T_{n-1} = \frac{\dot{e}_{gen,mm}\left[r_{i,sh,n}{}^2 - r_{i,sh,n-1}{}^2\right]}{4\,k_{fuel}} + T_n$$

```
end

smSurTempOne = transpose(smSurfaceTempOne);
smSurTempTwo = transpose(smSurfaceTempTwo);
smSurTempThree = transpose(smSurfaceTempThree);
smSurTempFour = transpose(smSurfaceTempFour);
smSurTempFive = transpose(smSurfaceTempFive);
fuelkone = transpose(calcFuelKOne);
fuelktwo = transpose(calcFuelKTwo);
fuelkthr = transpose(calcFuelKThr);
fuelkfou = transpose(calcFuelKFou);
fuelkfiv = transpose(calcFuelKFiv);
centerlineIMO = transpose(tempCenterlineIMO - 273.15);
changeOfKIMOFuel = transpose(deltaKIMOFuel);
```

Outputs fuel-centreline-temperature profile to tabs within an excel spreadsheet

```
xlswrite('ThO2_COS.xlsx',smSurTempOne,'SmallPinSurfaceTempOne','A1');
xlswrite('ThO2_COS.xlsx',smSurTempTwo,'SmallPinSurfaceTempTwo','A1');
xlswrite('ThO2_COS.xlsx',smSurTempThree,'SmallPinSurfaceTempThree','A1');
xlswrite('ThO2_COS.xlsx',smSurTempFour,'SmallPinSurfaceTempFour','A1');
xlswrite('ThO2_COS.xlsx',smSurTempFive,'SmallPinSurfaceTempFive','A1');
xlswrite('ThO2_COS.xlsx',fuelkone,'ThermCondSurface1','A1');
xlswrite('ThO2_COS.xlsx',fuelktwo,'ThermCondSurface2','A1');
xlswrite('ThO2_COS.xlsx',fuelkthr,'ThermCondSurface3','A1');
xlswrite('ThO2_COS.xlsx',fuelkfou,'ThermCondSurface4','A1');
xlswrite('ThO2_COS.xlsx',fuelkfiv,'ThermCondSurface5','A1');
xlswrite('ThO2_COS.xlsx',centerlineIMO,'IMOCenterlineTemperatures','A1');
xlswrite('ThO2_COS.xlsx',changeOfKIMOFuel,'IMOChangeInThermalConductivity','A1
');
xlswrite('ThO2_COS.xlsx',heatGenRateIMO,'HeatGenerationRate','A1');

disp(q)
disp(length(crossSectionLength))
```

Appendix C – MATLAB-Code Check Data

Table C.1. Comparison of MATLAB bulk-fluid temperatures to previous results and Excel spreadsheet calculations.

	Bulk Fluid Temperature, °C				
Distance, m	**Previous**	**MATLAB**	**Excel**	**% Difference w.r.t Previous**	**% Difference w.r.t Excel**
0	350	350	350	0.0	0.0
1	381	381	381	0.1	0.0
1.305	384	384	384	0.0	0.0
1.496	385	384	385	0.0	0.0
1.497	385	385	385	0.0	0.0
1.721	386	386	386	0.0	0.0
2	387	387	387	0.0	0.0
3	405	404	404	0.3	0.0
4	**454**	**451**	451	**0.6**	0.0
5	533	535	535	0.4	0.0
5.772	616	619	619	0.4	0.0
Max % Difference	–	–	–	0.6	0.0

Table C.2. Comparison of MATLAB HTC to previous results and Excel spreadsheet calculations.

	HTC, kW/m^2 K				
Distance, m	**Previous**	**MATLAB**	**Excel**	**% Difference w.r.t Previous**	**% Difference w.r.t Excel**
0	**20.8**	**17.8**	17.8	**14.4**	0.0
1	20.1	17.3	17.3	13.9	0.0
1.305	21.2	18.3	18.3	13.7	0.0
1.496	21.7	18.9	18.9	12.9	0.0
1.497	21.7	18.9	18.9	12.9	0.0
1.721	21.1	18.2	18.2	13.7	0.0
2	18.5	16.1	16.1	13.0	0.0
3	10.9	9.7	9.7	11.0	0.0
4	7.6	7.0	7.0	7.9	0.0
5	6.4	6.0	6.0	6.3	0.0
5.772	6.2	5.9	5.9	4.8	0.0
Max % Difference	–	–	–	14.4	0.0

Table C.3. Comparison of MATLAB outer-sheath temperatures to previous results and Excel spreadsheet calculations.

	Outer Sheath Temperature, °C				
Distance, m	**Previous**	**MATLAB**	**Excel**	**% Difference w.r.t Previous**	**% Difference w.r.t Excel**
0	**394**	**404**	404	**2.6**	0.0
1	426	437	437	2.5	0.0
1.305	427	436	436	2.3	0.0
1.496	427	436	436	2.1	0.0
1.497	427	436	436	2.1	0.0
1.721	430	439	439	2.0	0.0
2	438	447	447	2.2	0.0
3	492	503	503	2.3	0.0
4	578	590	590	2.1	0.0
5	684	696	696	1.8	0.0
5.772	766	784	784	2.4	0.0
Max % Difference	–	–	–	2.6	0.0

Table C.4. Comparison of MATLAB fuel centreline temperatures to previous results and Excel spreadsheet calculations.

	Fuel Centreline Temperature, °C				
Distance, m	**Previous**	**MATLAB**	**Excel**	**% Difference w.r.t Previous**	**% Difference w.r.t Excel**
0	**1280**	**965**	965	**24.6**	0.0
1	1340	1034	1035	22.8	0.0
1.305	1340	1033	1033	22.9	0.0
1.496	1341	1032	1032	23.0	0.0
1.497	1341	1032	1032	23.0	0.0
1.721	1347	1038	1038	22.9	0.0
2	1361	1057	1057	22.3	0.0
3	1462	1184	1184	19.0	0.0
4	1624	**1387**	**1388**	14.6	0.0
5	1817	1609	1609	11.5	0.0
5.772	1959	1753	1754	10.5	0.0
Max % Difference	–	–	–	24.6	0.0

Appendix D – Lisa Grande Publications

Publication summary: 1 paper in a refereed journal, 11 papers in refereed proceedings of international/national conferences and symposiums and 1 major technical report.

Paper in refereed journal:

1. **Grande, L.**, Villamere, B., Allison, L., Mikhael, S., Rodriguez-Prado, A., & Pioro, I. (2011). Thermal aspects of uranium carbide and uranium dicarbide fuels in supercritical water-cooled nuclear reactors. J. of Engineering for Gas Turbines and Power, 133, 7 pages.

Papers in refereed proceedings international/national conferences and symposiums:

1. Pioro, I., Mokry, S., Peiman, W., **Grande, L.**, & Saltanov, E. (2010). Supercritical water-cooled nuclear reactors: NPP layouts and thermal design options of pressure channels. Pacific Basin Nuclear Conference (PBNC-2010), (p. 31). Cancun, Mexico.
2. **Grande, L.**, Peiman, W., Villamere, B., Rodriguez-Prado, A., Mikhael, S., Allison, L., & Pioro, I. (2010). Thermal aspects of alternative fuels for use in supercritical water-cooled nuclear reactors. 11th International Conference on CANDU fuel (p. 15). Niagra Falls, Ontario: CNS.
3. **Grande, L.**, Rodriguez-Prado, A., Mikhael, S. V., Allison, L., & Pioro, I. (2010d). Thermal aspects of using uranium nitride, mixed oxide and thoria fuels as applied to supercritical water-cooled nuclear reactors. 34th CNS/CAN Student Conference (p. 9). Montreal, Canada: CNS.
4. **Grande, L.**, Peiman, W., Mikhael, S., Villamere, B., Rodriguez-Prado, A., Allison, L., & Pioro, I., (2010). Thermal aspects of using uranium nitride in supercritical water cooled nuclear reactors. ICONE-18 (p. 8). Xi'an, China: ASME.

5. Naidin, M., **Grande, L.**, Mokry, S., Peiman, W., Gupta, S., King, K., Farah, A. and Pioro, I., 2010. General Layouts of Supercritical Water NPPs, ICONE-18, Xi'an, China, ASME.
6. Pioro, I., Naidin, M., **Grande, L.**, Mokry, S., Villamere, B., Peiman, W., Allison, L., Rodriguez-Prado, A. and Mikhael, S., 2010. Supercritical Water-Cooled Nuclear Reactors: Thermodynamic-Cycles Plant Layouts and Thermal Aspects of Pressure-Channel Design, Abstract Accepted European Nuclear Conference (ENC 2010), Barcelona, Spain: ENS.
7. **Grande, L.**, Peiman, W., Rodriguez-Prado, A., Villamere, B., Mikhael, S., Allison, L., et al. (2010). Thermal aspects of using mixed oxide fuel in application to supercritical water-Cooled nuclear reactors. 2nd Canada-China Joint Workshop on Supercritical Water-Cooled Reactors (CCSC 2010) (p. 11). Toronto, Canada: CNS.
8. Naidin, M., Pioro, I., Duffey, R., Mokry, S., **Grande, L.**, Villamere, B., Allison, L., Rodriguez-Prado, A., Mikhael, S. and Chophla, K., 2009. SuperCritical Water-Cooled Nuclear Reactors (SCWRs): Thermodynamic Cycle Options and Thermal Aspects of Pressure-Channel Design, International Conference on Opportunities and Challenges for Water Cooled Reactors in the 21st Century, Book of Extended Synopses, IAEA, Vienna, Austria, Oct. 27-30, Paper 5S03, pp. 134-155.
9. **Grande, L.**, Villamere, B., Rodriguez-Prado, A., Mikhael, S., Allison, L., & Pioro, I. (2009). Thermal aspects of using thoria fuel in supercritical water-cooled nuclear reactors. ICONE 17 (p. 10). Brussels, Belgium: ASME.
10. Allison, L., **Grande, L.**, Villamere, B., Mikhael, S., Rodriguez-Prado, A., & Pioro, I. (2009). Uranium Carbide and Uranium Dicarbide in Axial Radial Uniform Heat Flux in SuperCritical Water-cooled nuclear Reactor. ICONE 17 (p. 10). Brussels, Belgium: ASME.
11. Villamere, B., Allison, L., **Grande, L.**, Mikhael, S. R.-P., & Pioro, I. (2009). Thermal aspects for uranium carbide and uranium dicarbide fuels in supercritical water-cooled nuclear reactors. ICONE 17 (p. 12). Brussels, Belgium: ASME.

Major Technical Reports:

1. Pioro, I., Saltanov, Eu., Naidin, M., King, K., Farah, A., Peiman, W., Mokry, S., **Grande, L.**, Thind, H., Samuel, J. and Harvel, G., 2010. Steam-Reheat Option in SCWRs and Experimental BWRs, Report for NSERC/NRCan/AECL Generation IV Energy Technologies Program (NNAPJ) entitled “Alternative Fuel-Channel Design for SCWR” with Atomic Energy of Canada Ltd., Version 1, UOIT, Oshawa, ON, Canada, March, 128 pages.

Appendix E – Lisa Grande Conference Attendance

Five conferences have been attended as well as paper presentations.

October 17 – 20th, 2010. 11th International Conference on CANDU fuel, Niagara Falls, Ontario: CNS.

May 24 – 27th, 2010. 34th CNS/CAN Student Conference. Montreal, Canada: CNS.

May 17 – 21st, 2010. ICONE-18. Xi'an, China.

April 25 – 28th, 2010. 2nd Canada-China Joint Workshop on Supercritical Water-Cooled Reactors (CCSC 2010). Toronto, Canada: CNS.

July 1 2– 16th, 2009. ICONE-17. Brussels, Belgium.

Appendix F – Lisa Grande Awards and Honours

Recipient of ICONE-18 “Best Presenter of North American Student Track” for:

Grande, L., Peiman, W., Mikhael, S., Villamere, B., Rodriguez-Prado, A., Allison, L., and Pioro, I., 2010. Thermal Aspects of Using Uranium Nitride in Supercritical Water-Cooled Nuclear Reactors, Proc. of the 18th International Conference On Nuclear Engineering (ICONE-18), Xi’an, China, May 17-21, Paper #29790, 8 pages.

Recipient of ICONE-17 “Best Paper of North American Student Track” for:

Villamere, B., Allison, L., **Grande, L.**, Mikhael, S., Rodriguez-Prado, A., and Pioro, I., 2009. Thermal Aspects for Uranium Carbide and Uranium DiCarbide Fuels in Supercritical Water-Cooled Nuclear Reactors, Proc. of the 17th International Conference On Nuclear Engineering (ICONE-17), Brussels, Belgium, July 12-16, Paper #75990, 12 pages.